The Role of microRNAs in Bladder Urothelium Development and Tumorigenesis

Angela Yuanyuan Jia

Submitted in partial fulfillment of the
requirements for the degree of
Doctor of Philosophy
under the Executive Committee
of the Graduate School of Arts and Sciences

COLUMBIA UNIVERSITY

2013

ABSTRACT

The Role of microRNAs in Bladder Urothelium Development and Tumorigenesis

Angela Yuanyuan Jia

There are two morphologically distinct cell types in the normal urothelium: umbrella cells and basal/intermediate cells. Immunohistochemical studies from our group suggest that there may be more than one urothelial progenitor. Bladder cancer is the fifth most common cancer in the United States and the second most prevalent genitourinary malignancy. Urothelial carcinoma accounts for 90% of bladder cancers. Based on clinical and histological studies, urothelial carcinomas are thought to develop through two independent pathways and are classified into two main phenotypic variants: low-grade tumors (usually papillary and “superficial” with high recurrence), and high-grade tumors (usually flat carcinoma *in situ* lesions that are often associated with and progress to muscle invasion).

MicroRNAs (miRNAs) are single-stranded non-coding RNA molecules, approximately 21-23 nucleotides in length, that regulate gene expression. Since their discovery in 1993, they have emerged as major mediators of cellular functions and tissue homeostasis. Importantly, distortion of their normal function is commonly observed in human malignancies, suggesting that they act as a new class of tumor suppressors and oncogenes. Despite the strong links reported between miRNAs and the pathogenesis of numerous human cancers, there are few studies centering on their characterization in normal urothelium and there is little consensus on which miRNAs contribute to urothelial tumor initiation and progression.

Through a series of studies, we profiled the expression of miRNAs in distinct compartments of the normal bladder, including umbrella and basal-intermediate urothelial cells, as well as the muscularis propria; and bladder carcinoma *in situ* (CIS) lesions. We discovered

and validated the expression of miR-133a and miR-139-3p in umbrella cells, and miR-142-3p in basal-intermediate cells. This study represents the first molecular characterization of miRNA expression in the normal urothelium. Strikingly, we found that miRNA expression levels of CIS most closely resembled the miRNA profile of umbrella cells. Finally, we examined well-established umbrella and basal-intermediate cell immunohistochemical biomarkers in an independent series of CIS samples. Once more, this analysis revealed that CIS lesions shared a common phenotype with umbrella cells through the expression of umbrella-specific markers.

Mechanistic studies were performed in parallel to further delineate the potential role of two critical miRNAs involved in cell invasion that were previously unassociated with urothelial carcinomas: miR-198 and miR-126. Overexpression of miR-198 increased cell invasion in non-invasive bladder cancer cells, an effect that was magnified with concurrent down-regulation of the miR-200 family. In contrast, elevated levels of miR-126 suppressed cell invasion in invasive bladder cancer cells, possibly through regulation of gene expression of the matrix metalloproteinase ADAM9. Correspondingly, knock-down studies of ADAM9 in invasive bladder cancer cells also inhibited cell invasion. We further demonstrated preferential expression of ADAM9 in muscle-invasive bladder tumors compared to non-muscle invasive tumors, and that ADAM9 expression significantly correlated with a poor prognosis in patients with urothelial carcinoma.

Our studies represent a comprehensive and accurate description of the different miRNAs expressed in distinct urothelial cellular compartments and CIS tumors. This study is also the first to provide evidence of the possible origin of CIS lesions from umbrella cells. Additionally, important translational results of our studies support the use of miR-198, miR-126, and ADAM9 as clinical biomarkers of disease progression, and provide a rationale for the therapeutic inhibition of ADAM9 in aggressive urothelial carcinomas. Overall, the findings reported here indicate that several miRNAs are differentially regulated in urothelium

development and tumorigenesis, and may form a basis for clinical development of new biomarkers for urothelial carcinoma.

Table of Contents

List of Figures and Tables

List of Abbreviations

The following is a list of abbreviations used throughout the dissertation.

3'UTR	3' untranslated region
ADAM9	ADAM metallopeptidase domain 9
ATF4	activating transcription factor 4
B/i	basal intermediate (bladder urothelium)
BBN	*N*-butyl-*N*-(-4-hydroxybutyl)nitrosamine
CDKN	cyclin-dependent kinase inhibitor
CIS	carcinoma *in situ* (bladder)
CK	cytokeratin
CSC	cancer stem cell
DBC1	deleted in bladder cancer 1
EGFR	epidermal growth factor receptor
EI24	etoposide induced 2.4 mRNA
EMT	epithelial-to-mesenchymal transition
FC	fold change
FGFR	fibroblast growth factor receptor
FL	firefly luciferase
GO	gene ontology
GTP	green fluorescent protein
HER	human epidermal growth factor receptor
HB-EFG	heparin-binding epidermal growth factor
HMWCK	high molecular weight cytokeratins
HRAS	v-Ha-ras Harvey rat sarcoma viral oncogene homolog
IHC	immunohistochemistry
ISH	*in situ* hybridization
KANK	KN motif and ankyrin repeat domains 1
KRAS	v-Ki-ras2 Kirsten rat sarcoma viral oncogene homolog
LCM	laser capture microdissection
LNA	locked nucleic acid
LOH	loss of heterozygosity
MI	muscle-invasive (urothelial carcinoma)
miRISC	miRNA-inducing silencing complex
miRNA	microRNA
MMP	matrix metalloproteinase
MNU	*N*-methyl-*N*-nitrosourea
MP	muscularis propria (bladder)
MYC	v-myc myelocytomatosis viral oncogene homolog (avian)
NKX3.1	NK3 homeobox 1
NMI	non-muscle-invasive (urothelial carcinoma)

PEX5	peroxisomal biogenesis factor 5
PI3KCA	phosphatidylinositol-4,5-bisphosphate 3-kinase, catalytic subunit alpha
PLXNB2	plexin B2
PTCH	Gorlin syndrome gene
PTEN	phosphatase and tensin homolog
qRT-PCR	quantitative reverse transcriptase polymerase chain reaction
RL	renilla luciferase
RPL41	ribosomal protein L41
SOX4	SRY (sex determining region Y)-box4
SPTBN1	spectrin, beta, non-erythrocytic 1
TSC	tuberous sclerosis complex gene
UC	urothelial carcinoma
UM	umbrella (bladder urothelium)
UPK	uroplakin
ZEB	zinc finger E-box binding homeobox

Acknowledgements

The following body of work would not have been possible without the guidance and dedication of my thesis mentor, Dr. Carlos Cordon-Cardo. His passion for research, optimism, and work-ethic have been an inspiration to me. Not only have I benefited greatly from his tremendous scientific and clinical expertise, Carlos also provided me the freedom and resources to follow my own research interests and develop as a scientist. I am indebted to the patience, wisdom, and generosity he has shown over the years.

I am very grateful to my thesis committee members, Drs. Jan Kitajewski, Ramon Parsons, Jose Silva, and Mitchell Benson, for their helpful critiques and objective insights to the development of my projects. I am especially thankful to Jose for his invaluable expertise and technical skills in the field of microRNAs, and the enormous generosity with his time. I would also like to thank Zaia Sivo and Dr. Ron Liem of the Pathology Department for being staunch advocates of student welfare and ensuring smooth passage throughout my PhD training. Zaia in particular has afforded countless hours ensuring the best experience possible at Columbia; I would be lost without her diligence and friendship.

I would like to acknowledge past and present members of the Cordon-Cardo and Silva labs for providing warm, collaborative, and encouraging work environments. Specifically, many thanks to Dr. David Llobet-Navas, Veronica Castro, and Dr. Berna Demircan in the Silva lab for their assistance in all things microRNA-related and sharing of reagents. In the Cordon-Cardo lab, I am especially thankful to Dennis Bonal, Joslyn Mills-Bonal, Dr. Orit Schmidt-Karni, and Todd Hricik for discussions and technical help. A special thank-you to Dr. Mireia Castillo-Martin, who has been instrumental in the progress of my thesis work. She is both a most talented pathologist and scientist; I am extremely grateful for her detailed critiques and technical guidance. I also thank Dr. Marta Sánchez-Carbayo in Spain for valuable scientific discussions and tumor

samples. I am grateful to the Molecular Pathology Core for their generous provision of work space and reagents, and especially Dr. Tao Su for scientific advice. Finally, I am ever grateful for the steadfast friendships of Drs. Sara Siddiqi, Alison Barber, and Fil Dela Cruz. Their unique perspectives, technical assistance, and wonderful senses of humor have made my journey such a memorable delight. It has been a privilege to work beside so many brilliant scientists.

Dedication

To my parents and my husband, David, for their unwavering love and support.

1. Chapter 1: Introduction

Bladder development and histology

The bladder sprouts as a tubular organ from the upper urogenital sinus and allantois in the embryo [1]. The primitive urogenital sinus develops from the expansion of the hindgut in the embryo between weeks four to six [1]. Mesoderm-derived mesenchymal cells that differentiate into fibroblasts and smooth muscle comprise the stroma, while endoderm-derived epithelial cells differentiate to form the urothelium. The urothelium coats the entire urinary tract, including the renal pelvis, ureter, bladder and female proximal urethra. In humans, the urothelium is pseudo-stratified, ranging from three to seven cell layers in thickness depending on distension. One layer of compact and cuboidal cells lines the basal membrane, a few layers of intermediate cells oriented perpendicular to the basal membrane constitute the majority of the urothelium, and a single layer of umbrella cells oriented parallel to the basal membrane face the lumen. The basal lamina separates the urothelium from the stromal part of the bladder, which includes the lamina propria and the muscularis propria. The lamina propria is composed of loose collagen, thin bundles of smooth muscle (muscularis mucosae), small blood, and lymphatic vessels, while the muscularis propria has thick interlacing bundles of smooth muscle fibers, nerves and foci of adipose tissue.

The three urothelial cell types (basal, intermediate, and umbrella cells) are distinct in both morphology and expression of specific biomarkers (**Figure 1.1**). While basal and intermediate (B/i) cells present clear and amphophilic cytoplasms, superficial umbrella (UM) cells display an eosinophilic cytoplasm and a large nucleus that is usually bi- or multi-nucleated. UM cells express high levels of uroplakin II (UPKII) [2], low molecular weight cytokeratins (e.g. CK18 and CK20) [3], and Lewis X determinant [4]; while none of these markers is expressed in

B/i cells. In contrast, B/i cells stain strongly for high molecular weight cytokeratins (e.g. CK5, CK10, CK14), p63 [5], and mature A and B blood group antigens – all of which are negative in UM cells. While it has been proposed that UM cells mature from the underlying B/i cells in a manner similar to epithelial development of the skin, the vast number of differences between the two cell types suggests that UM cells may originate from a precursor distinct from B/i cells.

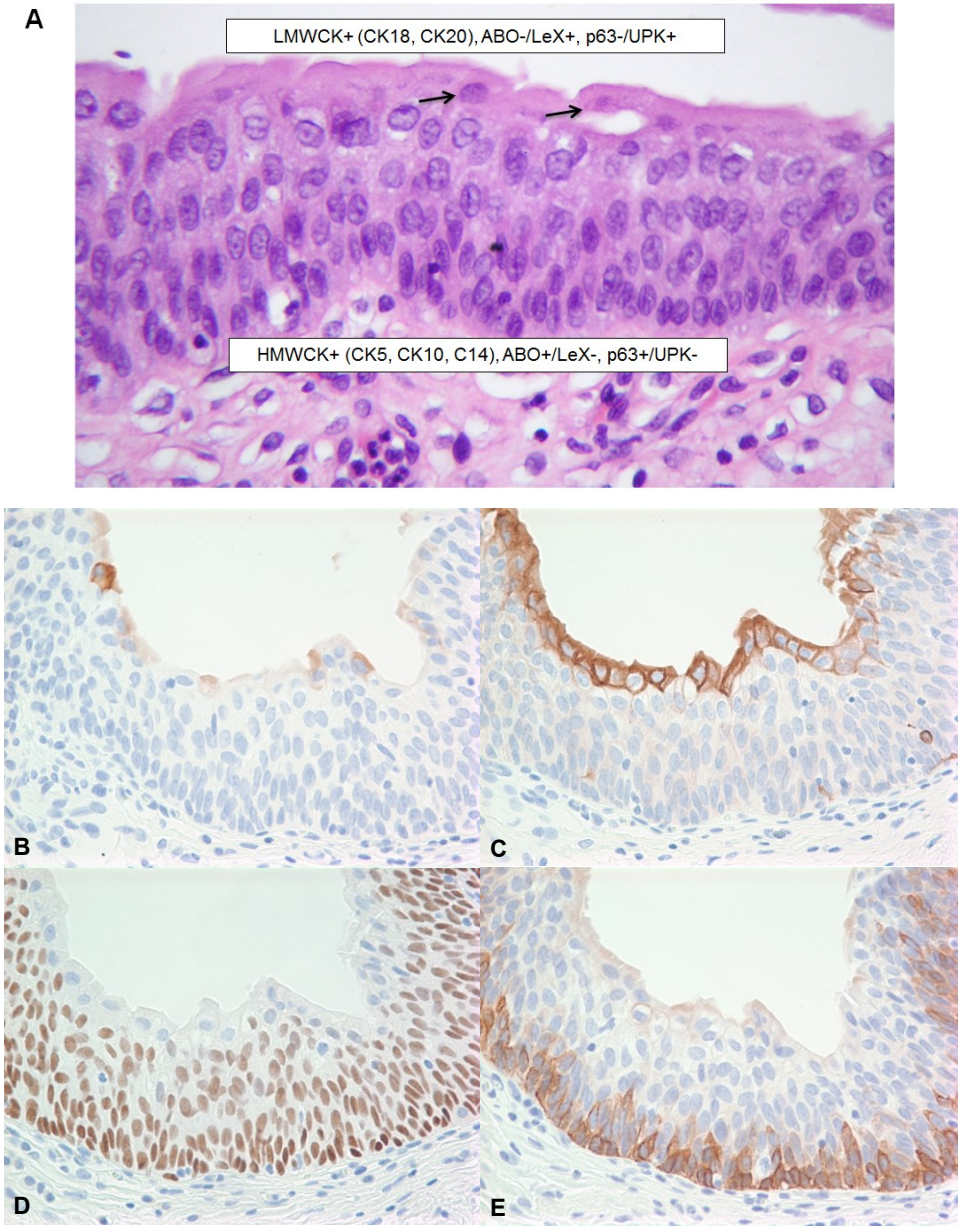

Figure 1.1 Normal bladder urothelium

(A) UM cells (indicated by arrows) form a single layer facing the lumen and are distinct from subsequent layers of B/i cells. Representative immunohistochemical analyses of **(B)** CK20, **(C)** CK18, **(D)** p63, and **(E)** HMWCKs (CK1, CK5, CK10, CK14) in normal urothelium.

The urothelium can undergo proliferation in response to injury, but is otherwise normally quiescent [6,7]. To date, urothelial stem or progenitor cells have not been identified. Although one research group has reported potential adult bladder stem cells to be CD43+CD45-, these

cells were not shown to possess stem cell features such as self-renewal and differentiation capacity [8]. Cells from the bladder trigone, a region with an elevated incidence of tumorigenesis, were shown to maintain higher proliferative capacity and colony-formation efficiency; however, a stem cell was not isolated [9]. Other approaches utilizing the unique label-retaining ability of stem cells [10] reported contradictory findings. Likely due to different labeling techniques, bladder "label-retaining cells" have been identified as confined to the basal layer [11] as well as throughout the urothelium in random distribution [12]. Given the distinct immunohistochemical profiles of UM and B/i cells, more than one urothelial progenitor may exist [13].

Bladder cancer

The association of bladder cancer with occupational exposure to certain organic compounds, such as β-naphthylamine, was first observed in 1895 in workers in the German dye industry [14]. Other risk factors include tobacco smoking, radiation therapy of neighboring organs, and chronic infection with *Schistosoma* species (also known as bilharzia, mainly associated with the squamous cell carcinoma variant) [15]. The urothelium functions as a permeability barrier between blood and urine and is constantly exposed to potential carcinogens in urine. Therefore, it is not surprising that 90% of bladder tumors originate from the urothelium [16]. Due to the pseudo-stratified and non-squamous nature of the epithelium, the urothelium is also called the transitional epithelium; the majority of bladder cancers are therefore transitional cell carcinomas, more commonly known as bladder urothelial carcinoma (UC).

Bladder cancer ranks second as the most commonly diagnosed genitourinary malignancy after prostate cancer and fifth among all cancers in the United States [17], with higher prevalence in developed countries [18]. Bladder neoplasms present as superficial bladder tumors (stages Ta, Tis, and T1) in 75-85% of initial diagnoses and are often multifocal with frequent recurrence, although only 2-5% of Ta and 20% of T1 bladder tumors progress to a

higher stage [16]. The remaining 15-25% of carcinomas are invasive (stages T2, T3, and T4) or metastatic lesions at initial clinical presentation [16].

Bladder UCs can be classified as either low-grade or high-grade tumors based on distinct phenotypic and molecular profiles (**Figure 1.2**). Low-grade tumors are always papillary (i.e. protruding into the lumen) and usually do not invade the muscularis propria (clinically termed "superficial"). These tumors include urothelial papilloma, papillary urothelial neoplasms of low malignant potential, and non-muscle invasive low-grade papillary UC. Chromosomal aberrations associated with the development of papillary tumors include deletion of chromosome 9 and activating mutations in oncogenes. Loss of heterozygosity (LOH) on 9q mapped to three regions: *PTCH* (Gorlin syndrome gene) at 9q22, *DBC1* (deleted in bladder cancer 1) at 9q33, and *TSC1* (tuberous sclerosis complex gene 1) at 9q34 [16]. Of these three genes, only *TSC1*, which encodes for hamartin, has an established role as a tumor suppressor. The TSC1/TSC2 complex regulates mTOR activity by inhibiting Rheb; loss of *TSC1* results in inactivation of the complex and leads to enhanced mTOR signaling [19]. Another frequently perturbed region is 9p21. This locus harbors *CDKN2A* (encodes p16 and $p14^{ARF}$) and *CDKN2B* (encodes p15) genes [20]. Homozygous deletion of CDKN2A is linked to papillary tumors of high grade and higher recurrence [21,22]. Although it remains unclear whether loss of 9q precedes the loss of 9p, the loss of 9q phenotype is more frequent in non-muscle invasive than muscle-invasive tumors [23].

Oncogenes frequently mutated in low-grade superficial tumors include *FGFR3* (fibroblast growth factor receptor-3), *PIK3CA* (the catalytic p110α subunit of phosphoinositide 3-kinase), and *HRAS* (v-Ha-ras Harvey rat sarcoma viral oncogene homolog). A missense mutation in *FGFR3* resulting in increased receptor stability and decreased degradation [24] is present in over 70% of all low-grade, non-muscle invasive papillary tumors [25,26]. Gain of function mutations in *PIK3CA* are rare in muscle-invasive tumors, predominately found in bladder tumors of low grade and stage, and show a significant association with *FGFR3* mutations [27]. In

contrast, *HRAS* and *FGFR3* mutations are mutually exclusive, likely because these proteins stimulate the same mitogen-activated protein kinase pathway [28]. Activating *HRAS* mutations are detected in 30-40% of UCs [29,30]. Furthermore, experimental overexpression of constitutively active *Hras* driven by the mouse uroplakin II promoter only produced low-grade papillary tumors [31].

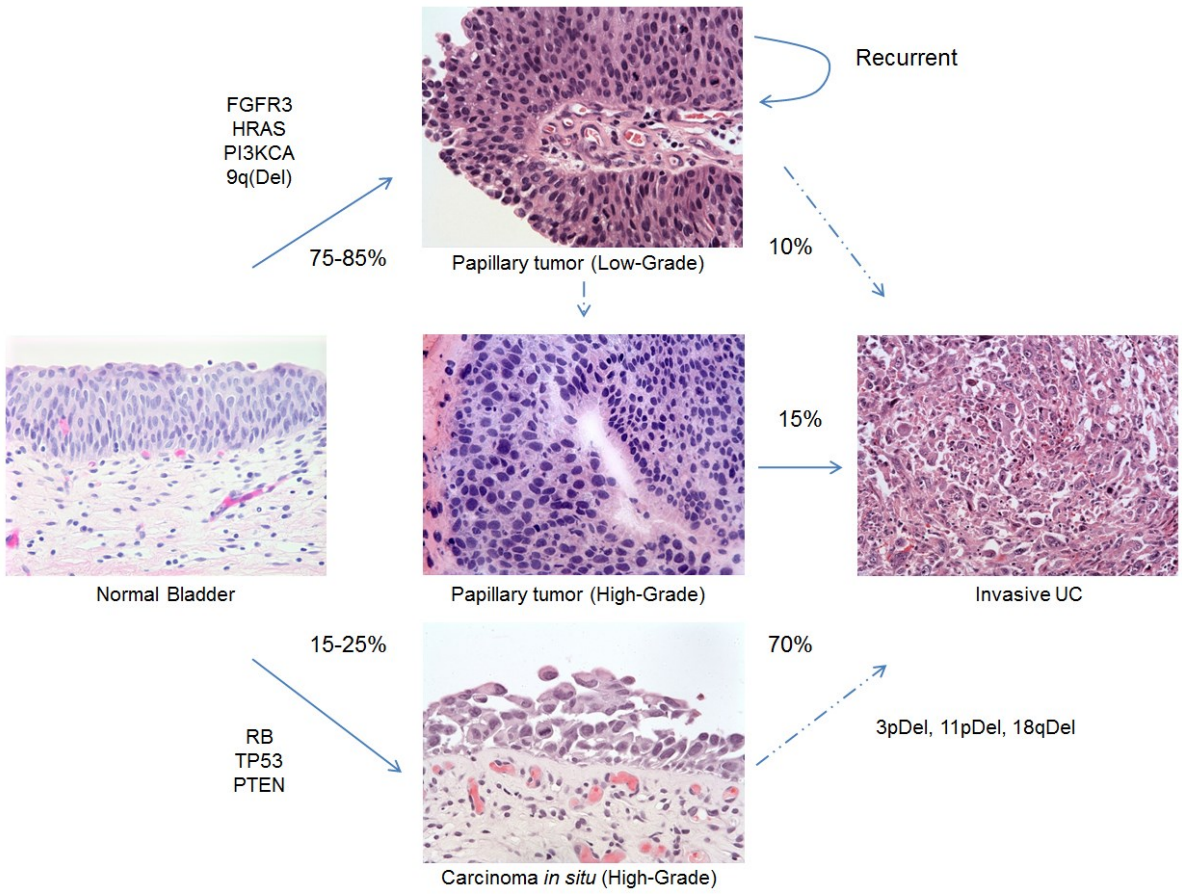

Figure 1.2 Molecular pathways in bladder tumorigenesis

Urothelial tumors initiate and progress via two distinctive pathways. The majority present as low-grade papillary tumors, characterized by the loss of regions on chromosome 9q and mutations that result in constitutive activity of FGFR3, HRAS, and PI3KCA. The remaining high-grade tumors frequently display loss of function of RB, TP53, and PTEN.

In contrast, high-grade tumors can be papillary or non-papillary, such as the flat carcinoma *in situ* (CIS) lesions, and often progress to muscle-invasive disease. These tumors

frequently display loss of key functional tumor suppressors, events that are rare or absent in low-grade bladder tumors. More than 50% of CIS and high-grade UCs are associated with a dysfunctional p53 protein [32], and the presence of *TP53* mutations corresponds to higher probability of disease progression [33]. Loss of function of RB, both through genomic deletions or mutations, primarily correlates with muscle-invasive UC [34] and is associated with aggressive clinical behavior [35]. LOH on chromosome 10 at the *PTEN* locus is another common occurrence in muscle-invasive UCs [36,37] and is an important prognostic predictor of poor overall survival [38]. Additional chromosomal abnormalities that contribute to progression of high-grade tumors into muscle-invasive UCs include deletion of 3p, 11p, and 18q [39,40].

The transformed cells within a bladder tumor are not homogeneous. One explanation attributes the source of intratumoral heterogenetiy to cancer stem cells (CSCs). By definition, these cells are capable of self-renewal and asymmetrical cell division to give rise to differentiated progeny that constitute the bulk of the tumor [41]. Recent studies have characterized putative bladder CSCs to resemble normal basal cells [42,43]. One group characterized CD44+ bladder tumor cells with tumor-initiating capabilities *in vivo* as basal-like due to positive CK5 expression [42], however, human xenograft tumors produced in another study did not identify preferential CD44 expression in basal-like cells [43]. Furthermore, human UCs do not uniformly express CD44 [42], suggesting that CD44 is not a universal marker for bladder CSCs. Therefore, the possibility of more than one cancer progenitor cell exists. It is conceivable that oncogenic events affecting different progenitor cells may give rise to two pathways of bladder cancer transformation (low-grade non-muscle invasive versus high-grade muscle-invasive).

microRNAs (miRNAs)

MicroRNAs (miRNAs) were first discovered in developmental studies of temporal gene expression control in *Caenorhabditis elegans* by the Ambros group in 1993 [44]. To date, more

than 21,000 distinct mature miRNA sequences have been identified in 193 different species (miRBase 19) with more than 2,000 miRNAs identified in humans [45,46]. Although first believed to be required only in multicellular organisms, the recent discovery of miRNAs in the unicellular algae *Chlamydomonas reinhardtii* [47] suggests that miRNAs are evolutionarily older than previously thought. miRNAs have been implicated in development and tumorigenesis, as reviewed in [48-50].

miRNA mechanism of function

Biogenesis

miRNAs can be transcribed from independent miRNA genes (intergenic) or as introns of protein-coding mRNAs (intragenic) into precursor molecules (pri-miRNA). Pri-miRNAs fold into hairpin structures that are cleaved by the RNase III family nuclease Drosha to generate hairpins known as pre-miRNA. The pre-miRNA hairpins are exported to the cytoplasm by exportin5, a Ran-GTP dependent exporter [51].

In the cytoplasm, pre-miRNAs are recognized and processed by Dicer, an endoribonuclease, to generate 22 base-pair miRNA duplexes with a two nucleotide overhang at the 3' end. miRNAs then complex with other ribonucleoproteins, the most studied of which is the Argonaute family, to generate miRNA-induced silencing complexes (miRISC). Asymmetry in the miRNA duplex determines which strand is loaded into miRISC and which one is degraded [52]; the strand whose 5' end is less thermodynamically stable, or less tightly paired to its complement, is kept as the mature miRNA that will guide miRISC to translationally repress specific mRNAs through base pairing [53] (**Figure 1.3, adapted from [51]**).

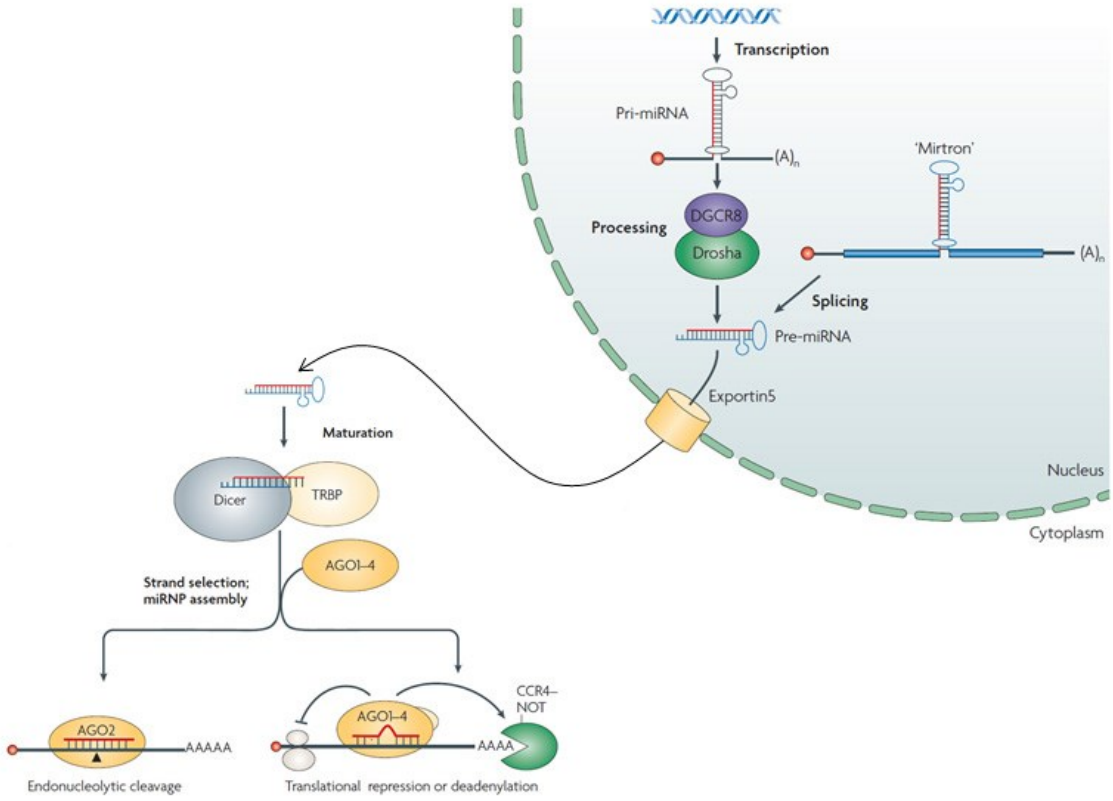

Figure 1.3 miRNA biogenesis and assembly into silencing machinery

miRNA-containing genes are transcribed into pri-miRNAs, processed by Drosha, and exported into the cytoplasm as pre-miRNAs. Pre-miRNAs are cleaved by Dicer to generate 22-nucleotide duplexes that associate with other ribonucleoproteins to form the silencing complex miRISC. miRNA-mediated repression results in mRNA endonucleolytic cleavage or translational repression. Figure adapted from Filipowicz and colleagues [43].

miRNA-mRNA interaction

miRNAs bind their targets at the 3' untranslated region (UTR) of the mRNA. A miRNA-mRNA duplex with nearly perfect complementarity usually results in endonucleolytic cleavage of the duplex through an RNAi like mechanism. This is often the case in plants, where the targeted mRNA is degraded [52]. By contrast, most metazoan miRNAs do not complement their targets exactly. Instead, base pairing is perfect and contiguous in the miRNA from the second to eighth nucleotides, known as the "seed" region, but mismatches are present in the central region of the

miRNA-mRNA duplex [51]. Although one binding site on the mRNA is sufficient to regulate gene expression, miRNAs have also been shown to bind cooperatively to their targets.

Mechanisms of miRNA-mediated repression from imperfect base pairing include proteolysis, deadenylation of the poly-A tail followed by mRNA decay, and translational block. For example, Argonaute proteins can compete with the eukaryotic initiation factor 4E subunit for binding to the mRNA 5'-terminal 7-methylguanosine cap. This blocks translational initiation [54]. In addition, miRNAs can cause ribosomes to "drop-off" or dissociate prematurely from the transcript to induce early termination [55].

While the ability to repress gene expression is well known, miRNAs can also up-regulate target expression. Vasudevan and colleagues [56] showed that miRNAs can coordinate both repression and activation of genes depending on cell cycle. Specifically, under serum-starved conditions, miR-369-3 is recruited by AU-rich elements in the tumor necrosis factor-α to promote downstream gene expression. Conversely, miR-369-3 represses the same targets during cell proliferation. This adds to the dynamic range of miRNA function. *In silico* studies suggest that up to 30% of all protein-coding genes may be controlled by miRNAs [51].

miRNAs share many similar features with transcription factors as gene regulatory molecules with numerous targets, however, miRNAs also maintain unique qualities. Owing to their small size and ability to function outside the nucleus, miRNA-mediated gene regulation can be compartmentalized and reversible [57]. Studies of miRNA regulation in neurons demonstrate the ability of miRNAs to modify gene repression at the synapse [58,59]. This level of subcellular specificity is not possible with transcription factors, which are limited to act within the nucleus. Furthermore, the miRISC can be disengaged from the mRNA to resume target expression [59,60]. This makes protein repression rapidly reversible, as opposed to transcription of new mRNA.

The role of miRNAs in human cancer

More than 50% of the miRNAs implicated in cancer map to areas of the genome highly susceptible to chromosome damage, such as sites of chromosomal amplification, breakage, and fusion [61]. These areas, known as fragile sites, are more vulnerable to replicative stress. miRNA are associated with genomic alterations, as such, their expression patterns differ from cancer cells as compared to normal tissue of the same organ. Based on this and their tissue and cell lineage specificity, miRNAs can be used to identify the tissue of origin in metastatic tumors and facilitate diagnosis [62]. As regulators of gene expression, aberrant expression of miRNAs can be tumorigenic if they target mRNAs that code for either a tumor suppressor or an oncogene.

Oncogenic miRNAs and tumor suppressive miRNAs

The first study reporting the oncogenic role of a miRNA was on the development of lymphomagenesis in chickens following overexpression of the gene *BIC* [63]. Due to lack of an open reading frame, *BIC* was believed to function as a noncoding RNA, and was later confirmed to encode for miR-155. miR-155 is overexpressed in many B-cell cancers, including diffuse large cell B-cell lymphoma, pediatric Burkitt lymphoma, and Hodgkin lymphoma. Elevated levels of miR-155 in a variety of tumor cell lines was shown to target cell cycle regulators and consequently undermine DNA damage response mechanisms [64]. Similarly, transgenic mice overexpressing *mir-155* in B cells exhibited pre-leukemic pre-B-cell proliferation in the spleen and bone marrow, and eventually developed B-cell malignancy [65]. The mouse model suggests that the gain of miR-155 may be an early event or a “first hit” that predisposes cells to tumor formation following secondary mutations.

miR-21 is another miRNA up-regulated in a multitude of solid tumors and hematopoietic malignancies. *mir-21*$^{-/-}$ mice reduced the formation of skin papilloma in a chemical-induced skin carcinogenesis model [66]. Genomic deletion of *mir-21* was observed to decrease proliferation

of the epidermis and increase apoptosis in papilloma cells [66]. On the other hand, overexpression of *mir-21* driven by an inducible nestin promoter, which drives miR-21 expression in the central and peripheral nervous system and in myogenic tissues, developed pre-B-cell lymphoma that was reversed when endogenous miR-21 levels were reestablished [67]; this demonstrated the dependence of tumors on a single miRNA. In a non-small cell lung cancer mouse model bearing a constitutively active KRAS mutant, overexpression of *mir-21* was shown to increase tumor burden [68]. However, miR-21 did not affect tumorigenesis in the absence of the oncogenic mutant KRAS, suggesting it may enhance tumor pathology and not be an instigator of tumor initiation [68]. KRAS activation was shown to increase miR-21 expression *in vivo*, therefore additional miR-21 expression may provide a "second hit" that accelerated tumor formation [68].

Similar to the autoregulatory loop connecting KRAS and miR-21, the miR-17~92 cluster, a cluster of six miRNAs, is activated by the MYC oncogene [69]. Located within a fragile site of the genome, the miR-17~92 cluster is amplified in many different human cancers [70]. The rate of tumor formation was significantly increased in a B-cell lymphoma transgenic model expressing both *c-myc* and a truncated version of the cluster, *mir-17~19b-1*, in the mouse hematopoietic stem cells [70].

The miR-15~16 cluster, composed of miR-15a and miR-16, is also situated within a fragile site, but unlike the miR-17~92 cluster, this cluster is lost in more than half of B-cell chronic lymphocytic leukemia. Both genomic deletion and conditional deletion in B-cells of the *mir-15~16* locus in mice resulted in a spectrum of symptoms associated with chronic lymphocytic leukemia, including lymphoma [71]. Interestingly, levels miR-15a and miR-16 are also reduced in fibroblasts surrounding prostate cancer [72]. Reintroduction of the two miRNAs in fibroblast cells impaired cell proliferation and conditioned the fibroblast media to inhibit prostate cancer cell migration *in vitro* and expansion of prostate cancer xenografts *in vivo* [72].

In accordance with the idea that miRNAs adopt tumor suppressive roles, miRNA processing machinery disruptions are commonly observed in tumors. For instance, single allele deletion of *DICER1* is observed in several different human cancers [73]. Notably, single copy loss of *Dicer1* in the mutant *Kras*-driven lung cancer mouse model led to shortened lifespans compared to control, and homozygous deletion of *Dicer1* was never observed in tumors from *Dicer1*$^{flox/flox}$ mice [73]. This implies that DICER may function as a haploinsufficient tumor suppressor, where complete deletion may inhibit tumor formation and is selected against [73]. Since DICER is crucial in the production of mature miRNAs, reduction in *DICER1* gene dosage would be expected to decrease global miRNA function, whereas full loss of *DICER1* would abolish miRNA activity and lead to cell death. Indeed, loss of *Dicer1* is embryonically lethal in mice [74]. Therefore, a fine balance of miRNA expression must be maintained to ensure cell viability but inhibit tumor proliferation.

miRNAs involved in metastasis

Metastasis accounts for more than 90% of mortality related to cancer [75]. To achieve tumor formation at the secondary site, neoplastic epithelial cells at the primary tumor first degrade the basal membrane and invade the surrounding extracellular matrix, enter the blood stream (intravasation), survive in circulation to distant organs, exit the blood stream (extravasation), adapt and proliferate in the foreign tissue (colonization) [75,76]. Propelled by both internal signals and interactions with the microenvironment, one pathway of invasion employs epithelial-to-mesenchymal transition (EMT), whereby epithelial cells adopt mesenchymal traits, most notably increased motility [76]. Many miRNAs are reported to affect various stages of metastasis. Detailed understanding of their roles may provide insights on how to manipulate miRNAs for therapeutic applications.

The miR-200 family (miR-200a, b, c, miR-141 and miR-429) has been show to target ZEB1 and ZEB2 [77-79]. These two transcription factors promote EMT by targeting E-cadherin,

a key protein that is responsible for preserving intercellular junctions by immobilizing epithelial cells in sheets. Loss of miR-200 is frequently associated with aggressive clinical outcome in lung, prostate and pancreatic cancers [80-82]. Specifically, in a mouse lung adenocarcinoma model driven by oncogenic *Kras*^{G12D} and dysfunctional p53, miR-200 expression determined whether or not tumors metastasized, where the absence of miR-200 resulted in metastasis and its restoration prevented muscle-invasion [80].

Other miRNAs lost in invasive carcinomas include miR-31, miR-335, and miR-126. There is a marked decrease in miR-31 expression in invasive breast cancer cell lines compared to primary normal human mammary epithelial cells [83]. Delivery of miR-31 expressing MDA-MB-231 human metastatic breast cancer cells into the mammary fat pad of mice impaired metastasis to the lung, but did not affect the growth of the primary tumor. miR-31 is shown to convert metastatic breast cancer into non-muscle invasive tumors in orthotopic implants by activating cell cycle arrest and apoptosis, and inhibiting Akt-dependent signaling [84]. Loss of miR-335 and miR-126 is associated with poor metastasis-free survival in breast cancer. Overexpression of miR-335 and miR-126 in MDA-MB-231 cells injected into mice prevented bone and lung metastasis. Specifically, miR-126 suppressed overall tumor growth while miR-335 reduced invasion, presumably by targeting the transcription factor SOX4 and extracellular matrix component tenascin C [85]. miR-126 is also reduced in invasive pancreatic ductal adenocarcinoma [86] and metastatic hepatocellular carcinoma [87]; in both cases, restoration of miR-126 *in vitro* attenuated cell migration and invasion.

Conversely, a forward genetic screen was used to identify miRNAs that promoted muscle-invasion. A library set of approximately 450 miRNAs was transduced into MCF-7, a non-migratory and non-metastatic breast cancer cell line. Repeated transwell migration assays found miR-373 and miR-520c to be enriched in the pool of migratory cells, and both miRNAs were confirmed to stimulate migration and invasion *in vitro* and *in vivo* [88]. Similarly, miR10b expression is positively correlated with high-grade breast cancer [89] as well as pancreatic

adenocarcinomas [90], glioblastomas [91], and metastatic hepatocellular carcinomas [92]. Systemic treatment with miR-10b antagomiRs in a breast tumor mouse model effectively silenced its expression and suppressed metastasis without affecting primary tumor [89].

miRNA-based therapeutics

Evidence of the role of miRNAs in carcinogenesis in various animal models suggests that inhibiting up-regulated oncogenic miRNAs and replacing lost tumor suppressive miRNAs may have therapeutic effects. The small size of miRNAs lends to easier cellular uptake and allows for less toxic methods of delivery compared to protein-coding gene moieties, which require viral-based expression mechanisms. They are also less antigenic. Intravenous and intratumoral injections are commonly used methods of delivery in animal models [93].

Molecules created to suppress of miRNA function are designed to bind to mature miRNA sequences and prevent miRNA interactions with downstream silencing complexes through either competitive inhibition or degradation. One strategy uses chemically modified antisense molecules directly complementary to the target miRNA, such as locked nucleic acid (LNA)-modified anti-miRNA oligonucleotides [94]. An alternate approach exploits the miRNA-mRNA interaction, where transcripts expressing multiple tandem repeats of the seed region for the miRNA of interest are introduced. These transcripts, aptly named miRNA sponges or miRNA decoys, contain miRNA-binding sites that are modified to prevent cleavage of the sponge by miRISC, thereby “soaking up” the existing pool of miRNAs [95]. Sponges and decoys can be expressed in a plasmid driven by an appropriate promoter, lending a higher level of context-dependent and temporal control for expression in animal systems. Furthermore, instead of targeting one specific miRNA at a time, a sponge can theoretically target an entire miRNA family that share a common seed region. So far, the most promising method of silencing endogenous miRNAs in non-human primate and mouse models uses antagomirs [96]. Antagomirs are 2’ *O*-methyl phosphorothioate-modified single-stranded RNA oligonucleotides complementary to the

target miRNA and covalently bound to a cholesterol moiety to facilitate cell entry. Antagomir-miR-122 suppressed hepatitis C viremia in primates [97] and antagomir-miR-10b reduced metastatic breast cancer in mice [89]; in both studies, effective silencing was achieved at non-toxic doses.

The expression of miRNA mimics traditionally employ adenoviral- and lentiviral-based systems. While viral systems are efficient, they pose risks such as insertional mutagenesis. Lipid-based nanoparticles are being explored as methods to deliver synthetic miRNA oligonucleotides [93]. Wiggins and colleagues formulated a nanoparticle vehicle composed of a commercially available lipid-based emulsion mixed with synthetic miR-34a, and was able to successfully administer both locally and systemically into a lung cancer mouse model to block tumor growth [98]. Following this technique with slight variations on the lipid complex used, therapeutic replacements of *let-7* and miR-34a in the lung [99], and miR-34a in the prostate [100] have led to persistent tumor reduction in the respective mouse models. Replacement miRNAs and antogmirs are also reported to have the ability to sensitize cancer cells in vitro to various chemotherapeutics, including tamoxifen [101], gefitinib [102], paclitaxel [103], 5-fluorouracil [104], gemcitabine [105], and cisplatin [106].

However, the use of miRNAs in treatment is not without potential problems. First, while it is difficult to direct a miRNA to a specified destination, it is equally challenging to make sure the miRNA does not escape the tumor cell. miRNAs are tissue specific, their role depends on cellular context. For instance, while overexpression of miR143 in pancreatic xenografts reduced tumor growth [107], miR-143 is elevated in hepatocellular carcinoma and anti-miR-143 is required to suppress liver tumor formation [108]. Second, overexpression of miRNAs could saturate components of the silencing machinery; elevated miRNA and siRNA levels led to reduction in exportin 5 and Argonaute 2 expression [109], which could affect proper processing of other unrelated miRNAs.

Although there are no current miRNA clinical trials in humans, therapy in non-human primates are promising. Development of safer methods of expression is necessary as the current strategy relies on adenoviral- and lentiviral-based systems. Future challenges in delivery method include optimizing particles involved in organ targeting, cellular uptake by cancer cells, maintaining controlled release of the miRNA, and crossing tissue barriers (such as the blood-brain barrier to target glioblastomas) [93].

Objectives

The objectives of this dissertation are to examine the mechanistic roles of miRNAs in urothelial tumorigenesis and progression. Different stages and grades of bladder UCs have distinct phenotypic and genotypic signatures. Therefore, accurate profiling of biological determinants, including miRNAs, can improve the molecular classification of heterogeneous UCs. This can translate to a better understanding of tumor initiation and progression, and may improve accuracy in diagnoses and proper supervision of treatments. For this purpose, I have divided my work into two projects as follows.

miRNA expression in bladder urothelium physiology

Our group and others have demonstrated the presence of distinctive cell types in normal bladder urothelium. However, since no definitive urothelial stem cell has been identified the development of the urothelium remains unknown. Given the vast number of differences between UM and B/i cells, we hypothesize that the two cell types may be derived from separate precursor cells. This also introduces the idea that the two pathways of UC initiation (low-grade papillary tumors versus high-grade CIS) may stem from different urothelial progenitor cells.

miRNAs are reported to distinguish tissue samples based on tissue of origin, and tumors based on their respective developmental lineage. The expression of miRNAs has not been examined in UM and B/i cells. The aim of this study is to profile the expression of miRNAs in bladder CIS and distinct cell compartments of the normal bladder, namely UM and B/i urothelial

cells, as well as the stroma (MP). Importantly, we will isolate UM, B/i, and CIS samples using laser capture microdissection (LCM) to ensure pure populations.

The role of miRNAs in bladder urothelial carcinoma progression

High-grade CIS tumors frequently develop to a muscle-invasive phenotype. Low-grade papillary tumors, on the other hand, have high recurrence rates while only a small portion progress to invade the musculature. Muscle invasion and metastasis is associated with very poor prognosis in bladder cancer and the ultimate cause of patient death. There is currently no reliable diagnostic marker for determining whether a papillary tumor will develop into a muscle-invasive disease.

miRNAs are frequently deregulated in tumors, making them attractive candidates for molecular diagnosis and prognosis as biomarkers. To determine whether dysregulation of miRNA expression contributes to muscle-invasion, we propose to compare miRNA expression between various grades and stages of bladder UCs. miRNAs that are significantly differentially expressed between non-muscle invasive and muscle-invasive tumors are worth further experimentation *in vitro*. These mechanistic approaches serve in the discovery of potential targets. As an initial screen, bioinformatics and computational tools will be used to predict downstream targets of candidate miRNAs in an effort to identify biomarkers for molecular classification of UC patients with respect to prognosis.

2. Chapter 2: A common miRNA profile clusters normal bladder urothelium with bladder carcinoma *in situ*

Compartments of normal bladder urothelium: umbrella and basal/ intermediate cells

While it has been proposed that bladder UM cells mature from the underlying B/i cells in a manner similar to epithelial development of the skin, the considerable differences between the two cell types suggests that UM cells may originate from a precursor distinct from B/i cells. UM cells are characterized by the expression of UPKII, low molecular weight cytokeratins, and Lewis X determinant. Conversely, B/i cells display specificity for high molecular weight cytokeratins, p63, and mature A and B blood group antigens.

Our group has reported the presence of an altered bladder urothelium in *p63*$^{-/-}$ mice [110] consisting of a single-cell layer with typical features of UM cells [13,111] (**Figure 2.1, adapted from [110]**). p63 is critical in epithelial development [112], therefore it is unsurprising that the B/i layers are absent in *p63*$^{-/-}$ mice. However, the presence of cells displaying a UM phenotype implies a developmental pathway independent of p63. Furthermore, the Sun group has generated two UPK knock-out mice, *UPKII*$^{-/-}$ and *UPKIII*$^{-/-}$, both of which formed hyperplastic urothelial layers that lacked superficial UM cells (**Figure 2.2, adapted from [113,114]**). Data from these mouse models allude to the concept of two different developmental pathways in the urothelium, where UM and B/i cells develop independently.

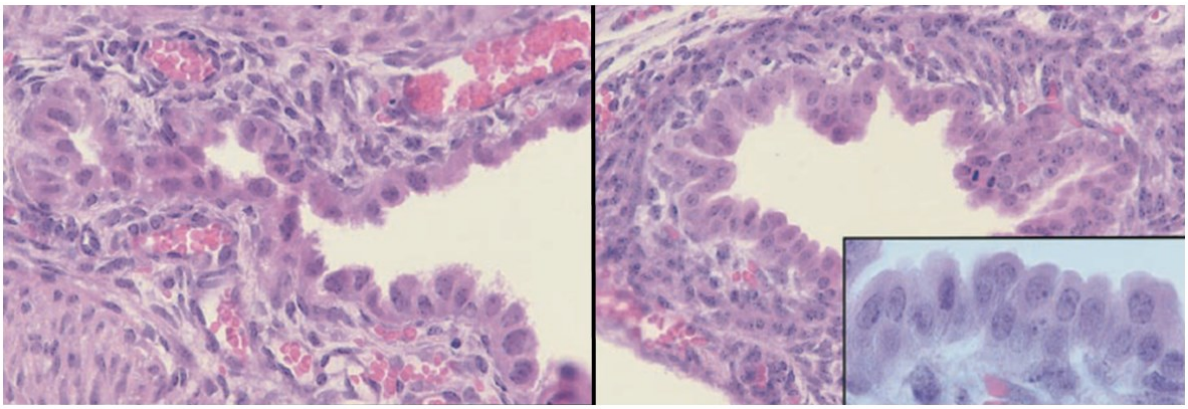

Figure 2.1 *p63*$^{-/-}$ mice develop a single-layer of UM cells

p63$^{-/-}$ mice develop a small bladder that is coated with a single layer of UM cells and no B/i cells. Figure adapted from Urist and colleagues [87].

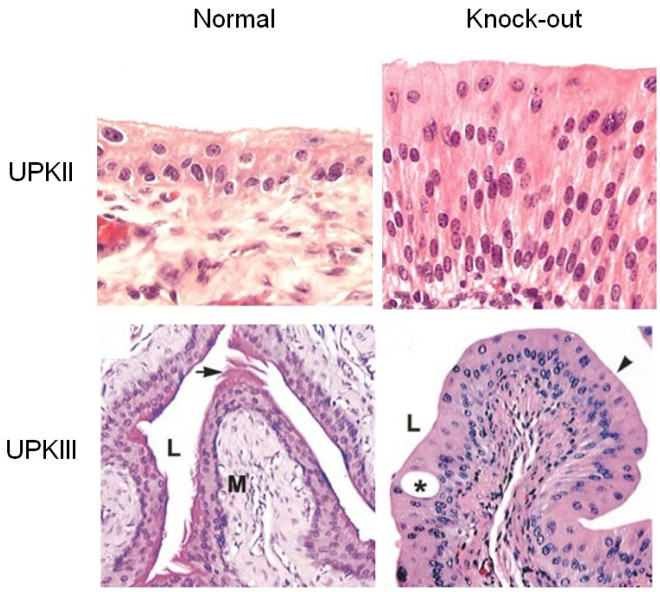

Figure 2.2 *UPKII*$^{-/-}$ and *UPKIII*$^{-/-}$ mice lack a superficial layer of UM cells

The urothelium of *UPKII*$^{-/-}$ and *UPKIII*$^{-/-}$ mice are hyperplastic and characterized by a smooth apical surface (arrowheads) that lack UM cells. L, bladder lumen; M, mesenchyme. UPKII figure adapted from Kong and colleagues [114]; UPKIII figure adapted from Hu and colleagues [113].

CIS is a flat lesion seen in association with up to 90% of high-grade papillary cases and present in 45-65% of all muscle-invasive urothelial tumors [115,116]. Presence of CIS greatly

increases the risk of disease progression to muscle-invasive UC; once the tumor is metastatic, the median survival rate is approximately 7-20 months [16,117]. Histologic and genetic abnormalities of CIS frequently include enlarged nuclei and nucleolus, hyperchromasia and aneuploidy [115]. Given the heterogeneity of bladder tumors, it is possible that the two distinct populations of normal urothelium – UM cells and B/i cells – may give rise to distinct subtypes of bladder tumors. A better characterization of both normal urothelium and bladder cancer cases is therefore needed to delineate the role of these cells in tumorigenesis.

To the best of our knowledge, miRNA profiles of UM and B/i cells have not been previously examined. miRNA expression profiling has been reported to be a powerful tool to classify tissue samples, including cancers, based on their developmental lineage [118]. Several groups have compared miRNA expression between normal mucosa and bladder tumors [119-127], but none has assessed miRNA expression in CIS samples relative to subpopulations of normal urothelium.

Experimental design

In order to elucidate the relationship between populations of the normal urothelium and CIS tumors, we employed LCM to obtain pure UM and B/i cell populations, as well as pure CIS cells. We then profiled the expression of both miRNAs and mRNAs in CIS tumors and three distinct histological areas of the urinary bladder: UM (lumen-facing cells), B/i cells, and muscularis propria (MP, stromal). We identified and verified the expression of several miRNAs differentially expressed between UM and B/i cells. Experimental set-up is depicted in **Figure 2.2**.

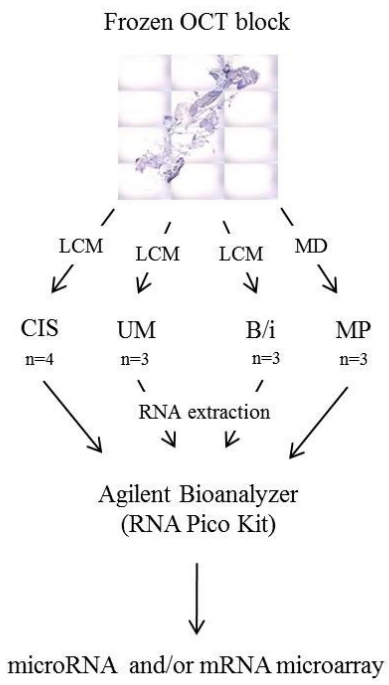

Figure 2.3 LCM experimental design

Microphotograph of frozen tissue section was taken with PALM Microbeam IV Laser Capture Microscope. UM, B/i, and CIS samples were isolated using LCM and analyzed with both miRNA and mRNA microarrays. MP samples were macrodissected (MD) and analyzed only in the miRNA microarray.

Results

1. Isolation of pure populations of urothelium by LCM

As we previously described [13,111], UPKII and CK5 were shown to be differentially expressed in UM versus B/i cells in normal bladder urothelium (**Figure 2.3A**). Membranous expression of UPKII was observed exclusively in the UM layer, while cytoplasmic CK5 expression was specific for the cells in the B/i layers. Three cases of normal bladder samples were used. The urothelium was microdissected to separate UM from B/i cells as explained in the material and methods section (**Figure 2.3B**). The MP population was obtained by removing the urothelium and lamina propria through macrodissection. Quantitative RT-PCR (qRT-PCR)

showed on average an eight-fold decrease in UPKII levels in B/i versus UM, and a two-fold increase in CK5 in B/i versus UM (**Figure 2.3C**). These results demonstrated that the distinct urothelial subpopulations could be efficiently separated by microdissection.

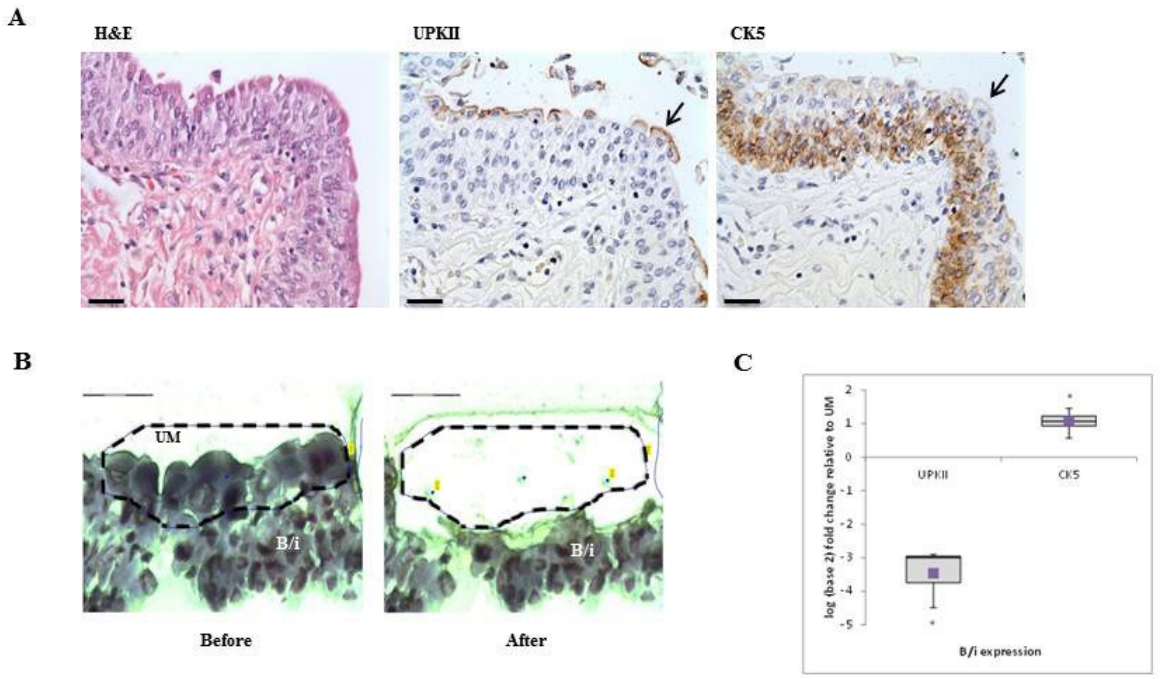

Figure 2.4 Isolation of UM and B/i cells from normal bladder urothelium

(A) Representative immunohistochemical analyses of UPKII and CK5 in normal urothelium; arrows point to prominent UM cells (scalebar, 50 μm). **(B)** Delineation of UM cells, before and after laser capture (scalebar, 75μm). **(C)** qRT-PCR on UM and B/i cells for UPKII and CK5. Graph shows B/i log2 fold expression; B/i expression normalized to UM. Sample median marked with horizontal line. Sample mean marked with square. *p < 0.05 by Student's T-Test.

2. miRNA microarray profiling associates CIS with normal UM cells

Once we had isolated pure populations of urothelial subtypes and stroma, we examined the miRNA expression in these cells, along with four CIS cases and a human urothelium cell line (HUC). Of the 984 human miRNAs evaluated there were 295 miRNAs differentially expressed (fold change ≥ 2) across normal bladder, HUC line, and CIS. Interestingly,

hierarchical cluster analysis of these 295 miRNAs separated samples based on cell type of origin instead of normal versus cancer. Endoderm-derived cells, including the urothelium, CIS, and HUC, clustered into one arm, while mesoderm-derived MP branched into another arm (**Figure 2.4**). Expression of individual samples was averaged into groups, with the exception of the HUC line. Notably, the level of expression of miRNAs in CIS most closely resembled the level observed in normal UM cells, whereas the HUC line shared greater similarity in miRNA expression with B/i cells. So far, analysis of a broad sampling of miRNAs indicates a correlation between UM and CIS cells.

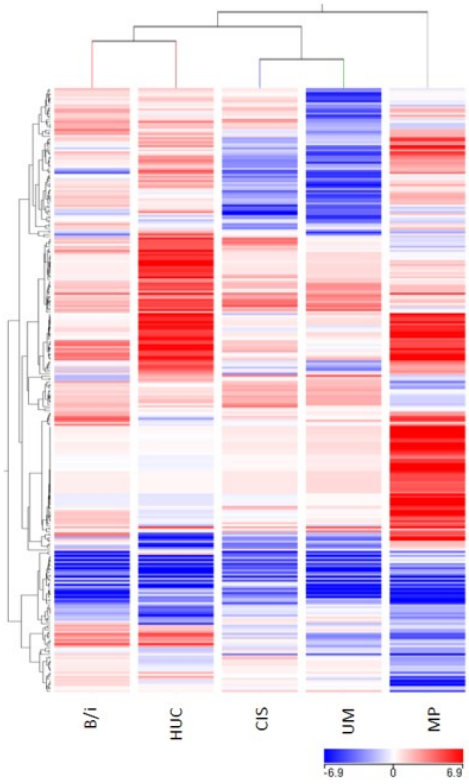

Figure 2.5 Hierarchical clustering of normal urothelium and CIS

Samples are in columns, miRNAs are in rows. Expression of individual samples were averaged into groups, with the exception of HUC, and clustered according to the expression signature of 295 differentially expressed miRNAs ($p \leq 0.05$). One-way ANOVA, Tukey HSD was performed as post-hoc (FDR ≤ 0.05).

We then focused our analyses on the individual miRNA and mRNA profiles of UM, B/i and CIS, since MP is not epithelial in origin and HUC is a cell line. With the removal of MP and HUC, there were 41 miRNAs and 1113 mRNAs differentially expressed across UM, B/i and CIS samples. Hierarchical cluster analysis of individual cases revealed distinct miRNA expression profiles between UM cells and B/i cells, while interestingly, the majority of CIS samples clustered with UM cells (**Figure 2.5A**). From these 41 miRNAs, four (let-7b*, miR-1281, miR-133a, and miR-139-3p) exhibited higher levels of expression in both CIS and UM cells when compared to B/i cells. Conversely, nine miRNAs (miR-142-3p, miR-199b-5p, miR-200a, miR-200b, miR-205, miR-21, miR-27b, miR-424, and miR-491-3p) displayed higher levels of expression in B/i cells than CIS and UM cells. Importantly, only five of the 41 miRNAs were significantly altered between UM and B/i cells (**Table 1**).

MicroRNA	Chromosome	FC (UM vs. B/i)	*p-value*	qRT-PCR verification	ISH verification
hsa-miR-139-3p	11q13.4	2.30	0.006	Yes	Yes
hsa-miR-199b-5p	9q34.11	-4.03	0.024	Yes	Not Detectable
hsa-miR-142-3p	2q35	-3.12	0.030	Yes	Yes
hsa-miR-133a	18q11.2	2.26	0.037	Yes	Yes
hsa-miR-221	Xp11.3	-5.04	0.048	Yes	Not Detectable

Table 1 miRNAs differentially expressed between UM and B/i cells

Statistical results and location of a set of miRNAs significantly differentially expressed between UM and B/i cells in the normal urothelium. FC = fold change. ISH = *in situ* hybridization.

In contrast, based on mRNA expression levels, normal urothelium (UM and B/i) and CIS formed two separate arms (**Figure 2.5B**). From the 1113 mRNAs differently expressed, 23 were commonly down-regulated in UM cells and CIS in comparison to B/i cells, while another 23 followed the opposite trend (**Table 2**). Notably, *TP63*, specific to B/i cells while absent in UM cells, was down-regulated in UM cells and CIS compared to B/i cells. Interestingly, amongst the genes that were up-regulated in UM cells and CIS compared to B/i cells, we found *CD24*, a

proposed marker of tumor-initiating cells (reviewed by Gires [128]), and genes involved in metabolism such as *GFOD2*, *NDUFB2* and *NQO1*.

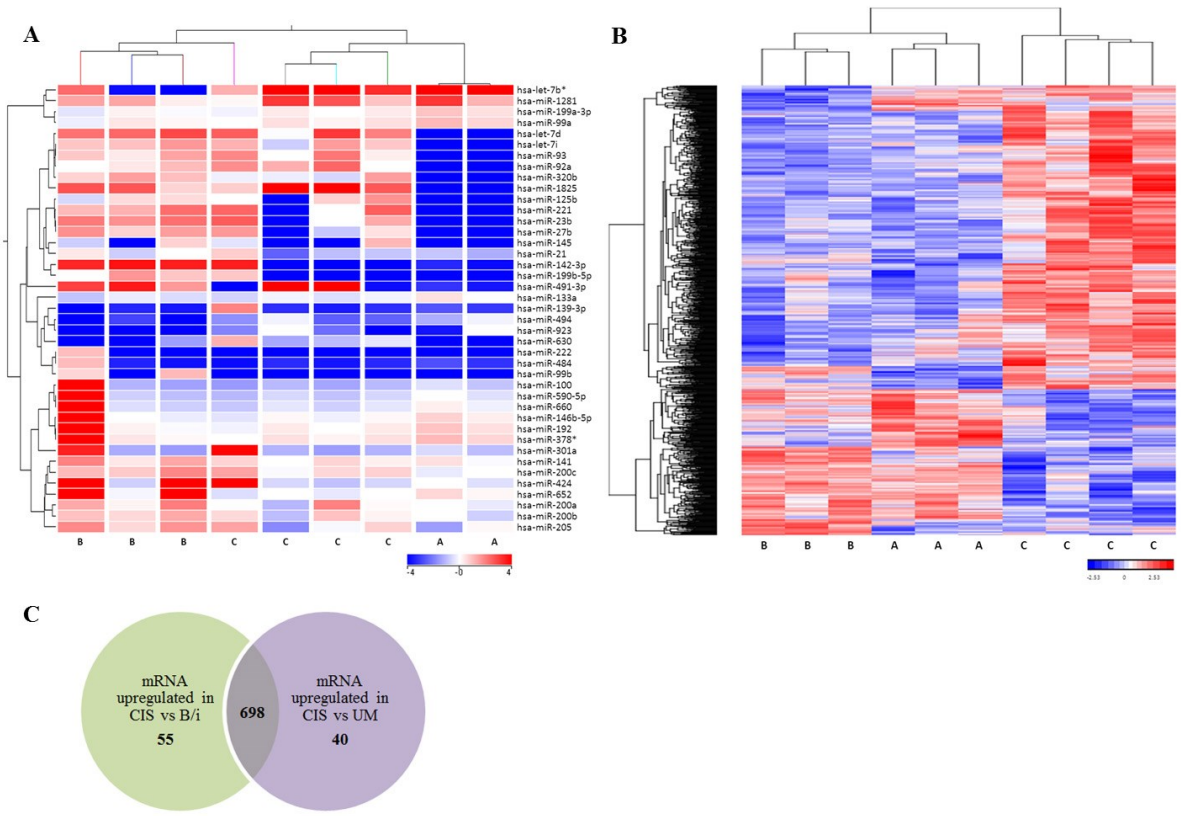

Figure 2.6 . Hierarchical clustering of normal urothelium and CIS

(A) Samples are in columns, miRNAs are in rows. Individual samples of normal urothelium and CIS were clustered according to the expression signature of 41 differentially expressed miRNAs ($p \leq 0.05$). **(B)** Samples are in columns, mRNAs are in rows. Normal urothelium and CIS samples were clustered according to the expression signature of 1113 differentially expressed mRNAs ($p \leq 0.05$). **(C)** Venn diagram illustrating 698 mRNAs up-regulated in common between CIS compared to normal UM and B/i cells. 753 mRNAs up-regulated in CIS compared to B/i cells; 738 mRNAs up-regulated in CIS compared to UM cells. Arbitrary assignment of cluster groups is as follows: A = UM cells, B = B/i cells, C = CIS.

Gene Symbol	Gene Title
Up in CIS and UM vs B/i	
PPP2R1B	protein phosphatase 2, regulatory subunit A, beta
TMED3	transmembrane emp24 protein transport domain containing 3
BMP8B	bone morphogenetic protein 8b
CFL1	cofilin 1 (non-muscle)
CD24	CD24 molecule
SHANK1	SH3 and multiple ankyrin repeat domains 1
HIST3H2A	histone cluster 3, H2a
RCAN1	regulator of calcineurin 1
NQO1	NAD(P)H dehydrogenase, quinone 1
SLC35A2	solute carrier family 35 (UDP-galactose transporter), member A2
GFOD2	glucose-fructose oxidoreductase domain containing 2
SND1	staphylococcal nuclease and tudor domain containing 1
CD80	CD80 molecule
CRAT	carnitine O-acetyltransferase
KCTD17	potassium channel tetramerisation domain containing 17
EN1	engrailed homeobox 1
PPAP2B	phosphatidic acid phosphatase type 2B
PDLIM2	PDZ and LIM domain 2 (mystique)
SEC24A	SEC24 family, member A (S. cerevisiae)
NDUFB2	NADH dehydrogenase (ubiquinone) 1 beta subcomplex, 2, 8kDa
TBCD	tubulin folding cofactor D
SLCO1C1	solute carrier organic anion transporter family, member 1C1
DLG3	discs, large homolog 3 (Drosophila)
Down in CIS and UM vs B/i	
CRLF3	cytokine receptor-like factor 3
ELP3	elongation protein 3 homolog (S. cerevisiae)
FZD6	frizzled homolog 6 (Drosophila)
SRSF11	serine/arginine-rich splicing factor 11
RBM26	RNA binding motif protein 26
ZNF571	zinc finger protein 571
TNFRSF11A	tumor necrosis factor receptor superfamily, member 11a, NFKB activator
SLC25A36	solute carrier family 25, member 36
DCAF8	DDB1 and CUL4 associated factor 8
PLP1	proteolipid protein 1
C5orf42	chromosome 5 open reading frame 42
HNRNPL	heterogeneous nuclear ribonucleoprotein L
ZNF302	zinc finger protein 302
MGEA5	meningioma expressed antigen 5 (hyaluronidase)
LOC100506168	hypothetical LOC100506168
ACVR1B	activin A receptor, type IB
NCOR1	nuclear receptor corepressor 1
TP63	tumor protein p63
EIF3M	eukaryotic translation initiation factor 3, subunit M
FUBP1	Far upstream element (FUSE) binding protein 1
PCGF3	polycomb group ring finger 3
GUCY1A2	guanylate cyclase 1, soluble, alpha 2
FAM149B1	family with sequence similarity 149, member B1

Table 2 Statistically significant genes altered between UM cells and CIS versus B/i cells

In fact, more than half of the differentially expressed mRNAs (698) were up-regulated in CIS compared to UM and B/i samples (**Figure 2.5C**). Gene ontology (GO) enrichment was performed on the 698 mRNAs to investigate biologically driven effects. This analysis revealed 74 biological processes with enrichment scores > 3 ($p \leq 0.05$), and as expected, the top seven ($p \leq 0.005$) are involved in genomic alterations, transcription regulation, and cell cycle (**Table 3**). We further examined differentially expressed pathways in the group of 698 mRNAs up-regulated in CIS using Pathway ANOVA (Partek Genomics 6.6). Statistically significant pathways with more than 10 genes involved include “metabolic pathways” and “pathways in cancer” (**Table 4**). Not surprisingly, the “bladder cancer” pathway was enriched (enrichment score 3.2) in this list (**Table 5**). As supported by GO analysis, hierarchical clustering by global gene expression separated samples based on normal (UM and B/i) versus cancer (CIS).

GO Function	E-score	*p-value*	% genes involved
rRNA transcription	7.60	0.0005	44.44
M phase of mitotic cell cycle	6.31	0.0018	13.10
pre-miRNA processing	6.30	0.0018	50.00
steroid hormone receptor signaling pathway	6.02	0.0024	30.77
chromatin modification	5.53	0.0040	9.60
regulation of primary metabolic process	5.44	0.0043	26.67

Table 3 GO enrichment of genes up-regulated in CIS

Biological processes with enrichment p ≤ 0.005 are shown.

Pathway Name	# of genes involved	*p-value*
Metabolic pathways	81	9.973E-05
Pathways in cancer	25	1.252E-02
HTLV-I infection	17	5.478E-04
Phagosome	16	8.687E-04
Cell cycle	15	6.688E-04
Protein processing in endoplasmic reticulum	14	4.469E-04
Systemic lupus erythematosus	13	9.570E-04
Focal adhesion	13	5.897E-02
Herpes simplex infection	12	1.979E-03
Ubiquitin mediated proteolysis	11	3.587E-04
Cell adhesion molecules (CAMs)	11	3.143E-04
Tuberculosis	11	5.594E-04
Dopaminergic synapse	11	5.298E-04
Neurotrophin signaling pathway	11	3.166E-03
Huntington's disease	10	4.607E-08
Oocyte meiosis	10	7.928E-05
Fc gamma R-mediated phagocytosis	10	4.341E-05
Lysosome	10	1.410E-04
Vascular smooth muscle contraction	10	2.680E-02
Hepatitis C	10	9.471E-04

Table 4 Statistically significant pathways in up-regulated genes in CIS

Statistically significant pathways that involve more than 10 genes in the set of 698 mRNAs that are up-regulated in CIS.

Pathway Name	E-score	*p-value*	% of genes involved
Cell cycle	5.24	0.0053	10.43
Steroid biosynthesis	5.11	0.0060	23.53
Mineral absorption	4.55	0.0106	14.29
Phagosome	4.38	0.0125	9.03
Systemic lupus erythematosus	3.98	0.0188	9.17
Herpes simplex infection	3.71	0.0245	8.05
Pathogenic Escherichia coli infection	3.48	0.0307	11.32
Alanine, aspartate and glutamate metabolism	3.35	0.0352	14.29
Rheumatoid arthritis	3.25	0.0389	9.30
Fanconi anemia pathway	3.24	0.0390	11.90
Bladder cancer	3.24	0.0390	11.90
Asthma	3.12	0.0440	13.33

Table 5 Pathways enriched in up-regulated genes in CIS

Pathway enrichment of statistically significant pathways composed of genes up-regulated in CIS.

3. Five miRNAs are differentially expressed between UM and B/i cells

Having examined miRNA and mRNA profiles globally in both normal urothelium and in CIS cases, we then decided to further explore the five miRNAs that were statistically differentially expressed between UM cells and B/i cells (**Table 1**), according to the microarray data. We performed qRT-PCR to determine the expression of the mature form of these five miRNAs (**Figure 2.6A**). qRT-PCR results showed an average Pearson correlation to the microarray data of 0.95. miR-133a and miR-139-3p were up-regulated in UM cells compared to B/i cells, while miR-142-3p, miR-199b-5p, and miR-221 were down-regulated in UM cells compared to B/i cells. Taken together, the qRT-PCR results confirmed that these five miRNAs were differentially expressed between UM and B/i cell populations.

We then went on to verify the localization of our miRNAs of interest via *in situ* hybridization. We used LNA oligonucleotide probes for detection of the miRNAs of interest in human and mouse bladders. Positive control using U6 gave strong signals in human and mouse urothelium, while no signal was detected using a non-specific probe for the miR-424/503 cluster

(**Figure 2.6B)**. Robust *in situ* hybridization conditions were established for three out of these five miRNAs. Expression of miR-133a and miR-139-3p was observed in UM cells, while miR-142-3p expression was localized to B/i cells with low expression in UM cells. In order to further validate the phenotypes described for human urothelial tissues, we extended the study to the analysis of mouse urothelium. We observed that the miRNA phenotypes of both human and murine bladder samples were consistent (**Figure 2.6C**).

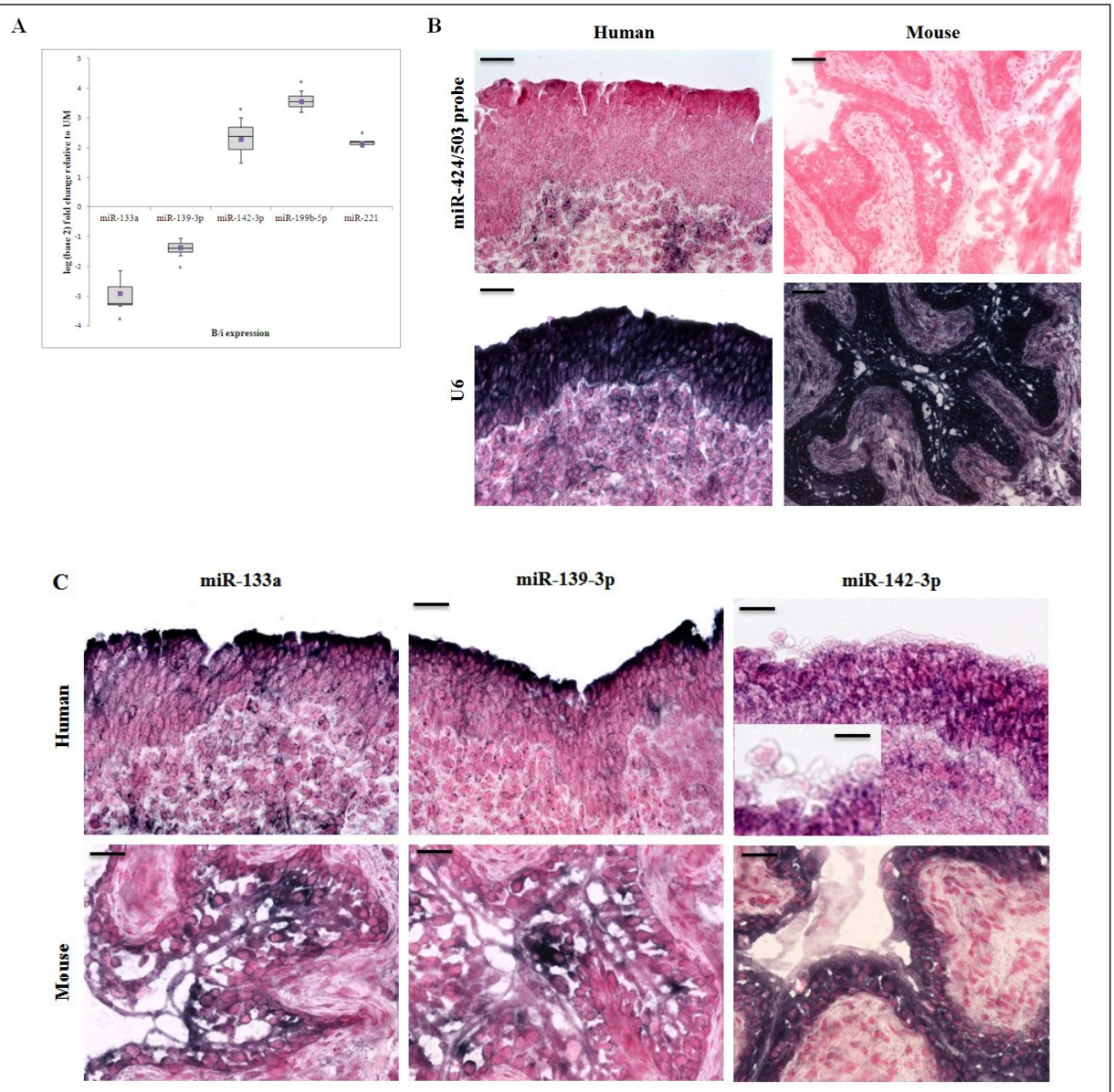

Figure 2.7 Validation of differentially expressed miRNAs from microarray data

(A) qRT-PCR on UM and B/i cells for various miRNAs. Graph shows B/i $\log_2$ fold expression; B/i expression is normalized to UM. Sample median marked with horizontal line. Sample mean marked with square. *$p \leq 0.05$ by Student's T-Test. **(B)** Localization of miR-133a, miR-139-3p, and miR-142-3p in human bladder samples by *in situ* hybridization (scalebar, 100μm). Inset for miR-142-3p shows umbrella cells (scalebar, 25μm). No staining was observed in a negative control ISH using the sense strand of miR-424/503, while a strong signal was observed in a positive control ISH using U6 in representative cases of normal bladder (scalebar, 100μm).

4. CIS samples express UM but not B/i urotehlium specific protein markers

To explore further whether CIS samples were more closely related to UM cells than B/i cells, as suggested by the miRNA microarray results, we examined the expression of miRNAs specific to UM cells in CIS. Compared to B/i cells, expression of the five miRNAs by qRT-PCR in six independent CIS biopsies were similar to that of UM cells. miR-133a and miR-139-3p were up-regulated in CIS compared to B/i, while miR-142-3p, miR-199b-5p, and miR-221 were down-regulated in CIS compared to B/i (**Figure 2.7A**).

Since miRNA expression revealed a correlation between CIS and UM cells, we decided to assess the expression of several well-established differentiation biomarkers of the urothelium in a cohort of CIS lesions. We have previously reported that B/i cells to be positive for high molecular weight cytokeratins (HMWCKs), while UM cells are characterized by low molecular weight cytokeratins and UPKII [13,111]. Indeed, a high percentage of CIS lesions revealed a positive UPKII (83.3%) and CK20 (84.2%) phenotype similar to that of UM cells, as well as a negative HMWCKs phenotype (only 10.5% of the cases expressed HMWCKs) (**Figure 2.7B, C**). **Table 6** summarizes the individual immunohistochemical profiles of the 19 CIS tissue samples.

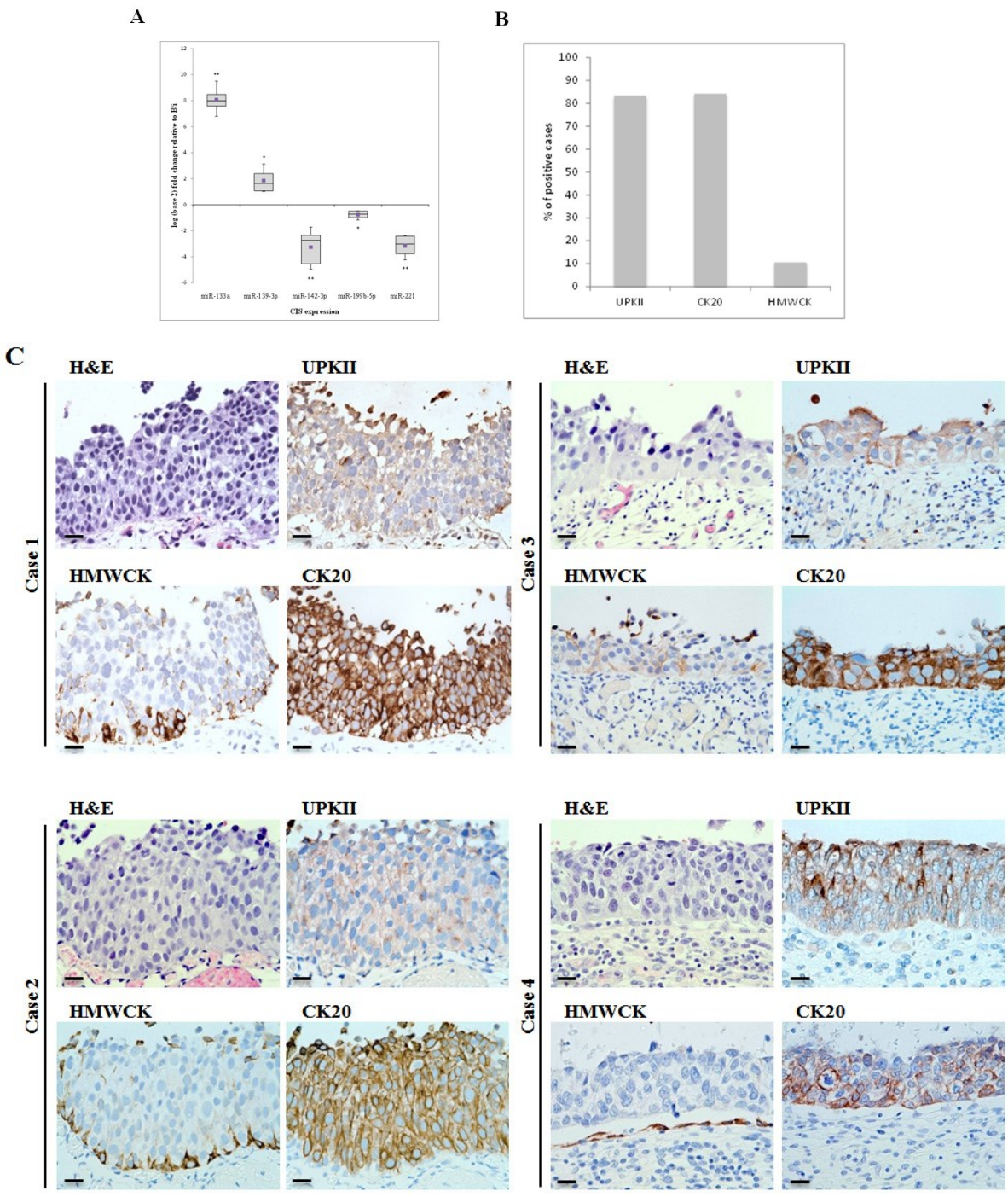

Figure 2.8 Phenotypic association of CIS with UM cells by qRT-PCR and IHC

(A) qRT-PCR results on B/i and CIS samples for various miRNAs. Graph shows CIS $\log_2$ fold expression; CIS expression is normalized to B/i. Sample median marked with horizontal line. Sample mean marked with square. $p \leq 0.05$, $^{**}p \leq 0.005$ by Student's T-Test. **(B)** Quantification of the percentage of cases with expression of the respective biomarkers. **(C)** Representative immunohistochemical analyses of UPKII, CK20, and HMWCKs in four different CIS tissue samples (scalebar, 100μm).

Case #	UPKII	CK20	HMWCK
1	-	+	-
2	+	+	-
3	+	+	-
4	+	+	+
5	+	+	-
6	+	+	-
7	+	+	-
8	+	-	-
9	-	-	-
10	+	+	-
11	+	+	-
12	+	+	-
13	-	+	-
14	NA	+	-
15	+	+	-
16	+	+	+
17	+	+	-
18	+	+	-
19	+	-	-
% positive	**83.3**	**84.2**	**10.5**

Table 6 Summary of IHC results in individual CIS tissue samples

NA: core not available

Discussion

To date, there have not been any studies examining miRNA expression within normal bladder urothelium and bladder CIS. Despite a limited number of samples, our study reveals that the phenotype of CIS most closely resembles that of UM cells, rather than B/i cells.

A novel approach undertaken in this study is the microanatomical isolation of normal bladder into three compartments: UM cells, B/i cells, and MP tissue. Thus far there is no consensus and there are several inconsistencies between different microarray studies for the majority of miRNAs reported as mis-expressed. For instance, Lin *et al*. reported miR-125b and miR-199b to be significantly down-regulated in tumors compared to normal tissue [126], while Veerla *et al.* reported high expression of the same two miRNAs in invasive (T2/T3) tumors [129]. One explanation for this discrepancy is that different populations of normal bladder tissue were

used. It is extremely difficult to obtain pure urothelium by macrodissection, as this method often leads to contamination of the urothelial sample with the lamina propria. Furthermore, while some groups use normal bladder mucosa [122,123,125], others use normal tissue adjacent to the tumor [126,127], which can include non-urothelium components such as the muscularis propria. Therefore, microdissection is necessary to ensure clean urothelial samples, and is the only method to dissect single-layer UM cells.

We profiled the expression of 984 human miRNA and 22,277 human mRNA genes in the sub-populations of normal bladder, CIS tumors, and a normal urothelial cell line (HUC). Surprisingly, miRNA expression profile revealed CIS tumors to share a molecular profile displayed by UM cells, while mRNA expression profile clustered B/i and UM cells together and separate from CIS. These data suggest that gene expression analysis is able to separate normal from tumor tissues. In fact, more than half of the differentially expressed genes that were up-regulated in CIS when compared to normal UM and B/i cells were related with proliferative phenotypes (e.g. cell cycle, metabolic pathways and pathways in cancer). In contrast, miRNA expression has been shown to classify tissue samples based on histogenesis [118], and our data show that CIS samples share more similarity with UM cells than B/i cells in the normal urothelium.

There were five miRNAs that were significantly altered between B/i and UM cells. qRT-PCR and *in situ* hybridization confirmed miR-133a and miR-139-3p to be specific to UM cells, while miR-142-3p was expressed only in B/i cells. Interestingly, the two UM cell specific miRNAs, miR-133a and miR-139-3p, are located on chromosome 18q and 11q, respectively. It is well known that deletions of chromosomes 18 and 11 are associated with invasive bladder carcinomas [40], which mainly arise from high-grade lesions such as CIS. Conversely, B/i specific miR-199b-5p is located on chromosome 9q, the deletion of which is associated almost exclusively with papillary, non-muscle invasive tumors [16,130]. It is plausible that deletion of these miRNAs may affect downstream targets involved in bladder tumorigenesis.

It is well accepted that there are two paths of bladder tumor progression [16,131-133]. The development of papillary, non-muscle invasive tumors is largely independent from that of CIS lesions, as demonstrated through transgenic mouse models [31,38,134]. While bladder-specific expression of mutant *HRAS* led to growth of papillary tumors [31], simultaneous deletion of tumor suppressors *p53* and *Pten* gave rise to CIS with progression to muscle-invasive tumors and metastasis [38]. Furthermore, the double inactivation of *p53* and *Rb* through UPKII-driven expression of SV40T also led to the development of CIS and high-grade muscle-invasive tumors [134], Although a clonal origin of bladder cancer has been suggested [135], the study did not include CIS tumors in the analyses. Therefore, it remains unclear whether oncogenic changes that give rise to two phenotypic variants occur within one cell, or arise in different progenitors (UM versus B/i). Our current study identifies a strong association between CIS and UM cells in miRNA expression and expression of a few well-established differentiation markers of the UM cell, and provides evidence of the possible relationship between the two.

Materials and Methods

Cell culture

The immortalized normal urothelial cell line, Human Urothelial Cell (HUC) from ScienCell Research Laboratories (Carlsbad, CA), was grown in Urothelial Cell Medium (ScienCell) at 37˚C in a humidified air atmosphere at 5% CO_2. RNA was extracted from the cells using the miRVANA Kit (Ambion, Foster City, CA).

Laser capture microdissection (LCM) of normal bladder urothelium and CIS biopsies

Human normal (n=3) and tumor bladder (CIS, n=4) tissue samples were obtained through IRB approved protocols. The three normal bladders were obtained from organ donors (males, ages 15, 25 and 28 years old) with no history of bladder cancer through the International Institute for the Advancement of Medicine (IIAM). Fresh tissues were processed and frozen in OCT molds, which were used for laser capture microdissection. CIS samples were obtained from patients who had undergone radical cystectomy for an invasive urothelial carcinoma, and sections that did not include the invasive area were chosen for further processing. Frozen normal bladder urothelium was microdissected to obtain pure populations of UM cells, B/i cells, and muscularis propria (MP). Frozen CIS samples were also microdissected to obtain pure populations of tumor cells. To rule out the possibility of normal urothelial cell contamination in CIS samples, only cases where the CIS lesion permeated the whole thickness of the epithelium were chosen. Cases in which we could histologically identify UM or B/i cells surrounding the malignant cells by H&E stain, and cases with pagetoid spread or denuded CIS were not used. Briefly, 20-µm sections from OCT blocks were cut and mounted on MembraneSlide NF 1.0 PEN (Zeiss, Munich, Germany) and stored at -80˚C until use. Slides were fixed in ethanol at -20˚C for 2 min, washed in DEPC-H_2O, stained with hematoxylin for 1 min, washed in DEPC-H_2O, and air-dried. PALM Microbeam IV Laser Capture Microscope was used to perform laser microdissection. A

total of 25 sections (20-µm) were prepared from each sample, where the microdissected tissue was pooled per patient to extract RNA. Formalin-fixed paraffin-embedded (FFPE) CIS samples (n=6) were macrodissected by scratching 40 sections (10-µm), where dissected tissue was pooled per patient.

RNA extraction and Microarray profiling and data analysis

RNA was extracted from microdissected samples using RNAquesous®-Micro Kit (Ambion, Carlsbag, CA). RNA was extracted using RecoverAll™ Total Nucleic Acid Isolation Kit for FFPE (Ambion) for macrodissected samples. The quality of all RNA samples was verified using a RNA Pico Kit (Agilent, Santa Carla, CA). Only sample qualities with RNA Integrity Number (RIN) > 6.0 with clean 18S and 28S peaks were used, as previously described [136].

Agilent Human miRNA Microarray (V3, based on Sanger miRbase release 12.0) were used for measuring miRNA expression in bladder samples. Samples used for the Agilent miRNA microarray were labeled as described by the manufacturer.

Affymetrix Human U133 Plus 2.0 arrays were used for measuring gene expression in bladder samples. Samples used for Affymetrix microarray were amplified using the Ovation RNA Amplification System (NuGEN, San Carlos, CA) and labeled using FL-Ovation cDNA Biotin Module V2 (NuGEN) following manufacturer's protocol. Raw intensity miRNA data were normalized and median transformed using GeneSpring GX 12 (Agilent). The raw mRNA data were log transformed and analyzed using Partek Genomics Suite 6.6 (Partek, Saint Louis, MO). Only detected probesets were used, compromised or undetected probesets were filtered out. One-way ANOVA and Tukey's honestly significant difference (HSD) post-hoc test were performed across all samples to obtain miRNAs or mRNAs differentially expressed ($p < 0.05$). Unsupervised hierarchical cluster analysis was performed on the list of differentially expressed probesets with a fold change ≥ 2 (295 miRNAs, 1113 mRNAs).

Quantitative reverse transcription-PCR (qRT-PCR) miRNA expression profiling

TaqMan microRNA Reverse Transcription Kit (Applied Biosystems, Foster City, CA) was used to convert miRNA to cDNA. Reverse transcription primers (44-nucleotide) were designed so that the first 36-nucleotide formed an internal stem loop and the last 8-nucleotide were complementary to the mature miRNA sequence of interest. A universal reverse primer was used: 5' GTGTCGTGGAGTCGGC 3'. Qiagen Reverse Transcriptase System (Qiagen, Valencia, CA) was used to produce cDNA from mRNA. The following primers were used to reverse transcribe miRNAs from **Table 1.**

miRNA	**Forward primer**
miR-139-3p	5' CTCAACTGGTGTCGTGGAGTCGGCAATTCAGTTGAGACTCCAAC 3'
miR-199b-5p	5' CTCAACTGGTGTCGTGGAGTCGGCAATTCAGTTGAGGAACAGAT 3'
miR-142-3p	5' CTCAACTGGTGTCGTGGAGTCGGCAATTCAGTTGAGTCCATAAA 3'
miR-133a	5' CTCAACTGGTGTCGTGGAGTCGGCAATTCAGTTGAGCAGCTGGT 3'
miR-221	5'CTCAACTGGTGTCGTGGAGTCGGCAATTCAGTTGAGGAAACCCA 3'

Qiagen QuantiTect PCR (Qiagen) was used to measure quantitative expression of miRNA and mRNA. PCR assays were performed as described by the manufacturer using a Stratagene MX3005P PCR system (Agilent). For normalization, we used *RNU6B* or *ACTIN* for miRNA and mRNA respectively.

Immunohistochemical (IHC) detection of biomarkers

Immunohistochemical analyses were conducted on formalin-fixed and paraffin-embedded (FFPE) tissue sections from 10 cases of normal human bladder, and 19 CIS specimens following the standard avidin-biotin protocol. The 10 cases of normal bladder included the three cases used for the laser microdissection (organ donors) and seven cases of histologically normal urothelium obtained from patients who had undergone a radical cystectomy for an invasive carcinoma. From the 19 CIS specimens, 10 corresponded to biopsies of patients with

primary CIS and the other nine were obtained from cystectomy specimens of patients with a diagnosis of invasive bladder cancer. Briefly, 5-μm sections were deparaffinized and submitted to antigen retrieval by steamer treatment for 15 min in 10 mM citrate buffer at pH 6.0. Subsequently, slides were incubated in 10% normal serum for 30 min, followed by primary antibody incubation overnight at 4˚C. Primary antibodies used were anti-UPKII goat polyclonal (Santa Cruz, Dallas, TX), anti-CK5 rabbit polyclonal (AF138, Covance), anti-CK20 mouse monoclonal (clone Ks20.8, DAKO, Carpinteria, CA) and anti-high molecular weight cytokeratin mouse monoclonal (clone 34βE12, DAKO). Then slides were incubated with biotinylated immunoglobulins at a 1:500 dilution for 30 min (Vector Laboratories, Inc, Burlingame, CA.) followed by avidin-biotin peroxidase complexes at a 1:25 dilution (Vector Laboratories, Inc.) for 30 min. Diaminobenzidine was used as chromogen and Hematoxylin as the nuclear counterstain. Slides were analyzed with a Nikon Eclipse 50i microscope equipped with a SPOT Insight™2MP Mosaic camera and SPOT™ Advanced software (Diagnostic Instruments, Sterling Heights, MI).

In situ detection of miRNAs

In situ detection of miRNAs was performed on 10-μm frozen tissue sections from normal human bladders obtained from healthy donor patients (n=3) and B6-wt mouse bladders (n=15). Sections were fixed in 4% paraformaldehyde, acetylated, and prehybridized in hybridization solution (50% formamide, 5X SSC, 0.5mg/ml yeast tRNA, 1X Denhardt's solution) for 3h at 25°C below the predicted T_m of the probe. Probe (5pmol; LNA-modified and FITC-labeled oligonucleotide; Exiqon, Woburn, MA) complementary to U6 (positive control), miR-133a, miR-139-3p, and miR-142-3p was hybridized to the sections overnight in a humidified chamber at pre-hybridization temperature. Posthybridization, slides were washed with 5X and 0.2X SSC, blocked in 10% normal goat serum for 30 min, and incubated in anti-FITC/alkaline-phosphatase antibody (Vector-Labs) at 1:400 at 4°C overnight. The sense-strand of the primary transcript of

the miR-424/503 cluster (5pmol; sequence in table below) was used as negative control. *In situ* hybridization signals were detected using BM purple (Roche, Indianapolis, IN). Slides were counterstained with Nuclear Fast Red (Sigma-Aldrich, Saint Louis, MO), mounted using 80% glycerol, and analyzed with a Nikon Eclipse 50i microscope equipped with a SPOT Insight™2MP Mosaic camera and SPOT™ Advanced software (Diagnostic Instruments).

miR-424/503 probe sequence	**Hybridization temperature**
GGGCAGTCAACGACATTTTTCTCCATTAATCCCAAAGTCAGTGT AAAAGTTGTTTGTAAATATCATTGCCAAAACAAGATGGAATGTAG AGATACTTGATTGTCGCAATTTAGGGAATGGGGTTATTGTTACTA ATGACTTTTTTTTTTTTACCATGACATAGTGTATTTGTTACCACTGG ATCTCAGTCTGGATGTTATAAATTCGATACTTAATCTTATTAAATA CTCTGCACATTTTATTAACTAATAAATAGGACACTTAACATTCATT GTACTGGTTTTGAAAAACCGACTTAATTTGTAAGTGTAACAAGAT ACTTACAGTTGGATAATTT	65˚C

3. Chapter 3: Invasive bladder urothelial carcinoma is characterized by distinct miRNA expression

Invasive bladder UC

At tumor initiation, bladder tumors can be classified into two groups: low-grade papillary tumors; and high-grade tumors (either papillary or non-papillary). Tumor cell invasion and metastasis in bladder cancer is a primary cause of patient mortality. Patients with unresectable metastatic bladder cancer have a median survival of 7-20 months despite systemic chemotherapy, while the 5-year survival rate is just 5.5% [137]. However, little is known regarding the transition from “superficial” papillary tumors to muscle-invasive tumors.

Changes in the tumor microenvironment that promote invasion and metastasis include loss of E-cadherin expression [138], increased levels of matrix metalloproteinases [139], and increased expression of angiogenic factors [140]. Chromosomal alterations that favor the transformation of non-muscle invasive high-grade tumors to muscle-invasive UCs have been identified in comparative genomic hybridization studies [141], although the specific genes have yet to be mapped. In addition, the genetic processes that promote the progression of low-grade superficial UCs to a muscle-invasive phenotype are unknown. Investigating miRNAs can improve the molecular classification of these heterogeneous tumors, which may translate to more effective and tailored treatments.

Experimental Design

The aim of this study is to identify miRNAs differentially expressed between non-muscle invasive and muscle-invasive UCs, and characterize their subsequent downstream targets. We profiled miRNA and mRNA expression on a repertoire of 22 bladder tumors: CIS (n=4), TaG1 (n=3), TaG2 (n=3), T1G1 (n=3), T1G2/3 (n=3), T2G2/3 (n=6). miRNAs differentially expressed

between non-muscle invasive Ta and muscle-invasive T2 tumors were selected for further study. Stable bladder cancer cell lines were generated to overexpress miRNAs potentially involved in tumor cell invasion. Transwell invasion assays were employed to quantitate invasive effects of candidate miRNAs.

Results

1. miRNAs and mRNAs clustered tumors based on tumor stage

There were 150 miRNAs differentially expressed (fold change ≥ 2) across 22 tumor samples (**Figure 3.1A**). Unsupervised hierarchical clustering grouped the tumors based on tumor stage. Interestingly, CIS tumors formed a separate branch from the rest instead of clustering with invasive tumors. 72 miRNAs were differentially expressed (fold change ≥ 2.5) between Ta and T2 tumors (**Table 7**); 31 miRNAs were up-regulated in T2 tumors, while 41 miRNAs were up-regulated in Ta tumors. qRT-PCR was performed on the 72 miRNAs in seven bladder cancer cell lines: HUC (normal primary urothelial cells), three non-invasive cell lines (BFTC-905, RT4, RT112), and three invasive cell lines (TCCSUP, J82, and EJ138). Of the 72, five miRNAs had a fold change > 10 according to qRT-PCR. The five miRNAs were: miR-200c, miR-141, miR-429, miR-126, and miR-198 (**Figure 3.2**). With the exception of miR-198 that had the opposite trend, the four other miRNAs were expressed at higher levels in non-invasive cells than invasive cells.

Similar to the miRNA profile, the cohort of 1493 differentially expressed mRNAs also clustered tumors based on stage (**Figure 3.1B**). 17 tumors were used instead of the original 22; five tumor samples were excluded from mRNA microarray analysis due to tissue scarcity. This set of genes will be used to identify downstream targets of candidate miRNAs using TargetScan.

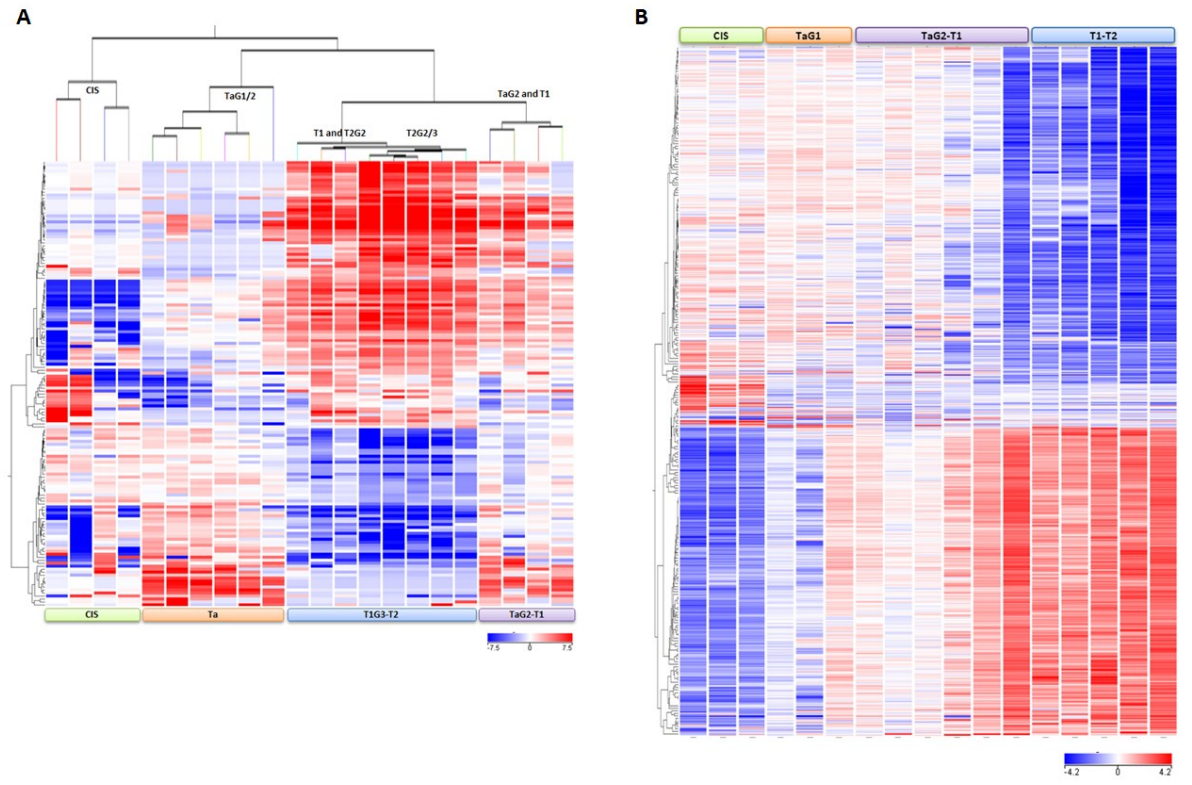

Figure 3.1 miRNA and mRNA expression profiles in non-muscle invasive and muscle-invasive bladder UCs

(A) Samples are in columns, miRNAs are in rows. Samples were clustered according to the expression signature of 150 differentially expressed miRNAs ($p \leq 0.05$). **(B)** Samples are in columns, mRNAs are in rows. Samples were clustered according to the expression signature of 1493 differentially expressed mRNAs ($p \leq 0.05$).

microRNA	*p-value*	FC (NMI vs. MI) microarray	microRNA	*p-value*	FC (NMI vs. MI) microarray
hsa-miR-148a	3.48E-03	8.09	hsa-miR-338-3p	3.18E-03	2.97
hsa-miR-10a	8.06E-04	7.81	hsa-miR-200c	4.03E-03	2.91
hsa-miR-29c	1.97E-04	7.79	hsa-miR-425	2.71E-03	2.83
hsa-miR-31*	3.99E-03	6.83	hsa-let-7i	2.81E-03	2.79
hsa-miR-26b	2.25E-03	6.65	hsa-miR-664*	1.34E-03	2.53
hsa-miR-195	3.29E-04	6.43	hsa-miR-296-5p	6.07E-04	-2.65
hsa-miR-29b	4.79E-04	6.10	hsa-miR-518c*	2.81E-03	-2.67
hsa-let-7g	1.32E-03	5.81	hsa-miR-422a	3.63E-03	-2.75
hsa-miR-140-5p	8.85E-04	5.71	hsa-miR-1236	2.81E-03	-2.75
hsa-let-7f	2.16E-03	5.65	hsa-miR-1225-5p	1.96E-03	-2.79
hsa-let-7a	1.63E-03	5.64	hsa-miR-1228	5.83E-04	-2.79
hsa-miR-15a	1.46E-03	5.41	hsa-miR-18b*	1.19E-03	-2.84
hsa-miR-98	1.28E-03	5.09	hsa-miR-133a	2.13E-03	-2.89
hsa-miR-497	5.99E-04	4.70	hsa-miR-1249	6.29E-04	-2.90
hsa-let-7d	3.15E-03	4.65	hsa-miR-526b	2.69E-03	-2.90
hsa-let-7c	4.07E-03	4.52	hsa-miR-933	1.23E-03	-2.92
hsa-miR-29c*	7.42E-05	4.47	hsa-miR-30c-1*	4.14E-03	-2.93
hsa-miR-150	2.32E-03	4.47	hsa-miR-767-3p	1.89E-04	-3.15
hsa-miR-200a	1.36E-04	4.43	hsa-miR-877	6.10E-04	-3.19
hsa-miR-140-3p	1.75E-03	4.40	hsa-miR-516b	1.97E-03	-3.22
hsa-miR-30c	2.29E-04	4.38	hsa-miR-1207-5p	3.62E-03	-3.26
hsa-miR-28-5p	1.92E-03	4.12	hsa-miR-432	4.65E-03	-3.36
hsa-miR-582-5p	3.39E-03	4.02	hsa-miR-150*	5.19E-04	-3.43
hsa-miR-374b	3.61E-03	4.02	hsa-miR-659	8.81E-04	-3.44
hsa-miR-16	1.39E-03	3.95	hsa-miR-320c	3.09E-03	-3.45
hsa-miR-30e*	3.48E-03	3.86	hsa-miR-601	6.60E-04	-3.56
hsa-miR-200b	4.51E-04	3.80	hsa-miR-92b	7.19E-04	-3.59
hsa-miR-26a	1.33E-03	3.77	hsa-miR-188-5p	6.72E-04	-3.63
hsa-miR-34b*	4.03E-03	3.74	hsa-miR-1243	1.44E-03	-3.68
hsa-miR-141	2.18E-03	3.70	hsa-miR-193a-5p	4.27E-03	-3.99
hsa-miR-126	2.75E-04	3.67	hsa-miR-339-3p	8.39E-04	-4.02
hsa-miR-429	7.74E-04	3.61	hsa-miR-134	1.46E-03	-4.27
hsa-miR-361-5p	4.78E-03	3.60	hsa-miR-1910	1.27E-03	-4.35
hsa-miR-30b	3.61E-03	3.48	hsa-miR-520e	9.32E-04	-4.71
hsa-let-7b	1.79E-03	3.47	hsa-miR-520b	1.06E-03	-4.92
hsa-miR-34a	1.25E-03	3.07	hsa-miR-198	3.33E-03	-5.02

Table 7 miRNAs differentially expressed between TaG1 and T2G2-3 tumors

FC = fold change; NMI = non-muscle invasive tumors (TaG1); MI = muscle-invasive tumors (T2G2-3)

A

microRNA	Chromosome	*p-value*	FC (NMI vs. MI) microarray	FC (NMI vs. MI) qRT-PCR
hsa-miR-126	9q34.3	2.75E-04	3.67	16.08
hsa-miR-429	1p36.33	7.74E-04	3.61	67.18
hsa-miR-141	12p13.31	2.18E-03	3.70	3373
hsa-miR-198	3q13.33	3.33E-03	-5.02	11.63
hsa-miR-200c	12p13.31	4.03E-03	2.91	1314

B

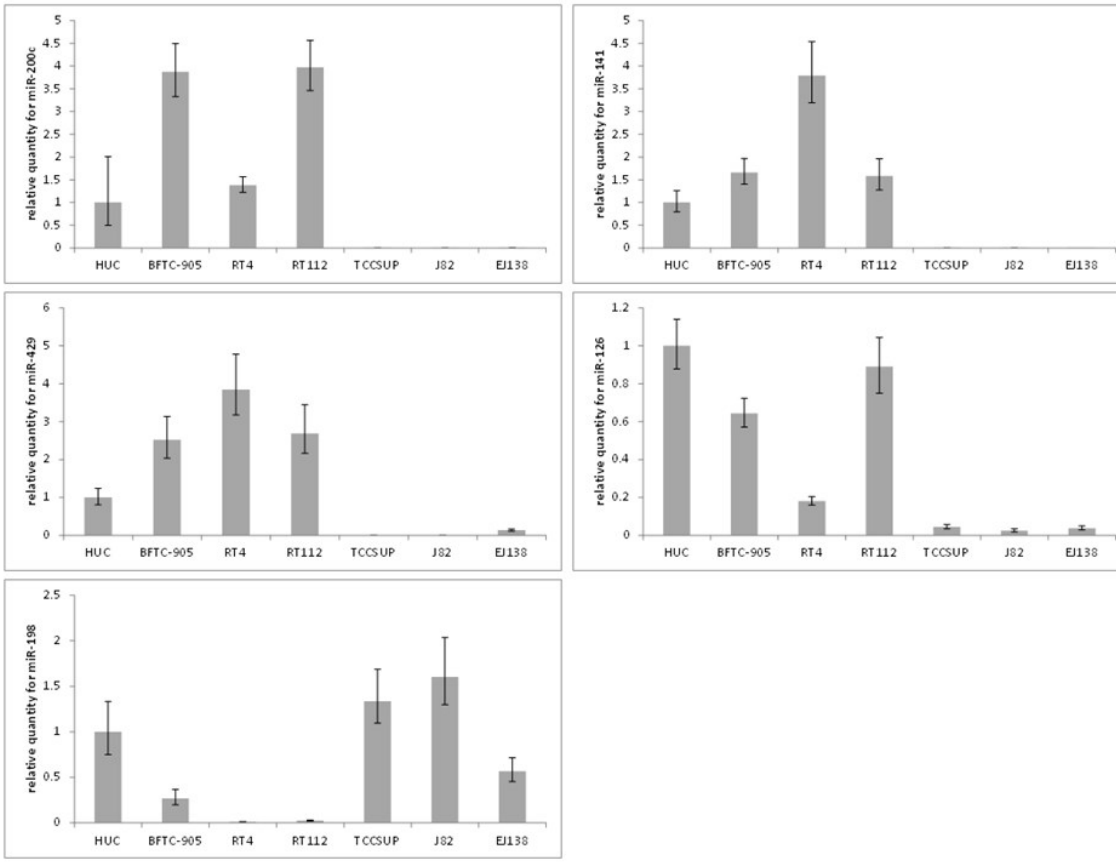

Figure 3.2 qRT-PCR validation of miRNAs differentially expressed between TaG1 and T2G2-3 tumors

(A) Table summarizing miRNAs with a calculated qRT-PCR fold change > |10| in bladder cancer cells. **(B)** qRT-PCR validation; fold changes are normalized to the HUC line. Non-invasive cells are: BFTC-905, RT4, RT112. Invasive cells are: TCCSUP, J82, EJ138.

2. Generation of firefly luciferase (FL) and renilla luciferase (RL) cell lines

To quantify the amount of cell invasion, stably expressing firefly luciferase (FL) and renilla luciferase (RL) were separately established in each cell line. Because the RL cells are not infected with miRNAs, these cells invade as would the native cell line. The RL cells can

therefore normalize differences between individual transwell chambers and serve as an internal control. Both FL and RL expression are directly proportional to the cell amount in a linear fashion (**Figure 3.3**).

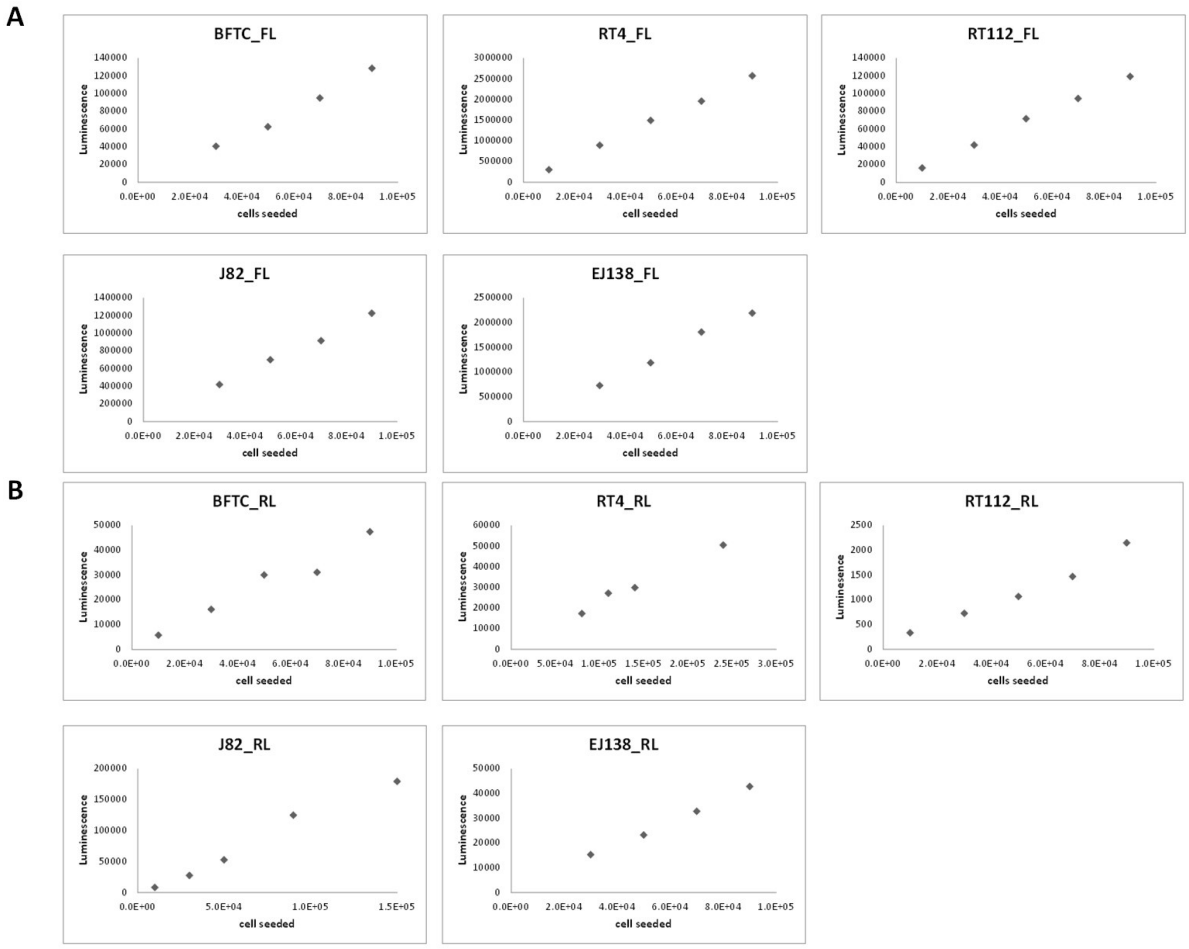

Figure 3.3 Establishing firefly luciferase (FL) and renilla luciferase (RL) cell lines. Firefly luciferase assays **(A)** and renilla luciferase **(B)** assays in respective cell lines.

In a transwell invasion assay, a 50% mixture of FL and RL cells were seeded in the well (**Figure 3.4**). After incubation, cells remaining in the well and those that have invaded through the matrigel were collected and subjected to luciferase assay. To evaluate the invasive potential of the miRNA, all quantifications of miRNA-induced invasion were calculated relative to invasion of the FL cell line. Comparisons to the FL line also correct for any potential secondary effects

produced by FL expression. Therefore, there are two levels of normalization: within each transwell chamber by RL cells, and between FL and FL_miR lines.

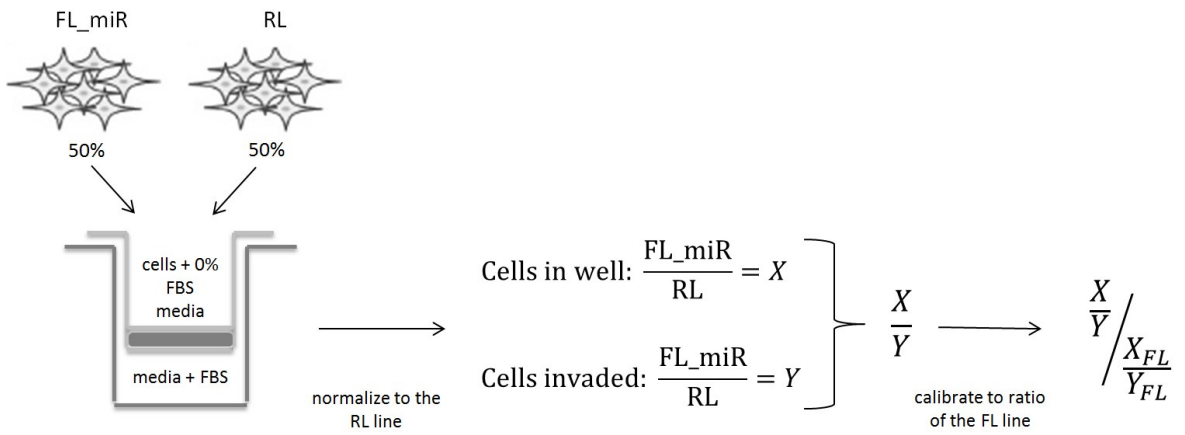

Figure 3.4 Invasion experimental design

Transwell matrigel chambers were used to assess invasion *in vitro.* miRNAs were stably infected into cell lines stably expressing FL. The same cell line expressing RL was used as an internal control. Non-invasive lines were incubated for 48h, invasive lines were incubated for 24h. Cells both on top and underneath the well were harvested and assayed for luciferase expression. The FL signal was normalized to the RL signal in the same well. Normalized luciferase ratios were then calibrated to the ratio of the FL line.

3. Generation of miRNA and HRAS overexpressing cell lines

Mature miRNA sequences expressed in a lentiviral vector were stably infected into bladder cancer cell lines. For each cell line, FL and the miRNA of interest were co-expressed in the same cell (with suffix FL_miR). Potentially invasive miR-198 was transduced into non-invasive cells BFTC-905, RT4, and RT112. The other five non-invasive miRNAs were transduced into invasive cells J82 and EJ138. qRT-PCR was performed to verify miRNA expression levels in the cell lines (**Figure 3.5**).

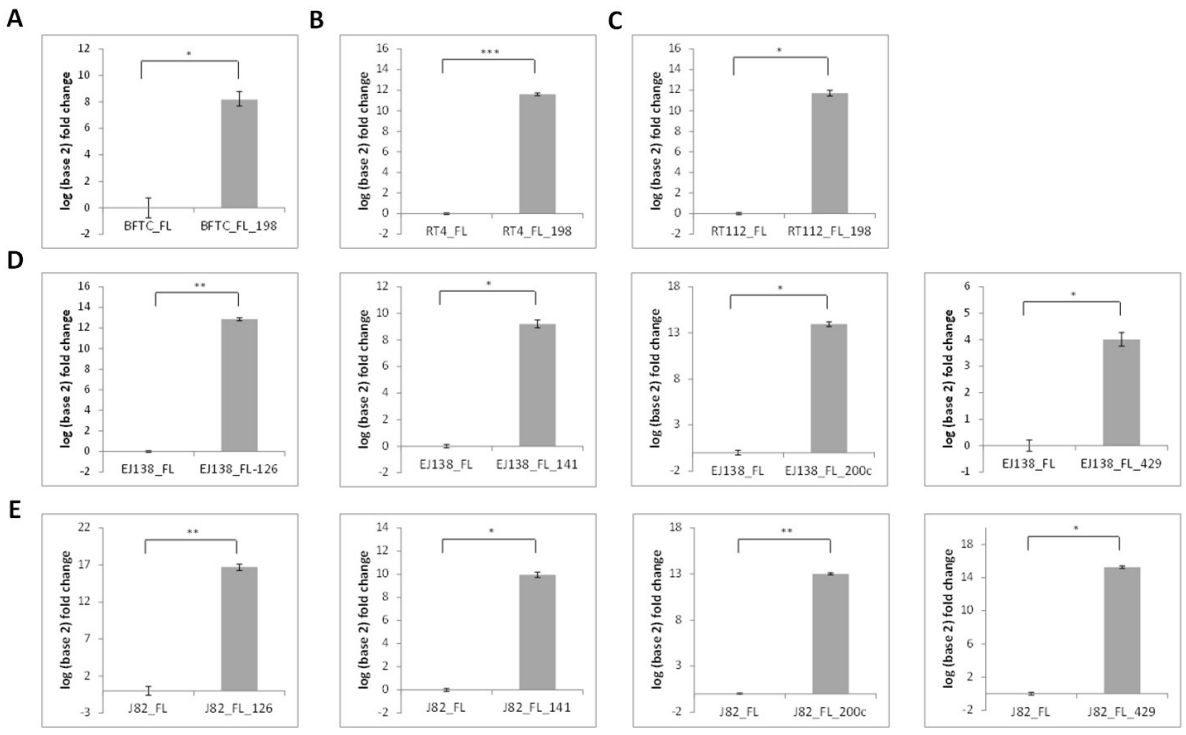

Figure 3.5 qRT-PCR validation of miRNA expression in FL_miR infected cell lines

Fold changes were calibrated to the respective FL line. Validation of miR-198 in BFTC-905 **(A)**, RT4 **(B)**, and RT112 **(C)**. Validation of miR-126, miR-141, miR-200c, and miR-429 in EJ138 **(D)** and J82 **(E)**. *$p < 0.05$, **$p < 0.005$, ***$p < 0.0005$ by Student's T-Test.

To generate a positive control for non-invasive cell lines, the constitutive active *HRAS*^{V12} was stably infected into FL expressing lines of BFTC-905, RT4, and RT112 (**Figure 3.6**). Non-invasive and invasive cell lines were subjected to transwell invasion assays to examine the native invasive potential of each cell line (**Figure 3.7**). As expected, mutant HRAS^{V12} significantly increased the invasiveness of the non-invasive cell lines; a two to six fold increase was observed in HRAS^{V12} lines.

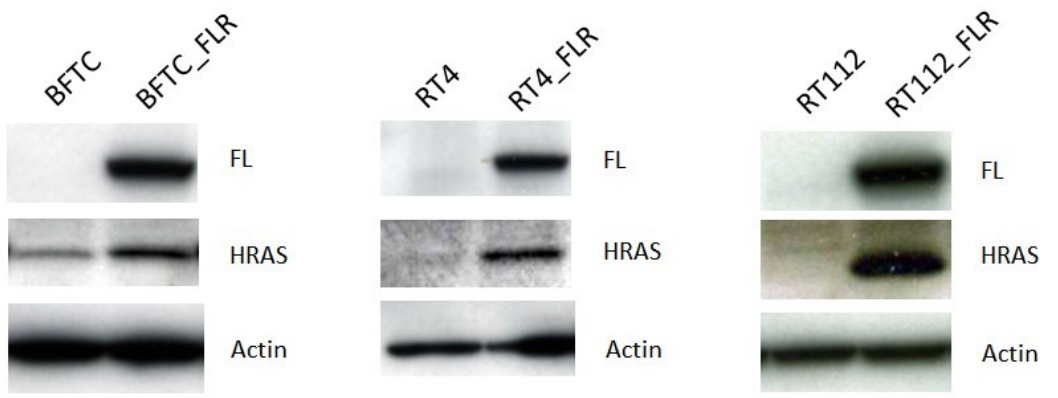

Figure 3.6 Establishing HRAS^{V12} in non-invasive FL cell lines

FL cell lines expressing HRAS^{V12} (FLR) were used as a positive control for invasion of non-invasive cells. Protein blots show presence of FL (82 kDa) and HRAS (21 kDa) in the FLR line.

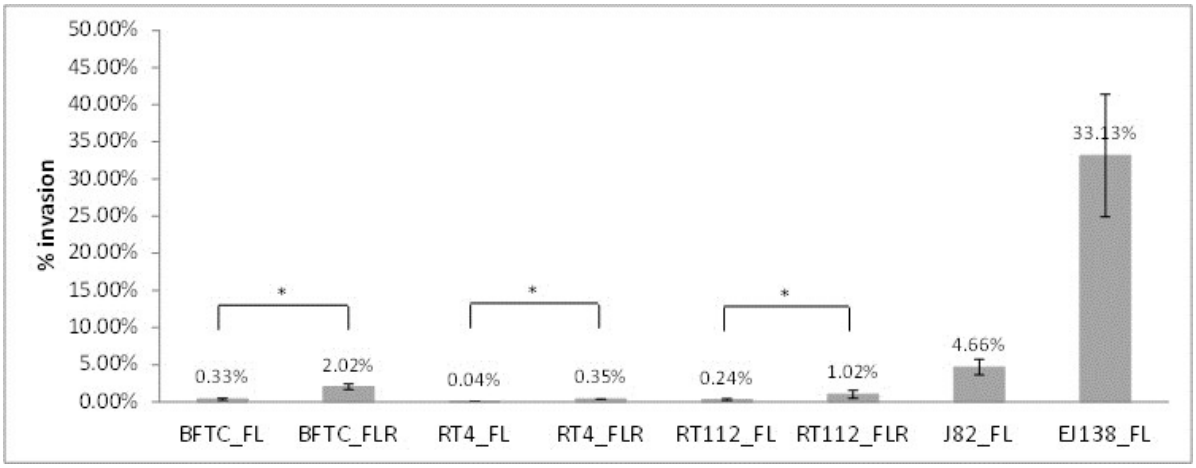

Figure 3.7 Invasion potential of bladder cancer cell lines

Percent invasion measured as the ratio of cells that have invaded relative to those that have remained in the well. *$p < 0.05$ by Student's T-Test.

4. Overexpression of miR-198 promotes invasion in non-invasive cells

Overexpression of miR-198 generated a six-fold and two-fold increase in invasion in RT4 and RT112, respectively, an extent comparable to that of HRAS^{V12} (**Figure 3.8A, B, C**). Similar to cells expressing HRAS^{V12}, miR-198 did not stimulate cell proliferation in any of the non-

invasive cell lines (**Figure 3.8C, D, E**). This ruled out the possibility that the rise in invasion was due to a confounding effect of an increase in proliferation.

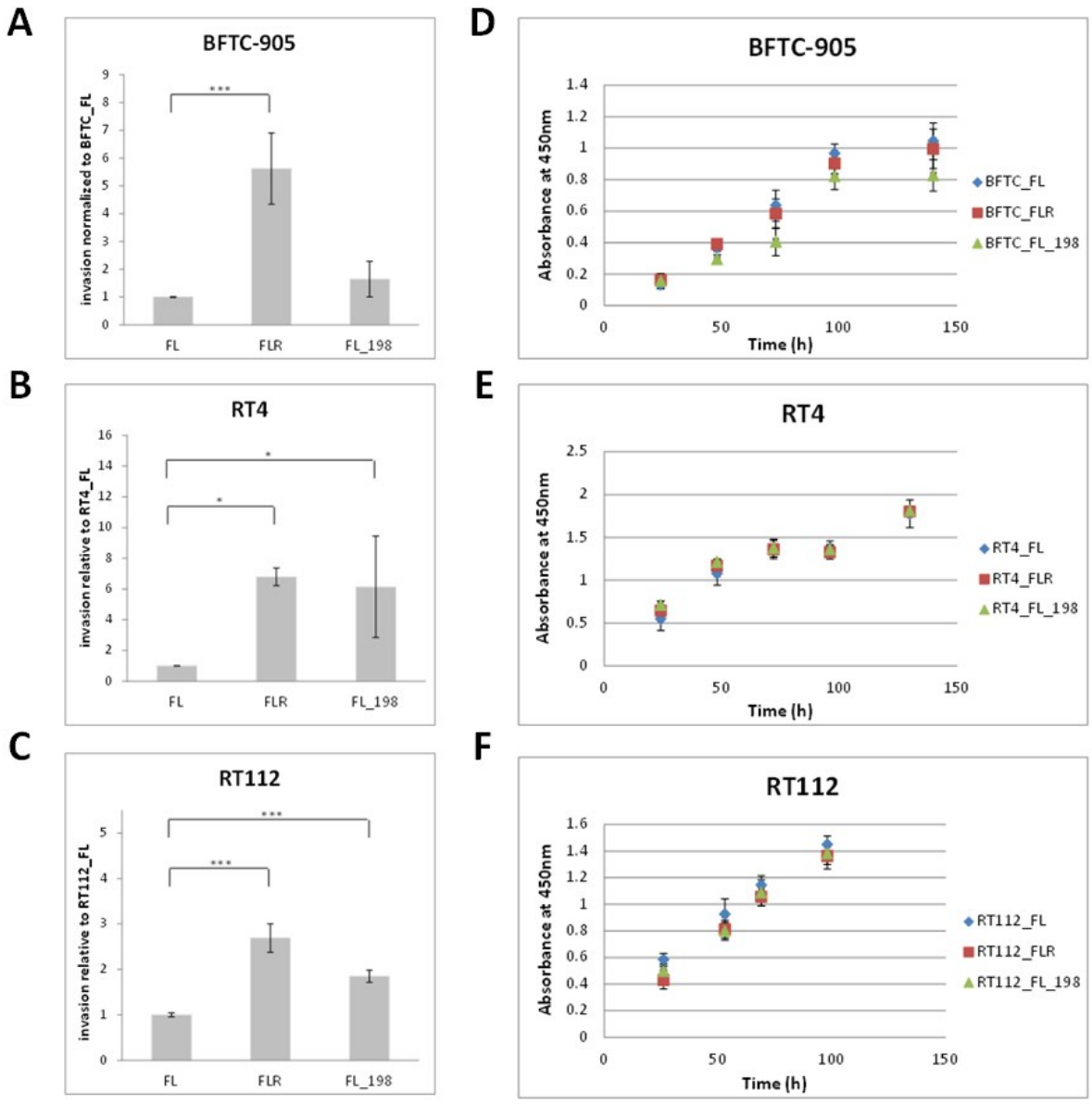

Figure 3.8 Effect of miR-198 overexpression in non-invasive cells

Matrigel invasion assay of BFTC-905 **(A)**, RT4 **(B)**, and RT112 **(C)**. FLR lines were used as a positive control for invasion. Cell proliferation assays performed on BFTC-905 **(D)**, RT4 **(E)**, and RT112 **(F)**. **p* < 0.05, ***p* < 0.005, ****p* < 0.0005 by Student's T-Test.

5. Concurrent knock-down of miR-200c, miR-141, and miR-429 promote invasion in non-invasive cells

Anti-miRNA inhibitors, chemically modified single stranded RNA complementary to the endogenous miRNA, were used to transiently knock-down miR-200c, miR-141, and miR429 in BFTC-905, RT4, and RT112 cells. Individual knock-downs of each miRNA did not produce a significant change in cell invasion. However, knock-down of all three miRNAs simultaneously resulted in a seven-fold and 1.5-fold increase in invasion in RT4 and RT112, respectively (**Figure 3.9**). Furthermore, combined knock-down of the three miRNAs against a background of miR-198 overexpression produced a cumulative effect in BFTC-905, RT4, and RT112; in RT4 the increase in invasion was additive (**Figure 3.9**).

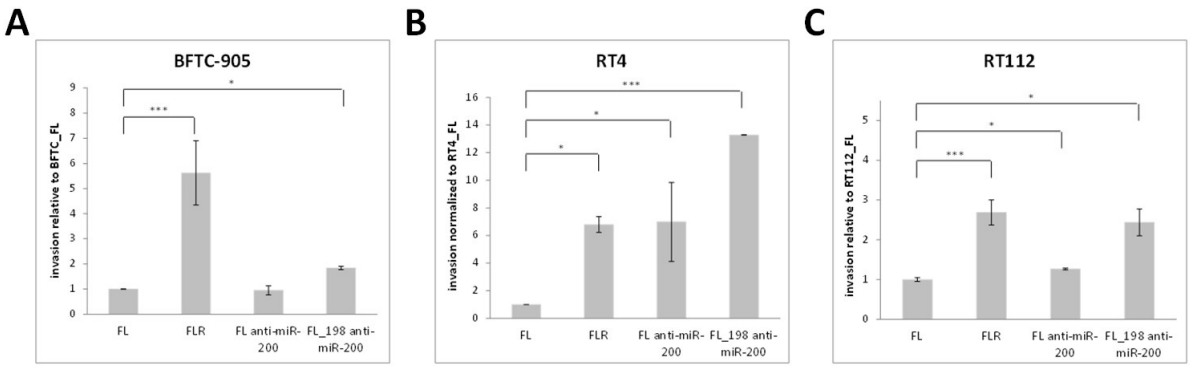

Figure 3.9 Effect of miR-200 family knock-down in non-invasive cells

Matrigel invasion assay of BFTC-905 **(A)**, RT4 **(B)**, and RT112 **(C)**. FLR lines were used as a positive control for invasion. A cocktail of anti-miR-200c, 141, 429 inhibitors (50nM; designated as anti-miR-200) was transiently transfected into the FL or FL_198 line. *p < 0.05, **p < 0.005, ***p < 0.0005 by Student's T-Test.

6. Overexpression of miR-200c and miR-126 inhibit invasion in invasive cells

Of the three miR-200 family members, only stable overexpression of miR-200c induced a statistically significant (two-fold) decrease in invasion in J82 and EJ138. miR-429 induced a noticeable decrease in magnitude of invasion EJ138 but was not statistically significant; while

no effect by miR-429 was observed in J82. miR-141 did not produce any appreciable effects on invasion in either cell line.

Transient concurrent overexpression of all three miRNAs resulted in a four-fold suppression of invasion in J82, a greater effect than miR-200c alone (**Figure 3.10A**). Such an effect was not observed in EJ138, where overexpression of all three miRNAs decreased invasion to a level similar to that of miR-200c alone (**Figure 3.10B**). miR-126 also inhibited invasion in J82 and EJ138 by two-fold. None of the miRNAs affected cell proliferation in EJ138 (**Figure 3.10D**), suggesting the reduction in invasion was not a consequence of inhibition of proliferation. However, expression of miR-200c, miR-429, and miR-126 decreased J82 proliferation (**Figure 3.10C**). This may account for the greater fold reduction from concurrent overexpression of the miR-200 family observed in J82.

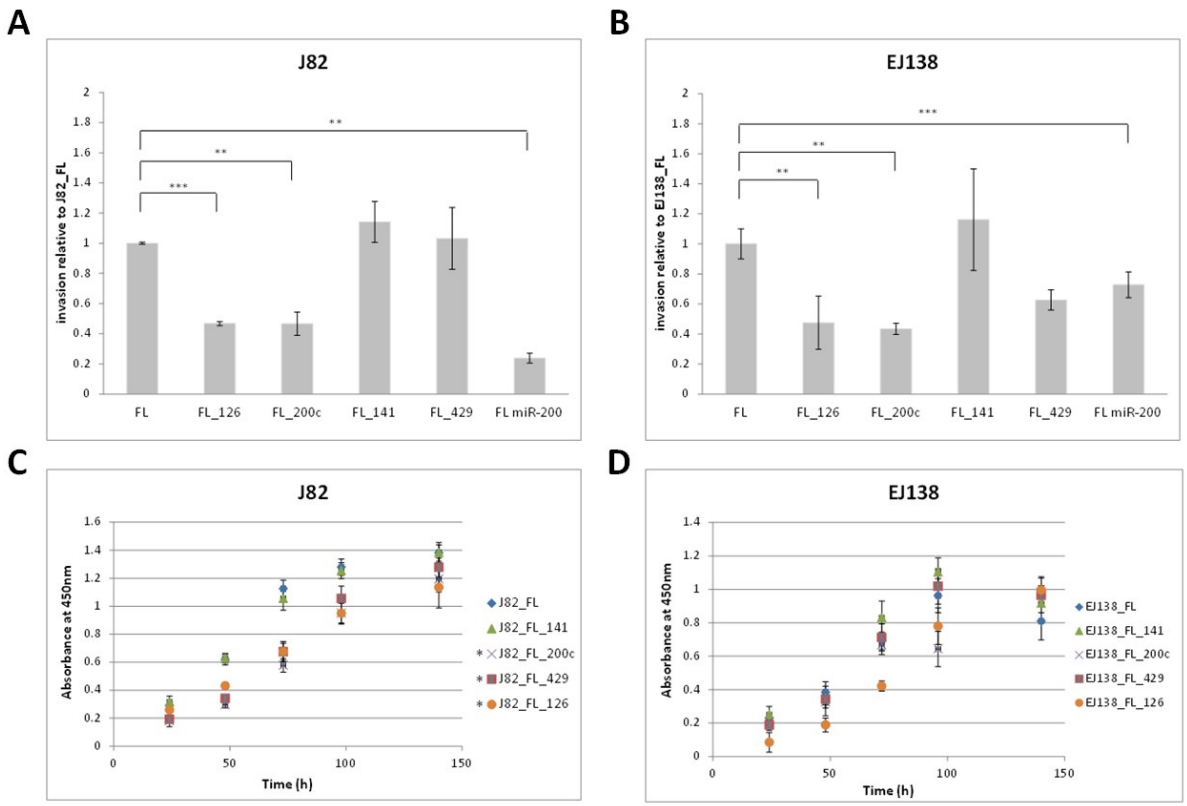

Figure 3.10 Effect of miR-126 and miR-200 family overexpression in invasive cells

Matrigel invasion assay of J82 **(A)** and EJ138 **(B)**. A cocktail of miR-200c, 141, 429 mimics (25nM; designated miR-200) was transiently transfected into the FL line. Cell proliferation assays performed on each miRNA infected cell line of J82 **(C)** and EJ138 **(D)**. *$p < 0.05$, **$p < 0.005$, ***$p < 0.0005$ by Student's T-Test.

7. Identification of potential downstream miRNA targets via TargetScan

In silico target prediction for the five miRNAs was performed using TargetScan on the list of 1493 differentially expressed mRNAs. The list of potential targets was modified to include only genes with expression patterns that inversely correlated with miRNA expression (e.g. a gene expressed at higher levels in muscle-invasive tumors than non-muscle invasive would not be a target of miR-198). miR-200c and miR-429 shared identical targets. There were four unique gene targets predicted for miR-126, 32 for miR-198, 215 for miR-141, and 306 for miR-200c/miR-429 (**Figure 3.11**). Between the three miR-200 family members there were 30 targets

in common. *KANK2* was a predicted target for both miR-126 and miR-200c/miR-429, and *PEX5* was a common target between miR-126 and miR-141. Since miR-198 affected cell invasion in the opposite manner as the miR-200 family and miR-126, there were no common targets.

A

B

Gene Symbol	Gene Title	*p-value*	FC (NMI vs. MI)
KANK2[a]	KN motif and ankyrin repeat domains 2	8.93E-04	-1.062
PEX5[b]	peroxisomal biogenesis factor 5	1.36E-02	-1.042
ADAM9	ADAM metallopeptidase domain 9	1.84E-02	-1.163
PLXNB2	Plexin B2	4.51E-02	-1.049

[a] miR-200c/miR-429 target
[b] miR-141 target

C

Gene Symbol	Gene Title	*p-value*	FC (NMI vs. MI)
DIXDC1	DIX domain containing 1	3.90E-04	-1.068
GJC1	gap junction protein, gamma 1, 45kDa	7.38E-04	-1.059
SGK269	NKF3 kinase family member	1.11E-03	-1.051
NCAM1	neural cell adhesion molecule 1	3.75E-03	-1.055
CALU	calumenin	4.13E-03	-1.056
NFASC	neurofascin	4.96E-03	-1.096
AFF1	AF4/FMR2 family, member 1	7.43E-03	-1.066
CCNE2	cyclin E2	8.75E-03	-1.047
KLF12	Kruppel-like factor 12	1.12E-02	-1.051
NPTX1	neuronal pentraxin I	1.17E-02	-1.063
ZCCHC24	zinc finger, CCHC domain containing 24	1.25E-02	-1.064
LASS6	LAG1 homolog, ceramide synthase 6	1.39E-02	-1.063
PHC3	polyhomeotic homolog 3 (Drosophila)	1.61E-02	-1.070
ZFAND5	zinc finger, AN1-type domain 5	1.63E-02	-1.047
MAF	v-maf musculoaponeurotic fibrosarcoma oncogene homolog (avian)	1.69E-02	-1.051
CDON	Cdon homolog (mouse)	1.93E-02	-1.052
ATXN1	ataxin 1	2.10E-02	-1.066
PRKACB	protein kinase, cAMP-dependent, catalytic, beta	2.24E-02	-1.062
PTEN	phosphatase and tensin homolog	2.40E-02	-1.031
WIPF1	WAS/WASL interacting protein family, member 1	2.48E-02	-1.042
HIPK2	homeodomain interacting protein kinase 2	2.85E-02	-1.046
PTCH1	patched 1	3.04E-02	-1.044
TCF4	transcription factor 4	3.17E-02	-1.051
CTBP2	C-terminal binding protein 2	3.26E-02	-1.054
ZNF148	zinc finger protein 148	3.29E-02	-1.055
MTF2	metal response element binding transcription factor 2	3.54E-02	-1.048
CHD2	chromodomain helicase DNA binding protein 2	4.01E-02	-1.071
LPIN2	lipin 2	4.33E-02	-1.027
DOCK4	dedicator of cytokinesis 4	4.76E-02	-1.040
RAPGEF2	Rap guanine nucleotide exchange factor (GEF) 2	4.86E-02	-1.059

D

Gene Symbol	Gene Title	p-value	FC (NMI vs. MI)
EI24	etoposide induced 2.4 mRNA	4.31E-04	1.039
STAT6	signal transducer and activator of transcription 6, interleukin-4 induced	8.48E-04	1.134
PCM1	pericentriolar material 1	9.40E-04	1.064
ERAP1	endoplasmic reticulum aminopeptidase 1	2.10E-03	1.039
PSD3	pleckstrin and Sec7 domain containing 3	2.26E-03	1.091
SPTBN1	Spectrin, beta, non-erythrocytic 1	2.65E-03	1.076
RPL41	ribosomal protein L41	3.01E-03	1.025
LRRC59	leucine rich repeat containing 59	3.85E-03	1.101
FAM136A	family with sequence similarity 136, member A	4.28E-03	1.073
MAP4	microtubule-associated protein 4	4.38E-03	1.134
CNOT4	CCR4-NOT transcription complex, subunit 4	5.35E-03	1.080
KPNA4	karyopherin alpha 4 (importin alpha 3)	5.43E-03	1.188
MET	met proto-oncogene (hepatocyte growth factor receptor)	5.52E-03	1.154
H3F3A /// LOC440926	H3 histone, family 3A /// H3 histone, family 3A pseudogene	6.21E-03	1.035
C1orf116	chromosome 1 open reading frame 116	6.35E-03	1.209
PUM2	pumilio homolog 2 (Drosophila)	6.79E-03	1.173

Gene Symbol	Gene Title	p-value	FC (NMI vs. MI)
MBNL2	muscleblind-like 2 (Drosophila)	9.06E-03	1.066
FBXO34	F-box protein 34	9.71E-03	1.046
EIF3B	eukaryotic translation initiation factor 3, subunit B	1.28E-02	1.083
VAPA	VAMP (vesicle-associated membrane protein)-associated protein A, 33kDa	1.35E-02	1.037
PBX2	pre-B-cell leukemia homeobox 2	1.57E-02	1.074
CA12	carbonic anhydrase XII	1.81E-02	1.095
PURA	purine-rich element binding protein A	1.88E-02	1.043
CLPTM1	cleft lip and palate associated transmembrane protein 1	2.02E-02	1.073
CDK4	cyclin-dependent kinase 4	2.25E-02	1.063
VCP	valosin-containing protein	2.44E-02	1.092
STAU1	staufen, RNA binding protein, homolog 1 (Drosophila)	2.59E-02	1.118
IPO9	importin 9	3.06E-02	1.037
NMT1	N-myristoyltransferase 1	3.08E-02	1.102
TCEA1	transcription elongation factor A (SII), 1	3.68E-02	1.080
FBXO41	F-box protein 41	4.18E-02	1.069
FBXW11	F-box and WD repeat domain containing 11	4.22E-02	1.042

Figure 3.11 miRNA targets predicted via TargetScan

Targets were predicted using TargetScan 5.0 by combining the miRNA and mRNA microarray data. **(A)** Venn diagram illustrating common targets shared between the miR-200 family and miR-126. miR-200c and miR-429 shared identical targets. **(B)** Four targets predicted for miR-126. **(C)** 30 targets in common between the miR-200 family members. **(D)** 32 targets predicted for miR-198.

Discussion

To investigate miRNAs potentially involved in invasion, we profiled the expression of miRNAs and mRNAs in bladder tumors of various stage and grade. Both miRNA and mRNA expression levels clustered tumors based on stage. Of the 72 miRNAs differentially expressed between non-muscle invasive (Ta) and muscle-invasive (T2) tumors, 31 were up-regulated and 41 were down-regulated in muscle-invasive tumors. From this list we identified two miRNAs, miR-198 and miR-126, previously not associated with bladder cancer invasion.

In this study we employed a novel method of assaying invasion. The standard method to measure transwell matrigel invasion is by staining invasion chambers with crystal violet to visualize cells. However, it is a challenge to procure an accurate cell count because many bladder cancer cell lines, especially RT4, grow in tight clusters. Because FL and RL levels increase linearly with cell amount, measurements of FL and RL expression could provide a more quantitative assessment of cell invasion. In our assay, errors that may arise due to physical variations between transwells and cell seeding irregularities are addressed by the use of RL expressing cells that do not express the miRNAs of interest and a measure of cells that remain in the transwell (i.e. cells that did not invade).

We focused on five miRNAs that displayed the highest differential expression between non-invasive bladder cancer cell lines and invasive cell lines by qRT-PCR (fold change > 10). Notably, three of the five miRNAs – miR-200c, miR-141, and miR-429 – belong to the miR-200 family. We found that simultaneous knock-down of all three miRNAs in non-invasive cells enhanced invasion, while forced overexpression of the three miRNAs in invasive cells inhibited invasion. The miR-200 family is previously reported to be silenced in muscle-invasive bladder tumors as well as undifferentiated bladder cancer cells (T24 cell line) [142]. Another study revealed that the miR-200 family was down-regulated in “mesenchymal” bladder cancer cells (UMUC2, UMUC3, UMUC13, T24, and KU7) compared to “epithelial” cells that express E-

cadherin (UMUC6, UMUC9, UMUC16, and UMUC5) [143], suggesting that miR-200 may function to maintain an epithelial phenotype in bladder cancer cells. Furthermore, miR-200c was shown to reverse the EMT process in UMUC3 cells and reduce migration, possibly through inhibition of ZEB1 and ZEB2. Unsurprisingly, *ZEB1* was also identified as a miR-200c and miR-429 target in our *in silico* screen.

miR-198 was up-regulated in T2 tumors compared to Ta. Although miR-198 was detected in HUC (normal bladder cells), it was highly expressed in invasive bladder cancer cell lines, and either at very low levels (BFTC-905) or non-existent (RT4 and RT112) in the non-invasive cell lines. High levels of miR-198 were reported in retinoblastoma [144] and squamous cell carcinoma of the tongue [145]. In contrast, miR-198 was found to be down-regulated in hepatocellular carcinoma, where overexpression of miR-198 reduced hepatocyte growth factor induced cell invasion *in vitro* by inhibiting c-MET [146]. Contrary to its effect in liver cancer cells, we found that overexpression of miR-198 in the non-invasive bladder cancer cell lines increased invasion. In addition, increased miR-198 expression augments invasion caused by suppression of the three miR-200 family members. This suggests that miR-198 and the miR-200 family may function in separate pathways. We have also identified several potential targets previously unassociated with miR-198: *EI24*, *SPTBN1*, and *RPL41*. EI24 is a proapoptotic factor regulated by p53 that is frequently mutated or deleted in invasive cervical [147] and breast carcinomas [148]. EI24 is expressed in ductal CIS of the breast but lost in invasive ductal carcinoma, suggesting a role in suppressing invasion [148]. Expression of EI24 also sensitizes breast cancer cells to the chemotherapy drug etoposide, which functions through p53 [149]. SPTBN1 is a member of the F-actin superfamily of cross linking proteins, essential for maintaining cytoskeletal integrity and may play a role in cell adhesion, migration, and invasion. This scaffolding protein has been implicated in the regulation of the TGF-β signaling pathway through Smad molecules [150]. SPTBN1 is present in chronic pancreatitis but lost in poorly differentiated tumor cells, where reduced expression is correlated with worsened prognosis of pancreatic

cancer [151]. Lastly, RPL41 is a microtubule-associated protein involved in proper chromosome segregation during mitosis, where depletion of RPL41 resulted in premature splitting of the centrosome [152]. RPL41 expression is reduced in breast carcinoma [152] and addition of RPL41 to lung carcinoma cells increased their sensitivity to cisplatin, presumably through degradation of the transcription factor ATF4 [153]. Since these targets have seemingly tumor invasion suppressive roles, it is reasonable that an oncogenic miR-198 may target them in bladder tumors. Further steps should be taken to verify the miR-198 regulation of these targets, such as through a 3'UTR assay.

We observed a significant decline in miR-126 in T2 compared to Ta tumors. The same trend was observed in bladder cancer cells, where miR-126 was expressed highly in HUC and non-invasive cell lines, but at barely discernible levels in invasive cells. As mentioned previously, down-regulation of miR-126 is observed in invasive tumors of the breast [85], pancreas [86], and liver [87]. In addition, low serum levels of miR-126 in a three-miRNA plasma signature served as a significant prognostic biomarker for tumor progression in lung adenocarcinoma [154]. Reduced miR-126 expression also correlated with tumor progression and nodal metastasis in oral squamous cell carcinoma [155]. Four genes with increased expression in invasive bladder tumors versus non-invasive were identified by TargetScan as potential miR-126 targets: *KANK2*, *PEX5*, *ADAM9*, and *PLXNB2*. Of these four, ADAM9 is of particular interest because of its implication in the progression of tumors [156]. The role of ADAM9 in bladder cancer cell invasion is further explored in Chapter 4.

Materials and Methods

Cell culture and human clinical samples

All cell lines were grown according to manufacturer's protocols at 37°C in a humidified air atmosphere at 5% CO2. The HUC line was purchased from ScienCell Research Laboratories. BFTC-905 cells were purchased from the Leibniz Institute DSMZ-German Collection of Microorganisms and Cell Cultures. RT112 and EJ138 were gifts from Dr. Sanchez-Carbayo (Tumor Markers Group, Madrid). MCF10A, RT4, TCCSUP, J82, and 293FT cells were purchased from the American Type Culture Collection (ATCC). The following human bladder tumor tissue samples were obtained through IRB approved protocols: TaG1 (n=3), TaG2 (n=3), CIS (n=4), T1G1 (n=3), T1G2/3 (n=3), T2G2/3 (n=6). CIS biopsies were dissected using laser capture microdissection as previously described in Chapter 2 to isolate tumor from adjacent normal urothelium.

RNA extraction

RNA was extracted from cell lines and tumor samples using the miRVANA Kit (Ambion). RNA from microdissected CIS samples were extracted using the RNAquesous-Micro Kit (Ambion). The quality of all RNA samples was verified using a RNA Pico Kit (Agilent). Only sample qualities with RIN above 6.0 with clean 18S and 28S peaks were used.

Microarray profiling and data analysis

Agilent Human miRNA Microarray (V3, based on Sanger miRbase release 12.0) and the Affymetrix Human U133 Plus 2.0 arrays were used for measuring miRNA and mRNA expression in bladder samples. All procedures were carried out according to manufacturer's protocol. Data analyses were performed as described in Chapter 2, with the exception that mRNA data were analyzed using GeneSpring GX 12 instead of Partek Genomics Suite 6.6.

Only detected probesets were used, compromised or undetected probesets were filtered out. One-way ANOVA and Tukey's honestly significant difference (HSD) post-hoc test were performed across all samples to obtain miRNAs or mRNAs differentially expressed ($p < 0.05$). Unsupervised hierarchical cluster analysis was performed on the list of differentially expressed probesets with a fold change ≥ 2 (150 miRNAs, 1493 mRNAs).

Plasmid generation

RNA from MCF10A cells were used to PCR amplify pre-miRNA regions. Amplified pre-miRNA fragments were subcloned into an empty pLemiR vector (Open Biosystems, Pittsburgh, PA) and verified by sequencing, hereby referred to as pLemiRNA. The following sense and antisense oligonucleotides were used:

miRNA	**PCR primers**
miR-198	Forward: 5' TCTGCTCGAGGAGCAAGGGTGCCTTAGA 3' Reverse: 5' ATGACTGGCGGCCGCAAGTCACAGTTT 3'
miR-126	Forward: 5' CATTCTCGAGTGGCTGTTAGGCAT 3' Reverse: 5' TGGGCGGCCGCCTCTGCACTTCTT 3'
miR-200c	Forward: 5' AAGGCTCGAGGGGGTAGGGGAAGGT 3' Reverse: 5' AGCGGCCGCCGACAGAGAACTA 3'
miR-141	Forward: 5' CGTCTCGAGCTGAGAGCGTTGCAC 3' Reverse: 5' AGACGCGGCCGCCCCAATCCTGAGT 3'
miR-429	Forward: 5' TAAGTCGACCGAGCTTCAGGAAGCCA 3' Reverse: 5' ACGGCGGCCGCAGCATCTGCCCGGGGACTACA 3'

Renilla luciferase was subcloned into a modified pLPCX (Clontech) plasmid that contains GFP, hereby referred to as pLPCX-Ren. The sense and antisense oligonucleotide sequences used to amplify renilla luciferase from pRL-SV40 (Promega) were 5'-AAAAACTCGAGCGCCACCATGA-CTTCGAAAGTTTATGATCC-3' and 5'-AAAAAGAATTCTTATTGTTCATTTTTGAGAACTC-3', respectively. Lentiviral plasmids PMB and CMV, retroviral plasmids VSVG and helper, firefly luciferase plasmid (FUW-Luc), and pBABE $HRAS^{V12}$ plasmids were gifts from Dr. Jose Silva.

Transient transfection and infection

Transient transfections using miRIDIAN microRNA Human Inhibitors or Mimics (Thermo Scientific) were performed using TransIT-TKO transfection reagent (Mirus). A final concentration of 50nM was used for miRIDIAN Inhibitors and 25nM was used for miRIDIAN Mimics.

293FT cells were transfected with lentiviral or retroviral particles using Lipofectamine 2000 (Invitrogen, Grand Island, NY). Media from 293FT 48 hours after transfection were collected to infect bladder tumor cell lines. Cell lines infected with FUW-Luc were subsequently infected with a pLemiRNA, and maintained using puromycin (0.5ug/ml) and geneticin (800ug/ml). Cell lines infected with pLPCX-Ren were maintained using puromycin (0.5ug/ml).

Quantitative real-time reverse transcription-PCR (qRT-PCR) miRNA expression profiling

TaqMan microRNA Reverse Transcription Kit (Applied Biosystems) was used to convert miRNA to cDNA. Reverse transcription primers (44nt) were designed so that the first 36nt formed an internal stem loop and the last 8nt were complementary to the mature miRNA sequence of interest. Qiagen QuantiTect PCR (Qiagen) was used to measure quantitative expression of miRNA. PCR assays were performed as described by the manufacturer using a Stratagene MX3005P PCR system. For normalization, we used *mir-92b* because it provided comparable expression levels across the bladder cell lines. miR-92b has also been cited as a stable reference gene for miRNA qRT-PCR [157].

Invasion and luciferase assays

In-vitro invasion assays were carried out using BD BioCoat Matrigel Invasion Chambers (8-µm pore, BD Biosciences, San Jose, CA) in 6-well tissue culture plates according to manufacturer's protocol. Cells were placed in serum-free media 24 hours prior to invasion assay set-up. Cells were seeded in a 50/50 mixture of FL to RL cell lines to a total amount of $2x10^6$ cells for non-invasive cell lines (BFTC-905, RT4, RT112) and $1.5x10^6$ cells for invasive cell lines (TCCSUP,

J82, EJ138) per well. Cells were suspended in serum-free media were added to each chamber and allowed to invade towards the underside of the chamber for 24h (invasive cell lines) or 48h (non-invasive cell lines) at 37°C. After incubation, remaining cells inside the chamber were collected along with cells that have invaded the membrane. FL and RL activities were measured using the Dual-Glo Luciferase Assay System (Promega, San Luis Obispo, CA).

FL signals were normalized to that of RL. Separate controls (invasion of FL cell line) were performed for each test condition (i.e. FL_miR cell line, over-expression or knock-down or miR-200c/141/429) but were pooled into the left bar in the graph for the purpose of simplicity (**Figures 3.8, 3.9, and 3.10**). Each test condition was normalized to the respective individual control. A student T-test was performed between each test condition and the individual control.

Cell proliferation assay

Cell viability was determined at 24, 48, 72, 96, 144 hours by using the CellTiter 96 Aqueous One Solution Cell Proliferation Assay kit (Promega) according to the manufacturer's protocol. Absorbance was measured at 490nm. Data are presented as the mean value for octuplicate wells.

4. Chapter 4: miR-126 inhibits invasion in bladder cancer cells via regulation of ADAM9

miR-126 and ADAM9 in cancer

As discussed in Chapter 3, miR-126 was down-regulated in muscle-invasive T2 tumors compared to non-muscle invasive Ta tumors. Overexpression of miR-126 in invasive bladder cancer cell lines produced a marked reduction in cell invasion. Conversely, *ADAM9* expression was significantly higher in T2 tumors than Ta tumors. ADAM9 is a predicted target of miR-126 via TargetScan and has also been shown to be suppressed by miR-126 in pancreatic cancer cells [86].

ADAMs are membrane-anchored cell surface proteins and members of the metzincin superfamily of matrix metalloproteinases (MMPs). Characteristic domains conserved across the ADAM family include: an N-terminal signal peptide, a prodomain, a metalloprotease domain, a disintegrin sequence, a cysteine-rich region, an EGF-like domain, a transmembrane domain, and a cytoplasmic tail [158]. The prodomain maintains the enzyme in an inactive state until it is removed by a furin-type proprotein convertase or by autocatalysis; the disintegrin domain has also been implicated in facilitating the removal of the prodomain [159]. As proteases, ADAMs have been reported to cleave and release the ectodomain of tumor-promoting factors such as ligands of the epidermal growth factor receptor (EGFR) and human EGFR (HER) family of receptors [158]. Specifically, ADAM9, an 84kDa protein, has been shown to release and activate EGF and heparin-binding EGF(HB-EGF) [160]. While ADAM9 expression is ubiquitous during mouse development, *adam9*$^{-/-}$ mice were viable, developed normally, and presented no abnormal phenotypes [161]. However, ADAM9 expression has been correlated with progression of many human cancers.

Elevated levels of ADAM9 have been correlated with breast cancer progression [162] and metastases to the liver and brain from colon and lung, respectively [163,164]. A soluble form of ADAM9 secreted by hepatic stellate cells has been found to promote colon cancer invasion through interactions with $\alpha_6\beta_4$ and $\alpha_2\beta_1$ integrins [165]. Inhibition of ADMA9 in prostate cancer cell lines resulted in apoptotic cell death [166]. Furthermore, loss of ADAM9 in prostate cancer mouse model led to the development of well-differentiated prostate tumors as opposed to poorly differentiated tumors in control littermates [167]. To the best of our knowledge, functional studies of ADAM9 in the context of bladder cancer has not been examined.

Experimental Design

To further investigate the role of ADAM9, we performed ADAM9 knock-down experiments in invasive bladder cancer cells followed by the luciferase invasion assay described in Chapter 3. Additionally, we stained transwell invasion chambers with DAPI to further visualize invasion and validate luciferase assay results. We also assessed ADAM9 expression in a cohort of 103 bladder tumors via immunohistochemistry; this is a separate panel of bladder tumors independent of the samples used in Chapter 3 microarray studies.

Results

1. miR-126 suppresses ADAM9 expression *in vitro*

As predicted by TargetScan, miRanda, and miRWalk, miR-126 targets the 3'UTR of ADAM9 (**Figure 4.1A**). Invasive bladder cancer cells stably infected with miR-126 displayed a significant decrease in ADAM9 mRNA (**Figure 4.1B**) and protein (**Figure 4.1C, D**). This confirms that miR-126 negatively regulates ADAM9 expression *in vitro*.

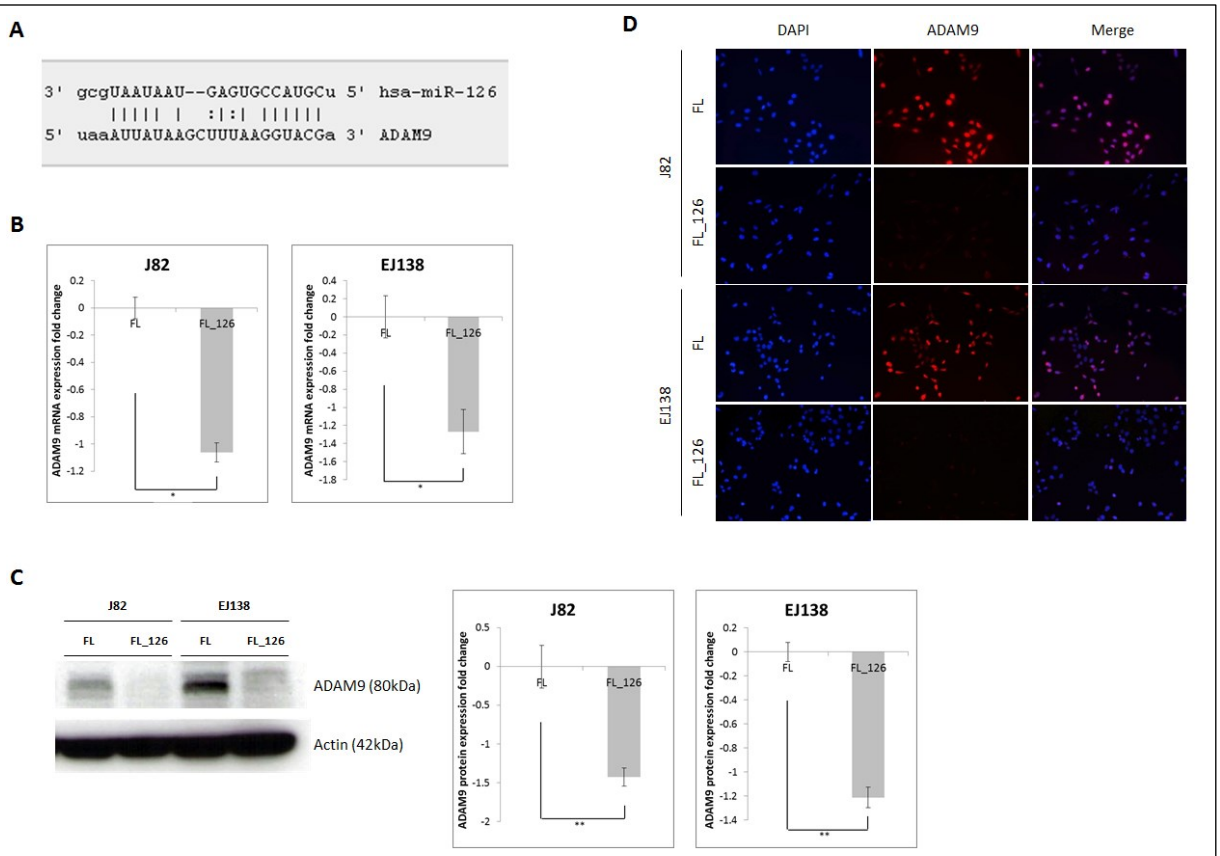

Figure 4.1 miR-126 targets ADAM9 in bladder cancer cells

(A) Complementary miR-126 binding sequences in the ADAM9 3'UTR as predicted by miRanda, miRWalk, and Targetscan. **(B)** ADAM9 mRNA expression in miR-126 infected cell lines (n = 3). **(C)** ADAM9 protein expression in miR-126 infected cell lines. Right, densitometric analysis of ADAM9 protein expression level (n = 5) relative to the respective FL line. Expression levels are calculated as $\log_2$ fold change. **(D)** Immunofluorescence detecting ADAM9 expression in miR-126 infected cell lines. *p < 0.05, **p < 0.005, by Student's T-Test.

2. Knock-down of ADAM9 inhibits invasion

Transient siRNA knock-down of ADAM9 at 25nM was complete in J82 but only 50% in EJ138 (**Figure 4.2**). There was no difference between an siRNA concentration of 25nM and 50nM.

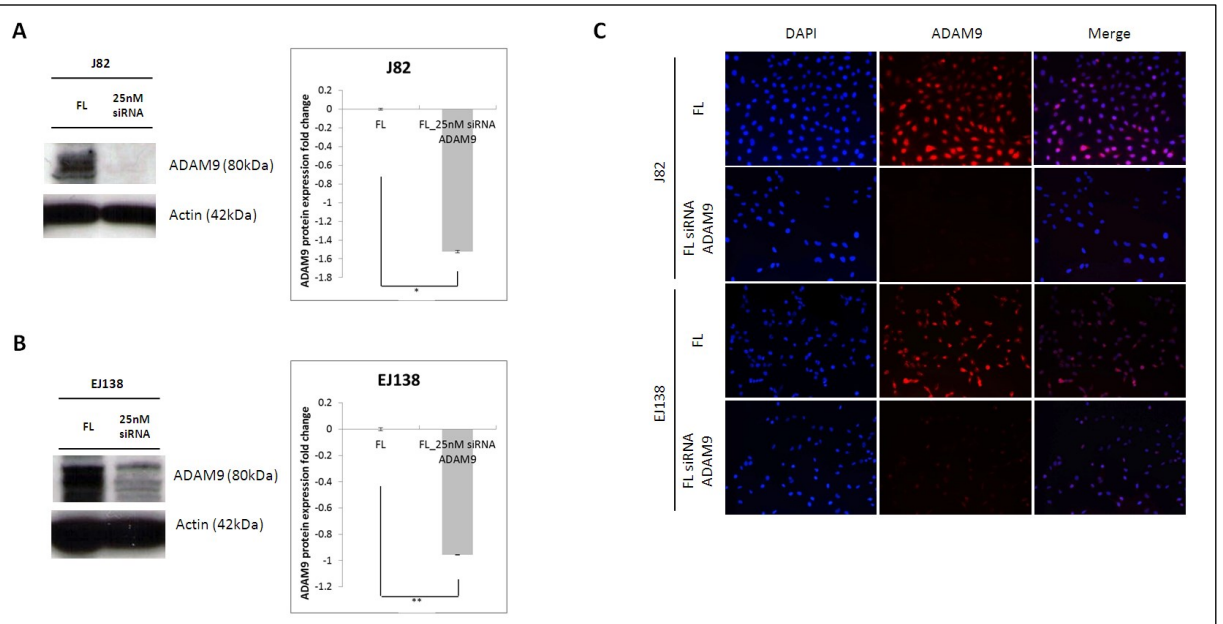

Figure 4.2 ADAM9 knock-down in invasive cells

ADAM9 protein expression at 48h after transfection of ADAM9 siRNA and matrigel invasion assay in J82_FL **(A)** and EJ138_FL **(B)**. Right, densitometric analysis of ADAM9 protein expression level (n = 5) relative to the respective FL line. Expression levels are calculated as $\log_2$ fold change. **(C)** Immunofluorescence detecting ADAM9 expression in cell lines transfected with ADAM9 siRNA. *$p < 0.05$, **$p < 0.005$, by Student's T-Test.

Transient knock-down of ADAM9 reduced cell invasion at a level comparable to miR-126 induced inhibition (**Figure 4.3A, C**) as quantified by the luciferase assay method described in Chapter 3. In a separate invasion set-up, we stained the transwell invasion chamber with DAPI to provide a qualitative assessment (**Figure 4.3B, D**). In this alternate set-up, RL cells were not mixed into the seeding population, therefore DAPI staining directly corresponded to the amount of FL cells that has invaded. Because this method lacks the internal control present in the luciferase assay method, the luciferase assay is provides a more rigorous quantitative measurement. This method also confirmed that transient knock-down of ADAM9 and overexpression of miR-126 suppressed cell invasion by a similar amount.

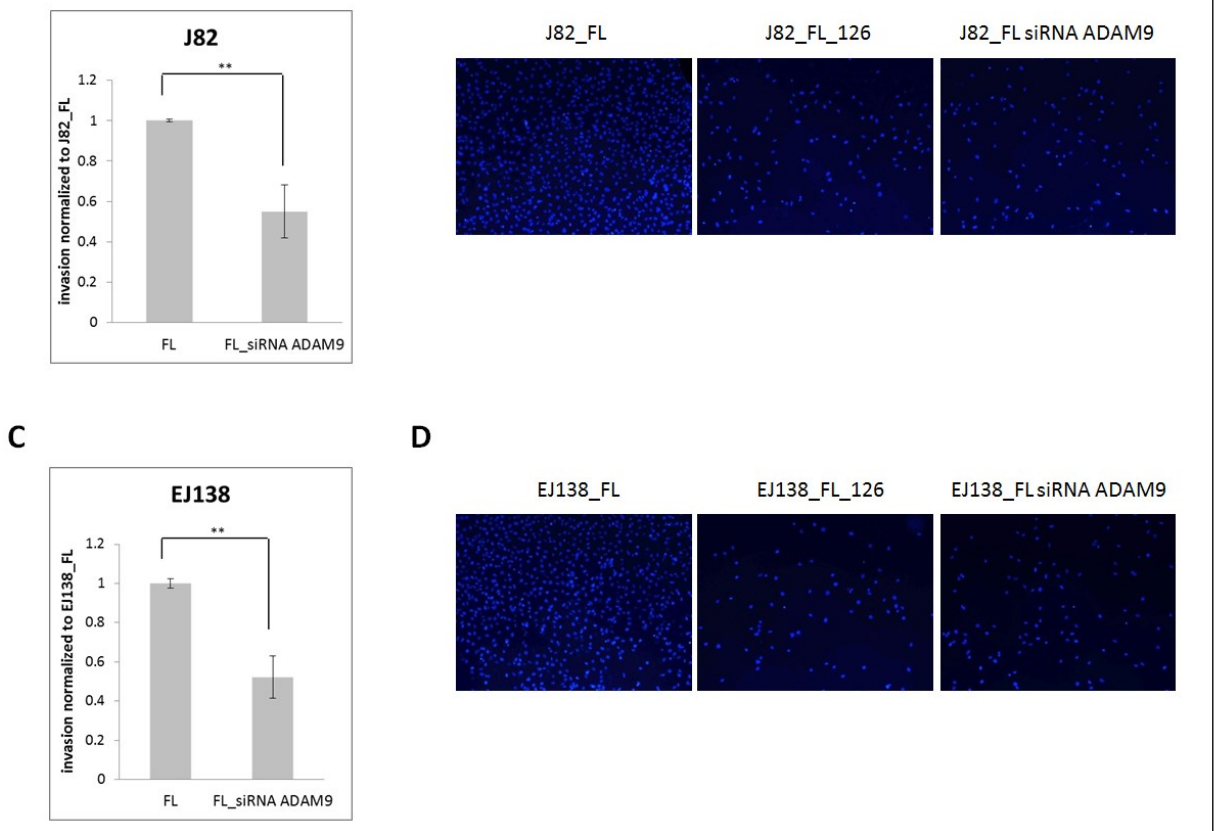

Figure 4.3 Effect of ADAM9 knock-down in cell invasion

Effect of ADAM9 knockdown (25nM) on J82_FL **(A)** and EJ138_FL **(C)** cell invasion. Representative images from FL cell invasion in J82_FL **(B)** and EJ138_FL **(D)**, stained with DAPI. *$p < 0.05$, **$p < 0.005$, by Student's T-Test.

3. Higher ADAM9 expression levels detected in invasive bladder tumors

Finally, to examine the prevalence of ADAM9 in human bladder tumors, we assayed the expression of ADAM9 in a panel of 103 UCs (**Table 8**). We observed that ADAM9 expression significantly correlated with tumor stage (**Figure 4.4A, B**). Indeed, the percentage of ADAM9 positive tumors increased with higher stage (from 44.8% of Ta tumors to 100% of T4 tumors; $p = 0.022$).

To determine whether ADAM9 has any prognostic significance, we performed Kaplan-Meier survival curve. High ADAM9 expression was associated with poor prognosis in patients, with

both a shorter disease-specific survival (DSS) and overall survival (OS). Patients with a positive ADAM9 phenotype had a median DSS of 52.5 months (95% CI 33.1 – 71.9 months), whereas patients with a negative phenotype did not reach median DSS ($p < 0.130$) (**Figure 4.4C**). Although not statistically significant, there is a clear trend that ADAM9 expression predicts a worse outcome for DSS. Similarly, patients displaying a positive ADAM9 phenotype had a significantly ($p = 0.019$) lower median OS (34.0 months, 95% CI 24.9 – 43.2 months) compared to patients presenting with an ADAM9 negative phenotype, for whom media OS was not reached at the current follow-up time (**Figure 4.4D**). However, multivariate analysis did not show ADAM9 to be an independent factor in affecting DSS or OS (data not shown). Therefore, stage could be a confounding factor in the Kaplan-Meier analyses since ADAM9 expression has a direct correlation with this pathological parameter. A larger cohort of patient data should be sampled to confirm this.

	Samples (%)
Stage (n = 103)	
Ta	29 (28.2%)
T1	25 (24.2%)
T2	22 (21.4%)
T3	20 (19.4%)
T4	7 (6.8%)
Final evolution (n = 88)	
AWOD	32 (36.4%)
AWD	22 (25.0%)
DOD	24 (27.2%)
DOOC	10 (11.4%)
Follow-up (range)	24.1 months (1.0-76.1)
ADAM9 positive phenotype (%)	65 (63.1%)

Table 8 Clinicopathological characteristics of patient cohort.

Outcome available in 88 out of 103 patients. AWOD: alive without disease, AWD: alive with disease, DOD: dead of disease, DOOC: dead of other causes.

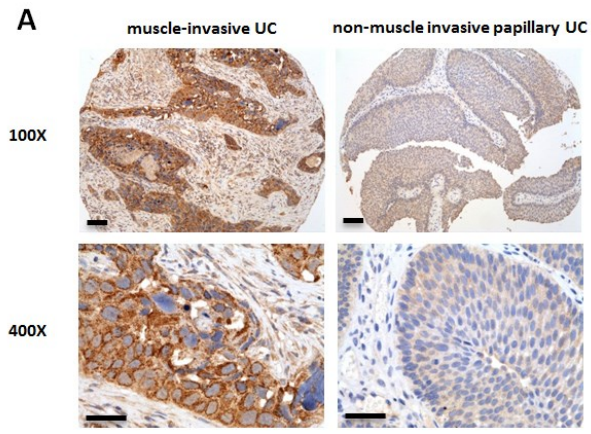

B

Stage	ADAM9 positive phenotype*
Ta	13 (44.8%)
T1	14 (56.0%)
T2	15 (68.2%)
T3	16 (80.0%)
T4	7 (100.0%)

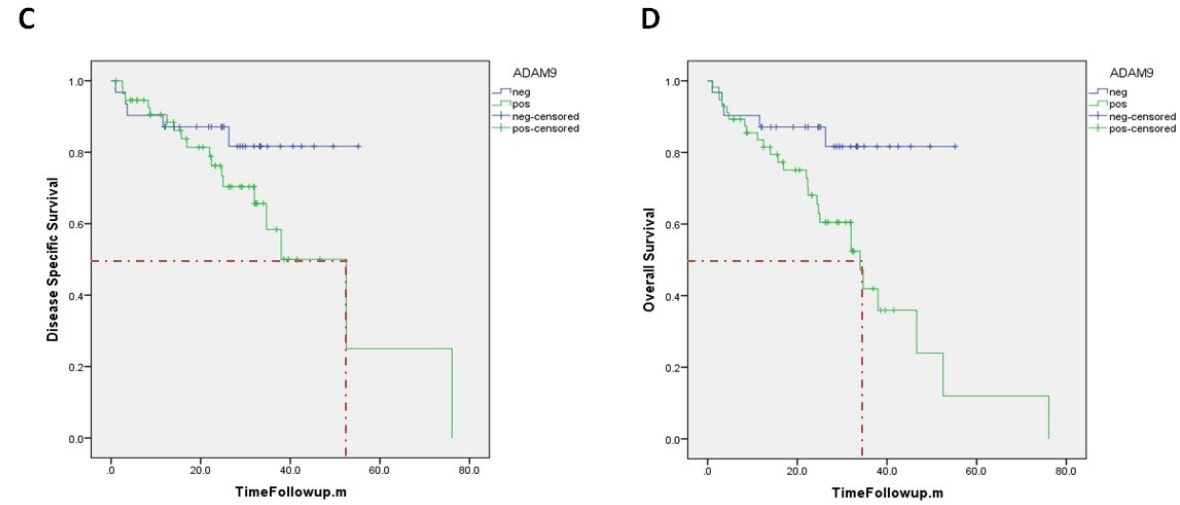

Figure 4.4 Prognostic significance of ADAM9 in bladder UCs

(A) Representative immunohistochemical analyses of ADAM9 in muscle-invasive UCs and non-muscle invasive papillary UCs. 100x, scalebar = 200μm; 400X, scalebar = 100μm. **(B)** Summary ofADAM9 IHC results, **p* = 0.022 by χ^2-distribution. Kaplan-Meier analysis for disease-specific survival (*p* < 0.130) **(C)** and overall survival (*p* = 0.019) **(D)** based on ADAM9 expression. Median survival is indicated by dotted red line.

Discussion

Metastatic bladder cancer manifests an extremely poor prognosis and is the primary cause of patient death [137]. While low miR-126 expression has been associated with an invasive phenotype in many tumors, we confirm this trend in bladder cancer and show for the first time the invasion suppressive activities of miR-126 in bladder cancer through ADAM9.

In this study, introduction of miR-126 in invasive bladder cancer cells caused a significant reduction in ADAM9 mRNA and protein levels. This is consistent with experiments in pancreatic cancer cells, where miR-126 was shown to directly target the 3'UTR of ADAM9 [86]. We showed previously in Chapter 3 that overexpression of miR-126 inhibited bladder cancer cell invasion (**Figure 3.10**). We were able to reproduce the same level of suppression of cancer cell invasion by a transient knock-down of ADAM9.

Upon ligand-induced receptor dimmerization, EGFR activation stimulates a multitude of signaling cascades that results in cell proliferation, survival, angiogenesis, and migration [168]. A prominent downstream pathway turned on by EGFR signaling is the PI3K/AKT axis. Although up-regulated PI3K/AKT signaling in invasive bladder cancer can be attributed to loss of function of PTEN, it is possible that enhanced EGFR activity also contributes to this anti-apoptotic pathway. EGFR signaling can be augmented either through activating mutations of the receptor or abnormal abundance of either receptor and/or ligand. While overexpression of EGFR has been identified in some bladder cancer cases, mutations in EGFR have not been reported [169]. Increased expression of ADAM9 would lead to increased ectodomain shedding of EGF, releasing the membrane-anchored ligand that would otherwise only engage with EGFRs on the same cell or neighboring cell to participate in paracrine signaling. This ultimately augments EGFR signaling and subsequently the PI3K/AKT network, as seen in muscle-invasive bladder UCs. Consistent with this, we observed elevated *ADAM9* levels in muscle-invasive bladder tumors compared to non-muscle invasive tumors.

While ADAM17 (tumor-necrosis factor α-converting enzyme) and ADAM10 (Kuzbanian) have been well studied, it is unclear what regulates ADAM9 expression [156,158]. It is possible that reduced levels of miR-126 in invasive bladder cancer de-repress ADAM9 expression, leading to its accumulation. Although our data suggest ADAM9 to have prognostic clinical implications, our cohort is too small to perform separate analyses in the different UC stages.

Therefore, further studies in larger cohorts of both non-muscle invasive and muscle-invasive UC should be performed to validate our findings.

Materials and Methods

Cell culture

J82 and EJ138 cell lines in addition to each cell line's derivations (e.g. FL, RL, FL_126) were generated and maintained as outlined in Chapter 3.

Quantitative real-time reverse transcription-PCR (qRT-PCR) expression profiling

QuantiTect Reverse Transcription Kit (Qiagen) was used to convert RNA to cDNA. QuantiTect PCR (Qiagen) was used to measure quantitative expression of *ADAM9* using the following sense and antisense primers: 5'-GTTCCTGTGGAGCAAAGAGC-3', 5'- CCAGCGTCCACCAAC-TTATT-3'. PCR assays were performed as described by the manufacturer using a Stratagene MX3005P PCR system. *ACTIN* was used for normalization.

Transient transfection and infection

Transient knock-down of ADAM9 was conducted using the ON-TARGET plus SMARTpool siRNA against ADAM9 (Thermo Scientific, Pittisburgh, PA) using Lipofectamine 2000 (Invitrogen). A final siRNA concentration of 25nM was used.

293FT cells were transfected with lentiviral or retroviral particles using Lipofectamine 2000 (Invitrogen). Media from 293FT 48 hours after transfection were collected to infect bladder tumor cell lines. Cell lines infected with FUW-Luc were subsequently infected with a pLemiRNA, and maintained using puromycin (0.5ug/ml) and geneticin (800ug/ml). Cell lines infected with pLPCX-Ren were maintained using puromycin (0.5ug/ml).

Invasion and luciferase assays

In-vitro invasion assays were carried out using BD BioCoat Matrigel Invasion Chambers (8-µm pore, BD Biosciences) in 6-well tissue culture plates according to manufacturer's protocol. Cells

were placed in serum-free media 24 hours prior to invasion assay set-up. Cells were seeded in a 50/50 mixture of FL to RL cell lines to a total amount of $1.5x10^6$ cells per well. Cells were suspended in serum-free media were added to each chamber and allowed to invade towards the underside of the chamber for 24h at 37˚C. After incubation, remaining cells inside the chamber were collected along with cells that have invaded the membrane. FL and RL activities were measured using the Dual-Glo Luciferase Assay System (Promega). FL signals were normalized to that of RL.

An alternate method of visualizing invasion was established by seeding only FL cells in 24-well tissue culture plates of BD BioCoat Matrigel Invasion Chambers (8-μm pore) at $5x10^4$ cells per well. Cells were placed in serum-free media 24 hours prior to invasion assay set-up. Cells were allowed to invade for 20h at 37˚C. After incubation, a Q-tip was used to remove remaining cells in the chamber. Each chamber was fixed in cold 4% paraformaldehyde and washed in PBS. The membrane at the bottom of each chamber was excised and mounted onto glass coverslips using ProLong-Gold with DAPI (Invitrogen).

Immunoblotting

For immunoblotting, cells were lysed in RIPA lysis buffer (Boston BioProducts) and protease inhibitor cocktail (Roche). Proteins were resolved by 4-20% SDS-PAGE and transferred to a nitrocellulose membrane. Blots were blocked with 5% non-fat dry milk and probed with primary antibodies, as follows: ADAM9 rabbit monoclonal (2099; Cell Signaling, Danvers, MA), and Actin rabbit monoclonal (A2066; Sigma-Aldrich). Horseradish peroxidase (HRP)-conjugated anti-rabbit antibody (GE healthcare, Pittsburgh, PA) was used. Reactive bands were visualized using ECL plus Western blotting detection reagents (GE Healthcare).

TMAs of bladder cancer samples

To perform ADAM9 expression analysis in UC, we used three different tissue microarrays (TMAs) from two different institutions (Columbia University, New York and Centro Nacional de Investigaciones Oncologicas (CNIO), Spain). The TMAs were built following institutional review board (IRB) approved protocols. From each specimen, triplicate tissue cores with diameters of 0.6mm were represented. Follow-up clinical information of the 103 patients included in these TMAs and their clinicopathological characteristics are summarized in **Table 8**. Tissues analyzed corresponded to different stages of bladder cancer from Ta to T4.

Immunohistochemistry analysis

Immunohistochemical analyses were performed on three TMAs (mentioned above) following standard avidin-biotin procedure as outlined in Chapter 2. To confirm the sensitivity and specificity of antibodies (ADAM9 rabbit monoclonal (2099; Cell Signaling)), we ran positive and negative controls in parallel with the TMAs. ADAM9 expression was characterized by cytoplasmic staining. Immunoreactivity was scored by assessing the percentage of cells that displayed a positive immunostaining profile [from undetectable (0%) to homogeneous expression (100%)], as well as the intensity of expression [from negative (0) to high intensity (2)]. Average values of the representative cores from each arrayed sample were obtained and only cases that displayed a high intensity of expression in more than 10% of the tumor cells were considered positive for statistical purposes.

Statistical analysis

The associations between protein expression values and stage were assessed using the χ^2 test. The association of ADAM9 expression with disease-specific survival and overall survival were assessed using the log-rank test. Survival curves were plotted using standard Kaplan-Meier methodology. A two-sided value of $p<0.05$ was considered statistically significant. Statistical analyses were carried out with SPSS v19.0 (SPSS Inc., IL).

5. Chapter 5: Conclusions and Future Directions

A common signature clusters CIS with normal UM cells

Bladder tumors are not homogeneous. The development of low-grade superficial tumors with frequent recurrence verses high-grade tumors that often become invasive follows distinct courses of tumor progression. Similarly, normal bladder urothelium contains two phenotypically different cell types. Contrary to the process by which epithelium development in the skin occurs, whereby stem cells reside in the basal layer and differentiates into subsequent superficial layers, UM and B/i cells in the urothelium may stem from separate progenitors. Unlike the pseudo-stratified urothelium, the epidermis maintains p63 expression throughout all layers, and there is no biomarker that can distinguish one cell from another. Rather, the urothelium shares more similarities with epithelium of the breast and prostate. Superficial luminal cells in the breast and prostate, like UM cells in the bladder, are negative for p63 expression, while basal-like myoepithelial cells express p63, similar to the B/i cells in the bladder [170,171]. *In vitro* colony assays have identified three independent progenitor groups: luminal-restricted, myoepithelial-restricted, and bipotent [172]. While luminal and myoepithelial developed into the respective cell types, the bipotent collection of cells formed luminal clusters surrounded by myoepithelial cells [172]. Flow cytometry-based approaches isolated a multipotent mammary population in adult mouse that was able to form an entire mammary gland *in vivo* [173]. Immunohistochemical analyses of these putative mammary epithelial stem cells revealed discrete cell fractions that expressed either basal (smooth muscle actin and CK4) or luminal (CK18) biomarkers, but not both [173]. This suggests a hierarchical structure by which a bipotential progenitor develops into lineage-restricted progenitors that then give rise to luminal and myoepithelial cells. While adult mammary tissue has a large regenerative potential, where it can expand and regress during pregnancy and each menstrual cycle, the human prostate epithelium is normally quiescent [171].

The prostate regresses following castration, but androgen treatment can restore the organ to its original size [171]. Evidence exists for both a basal and a luminal location for prostate epithelial stem cell. A fraction of prostate epithelial cells expressing basal cell markers was isolated by flow cytometry and shown to reconstitute tubular structures *in vivo* that contained both basal and luminal cell types [174]. Alternatively, lineage tracing studies identified a luminal epithelial cell population that express the homeobox gene *Nkx3.1*, the earliest marker for prostate epithelium, in the absence of androgens [175]. These cells gave rise to both basal (CK5, p63) and luminal (CK18) cells *in vivo* [175]. These studies suggest that prostate epithelial lineage-specific progenitors may maintain some bipotentiality to develop into the other cell type. As seen in breast and prostate progenitor development, a similar situation may exist in the bladder urothelium, where luminal-like UM cells and B/i cells are derived from independent precursors. Understanding normal development is central in understanding the origin of bladder cancer.

To our knowledge, we are the first to examine miRNA expression in pure populations of UM and B/i cells. Five miRNAs were differentially expressed between UM and B/i cells; *in situ* hybridization validated the expression of miR-133a and miR-139-3p in UM cells and miR-142-3p in B/i cells. It remains unknown whether these miRNAs affect urothelial cell-fate determination or are a by-product of cell differentiation. One method to determine the role of these miRNAs is by lineage tracing. In theory, cells that express the miRNA of interest can be marked using a genetically engineered mouse line in which Cre recombinase is driven by the endogenous promoter for the host gene the miRNA resides on. The Cre-expressing mouse can be crossed with a mouse carrying a reporter, such as green fluorescent protein (GFP), whose expression is turned on following Cre-induced recombination. GFP is then expressed wherever there is Cre recombinase. Cells that express the miRNA promoter should be green. A preliminary three-layered urothelium develops by embryonic day 15 in mice [176]. The presence of green cells during urothelial formation and prior to differentiation into UM and B/i layers would suggest that

the miRNA is involved in cell-fate determination. On the other hand, if cells only turn green after a well-defined urothelium has formed, then the miRNA is likely a consequence of differentiation.

While the reporter would reflect endogenous levels of miRNA expression, one drawback is that knock-in of Cre recombinase effectively generates a null allele for the miRNA of interest and disrupts gene dosage. Another limitation with this approach is the lack of definitive miRNA promoters. While *mir-139-3p* is located in the intron of *PDE2A* (phosphodiesterase 2A, cGMP-stimulated) and may be co-transcribed with its host gene, recent studies suggest that up to one-third of intronic miRNAs (i.e. intragenic) do not share the same transcription initiation regions as their host [177,178]. *mir-133a* and *mir-142-3p* reside in non-coding transcripts, further signifying that miRNAs may have their own promoters. Chromatin immunoprecipitation experiments characterized putative miRNA transcription initiation sites as nucleosome-free regions as far as 40kb upstream of the pre-miRNA sequence [177,178]. However, there is no conclusive evidence of where a miRNA promoter may be located and further studies are needed in elucidating transcriptional regulation of miRNAs. Additionally, assuming that *mir-139-3p* is co-transcribed with *PDE2A*, another problem is how to separate the effect of the gene product from that of the miRNA if both are driven by the same promoter. To tease apart the role of miR-139-3p from PDE2A in mice, *mir-139-3p* can be removed, since it is located in an intron, without disturbing *Pde2a* expression, in a manner similar to deleting only the *mir-15a~16* cluster from its host gene *Dleu2* [71].

An alternative strategy to lineage tracing is to conditionally knock-down the miRNA of interest in the bladder, as previously described with *mir-21* knock-out studies [66]. If the deletion of *mir-142-3p* produces the same bladder phenotype as the *p63*$^{-/-}$ mice, where only the UM layer exists, it would suggest a differentiation role for the miRNA. However, a lack of phenotype does not necessarily imply the miRNA as no role in determining cell-fate. Compensatory mechanisms may be activated to correct for the loss of function of the miRNA. This is seen in mice that still produce urothelial plaques even in absence of UPKIII. *UPKIII* deletion induced a

five-fold increase in *UPKIb* expression, and two-fold increase in *UPKIa* and *UPKII* expression [113]. Therefore, expression levels of other B/i-specific miRNAs, such as miR-199b-5p and miR-221, should be examined following *mir-142-3p* knock-out in the bladder to uncover any functional redundancies.

Another aspect of our study was to investigate the relationship between CIS and normal urothelium. CIS tumors are high-grade and frequently become invasive. Unfortunately, unlike papillary tumors that protrude into the lumen, CIS is embedded within the urothelium and is difficult to detect in cystoscopies. Although gene expression abnormalities in CIS have been reported [179], alterations in miRNA expression between normal urothelium and CIS were unknown. In line with previous reports that miRNAs can classify tissues based on lineage, our study revealed that cluster analysis of miRNA expression grouped samples based on developmental origin (endoderm versus mesoderm). While CIS is epithelial in origin and is predicted to cluster separately from the stromal compartment, it is highly unexpected that CIS would display the closest resemblance to normal UM cells in miRNA expression. Gene expression, on the other hand, segregated samples based on histological variation. More than half of the genes differentially expressed across CIS, UM, and B/i were up-regulated in CIS and were associated with pathways involved in cancer. Given the high degree of similarity between CIS and UM cell, both in genetic profile and histology, and that the UM cell is the only normal cell in the body that can be multi-nucleated, we postulate that CIS may arise from transformation of UM-like precursors (**Figure 5.1**). Interestingly, miRNA expression levels across different UC stages and grades shared the same pattern as those observed in UM and B/i cells. Higher levels of B/i specific miRNAs (miR-142-3p, miR-199b-5p, and miR-221) were observed in papillary tumors relative to other tumor stages, while UM specific miRNAs (miR-133a and miR-139-3p) were generally expressed at greater amounts in CIS and muscle-invasive (T2) tumors (**Figure 5.2**).

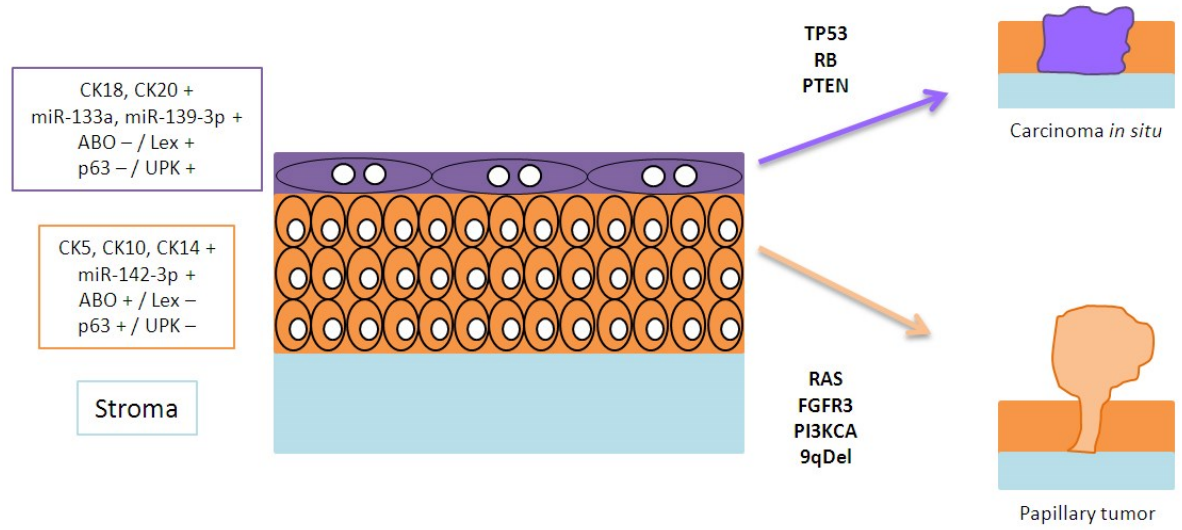

Figure 5.1 A proposed model of urothelial development and tumorigenesis

Different urothelial progenitor cells may give rise to two independent cell lineages, UM and B/i. UM cells are characterized by the expression of CK18, CK20, Lewis X factor, and UPK. In contrast, B/i cells express CK5, CK10, CK14, mature A/B blood group antigens, and p63. Transformation of UM and B/i precursors may result in the development of CIS and papillary tumors, respectively.

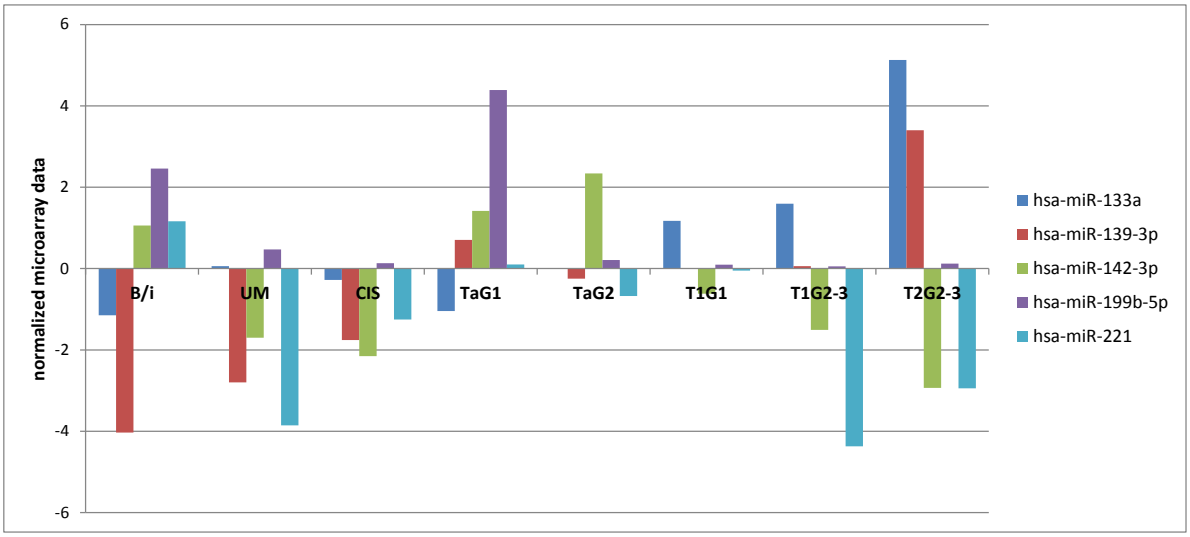

Figure 5.2 Expression levels of five urothelium-specific miRNAs in UCs

miRNA levels in UC tumors are acquired from miRNA microarray results.

Transgenic mouse models may be used to test the our hypothesis that the two pathways of bladder tumorigenesis evolve from oncogenic changes acquired by distinct UM and B/i precursors. The aforementioned *p63*$^{-/-}$ mice is non-viable due to the lack of epidermis, however, a small bladder exists that contains a single layer of UM-like cells [13,111]. A UPKII-driven Cre recombinase mouse can be crossed with a *p63*$^{flox/flox}$ to conditionally delete *p63* in the bladder. Provided that the bladder is still functional, conditional *p63*$^{-/-}$ mice can be fed *N*-butyl-*N*-(-4-hydroxybutyl)nitrosamine (BBN) or *N*-methyl-*N*-nitrosourea (MNU), two carcinogens commonly used to induce UCs *in vivo* [180]. Following our model, since B/i cells do not form in *p63*$^{-/-}$ mice, BBN or MNU should only induce the formation of CIS tumors. However, BBN caused primarily muscle-invasive tumors in mice [181], and while treatment with MNU produced multi-focal lesions in rats that were mainly non-muscle invasive tumors, further experimentation is needed to determine its effect in mice [182]. Therefore, development of CIS tumors in conditional *p63*$^{-/-}$ mice from BBN may not provide conclusive evidence that UM cells give use to CIS. This can be addressed by examining whether papillary tumors form in *UPKIII*$^{-/-}$ and *ARF*$^{-/-}$ mice, discussed below.

UPKII$^{-/-}$ and *UPKIII*$^{-/-}$ mice developed a urothelium that lacked UM cells. While *UPKII*$^{-/-}$ mice died approximately 10 days after birth from renal defects [114], *UPKIII*$^{-/-}$ mice enjoyed a normal lifespan albeit with a compromised leaky urothelium due to reduction in urothelial plaques [113]. Following our hypothesis, BBN- or MNU-induced tumor formation in *UPKIII*$^{-/-}$ should lead to the development of only papillary tumors. Alternatively, bladder tumorigenesis in *ARF*$^{-/-}$ mice may also be used to test our model. p19^{ARF} expression is confined to UM cells (unpublished data). *ARF*$^{-/-}$ mice developed a broad range of tumors spontaneously, including fibrosarcoma, salivary gland carcinoma, and lymphoma [183]. However, while bladder abnormalities were not noted, bladder histology in these mice was not characterized. It would be interesting to determine whether UM cells are present in *ARF*$^{-/-}$ mice. If only B/i cells subsist,

then treatment of *ARF*$^{-/-}$ mice with BBN or MNU should give rise to papillary tumors in the bladder, according to our model.

In summary, our findings support a novel model of urothelial tumorigenesis in which UM and B/i originate from different cell lineages, which may account for the divergent pathways of bladder tumorigenesis. Further studies are needed to identify and characterize these putative urothelial progenitor cells in order to understand their contribution to bladder tumorigenesis.

Characterization of miRNAs differentially expressed between muscle-invasive and non-muscle invasive UCs

The management of bladder cancer requires intensive physician-patient surveillance and costly procedures due to the high risk of recurrence in superficial papillary tumors, the most common form at initial presentation, thus making this one of the most expensive neoplasms to treat [16]. While the majority of high-grade CIS tumors progress to invade the musculature because it shares many genomic alterations as muscle-invasive tumors, it remains largely unknown the genetic processes that promote the progression of low-grade papillary tumors to a muscle-invasive phenotype. Patients with muscle-invasive and metastatic bladder tumors have a very poor prognosis. Therefore, identifying miRNAs and genes that participate in the transition from papillary to invasive tumors is necessary for development of effective therapies.

In line with previous studies [122,184], we found reduced expression of miR-200 family members (miR-200c, miR-141, miR-429) in invasive tumors. Re-expression of miR-200c was able to decrease cell invasion by two-fold in invasive bladder cancer cells. Of note, concomitant expression of the three miR-200 family members produced a cumulative effect in J82 and decreased cell invasion by four-fold. This could be explained by anti-proliferative effects of miR-429 and miR-200c in J82 cells. In addition, the unique molecular profiles of J82 and EJ138 could account for the differences observed in each cell line's response to variations in the

expression of miR-200 family members. For instance, immunohistochemical data in our lab show that J82 has the normal wild-type HRAS while EJ138 has the activated mutant $HRAS^{V12}$.

We also identified two miRNAs previously unassociated with bladder cancer with opposing effects: miR-198 and miR-126. miR-198 is located on chromosome 3q (3q13.33), a fragment that is amplified in up to 24% of UCs [141]. miR-198 was up-regulated in muscle-invasive UCs and its overexpression in non-invasive bladder cancer cells, RT4 and RT112, increased cell invasion by two- to six-fold. A combination of miR-200 family knock-down and miR-198 overexpression produced a greater increase in cell invasion than either condition alone. Interestingly, a statistically significant increase in BFTC-905 cell invasion was only observed with concurrent miR-200 family knock-down and miR-198 overexpression. This is the first reporting of a tumor invasive role of miR-198 *in vitro* (**Figure 5.3**). Since invasion is a multi-genic phenotype, it is unclear whether miR-198 and miR-200 operate in close proximity in a signaling pathway. This is reflected in the results from bladder cancer cell lines. While the effect of miR-198 addition and miR-200 knock-down appear additive in RT4, suggesting the miRNAs may operate in separate pathways, the increases in invasion in BFTC-905 and RT112 are non-additive, which is indicative of the miRNAs functioning in the same pathway. It is unlikely that miR-198 and miR-200 share the same gene targets since they affect invasion in opposite ways. Additional *in vitro* experiments should be done to determine if inhibition of miR-198 in invasive cells can decrease invasion, and whether an additive or a cooperative effect with the miR-200 family is observed (i.e. knocking-down miR-198 in J82_FL_200c cells).

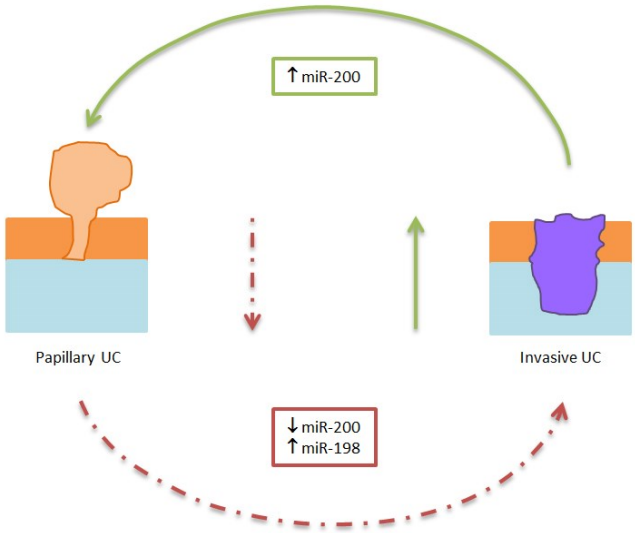

Figure 5.3 Potential regulation of invasion by miR-200 and miR-198 in bladder UCs

An increase in the expression of miR-200 family members is sufficient to reduce invasion of bladder cancer cells. Down-regulation of miR-200 promotes invasion of non-invasive bladder cancer cells, an effect that is augmented by addition of miR-198.

Contrary to miR-198, miR-126 was down-regulated in muscle-invasive UCs and its restoration in invasive bladder cancer cells decreased cell invasion by two-fold. miR-126 resides on chromosome 9q, a region that frequently undergoes heterozygous deletion in superficial papillary tumors [16,20]. It is unknown whether both copies of the 9q region are lost in muscle-invasive UCs. In addition to suppressing invasion, miR-126 also reduces J82 proliferation. Both roles have been observed in tumor cells previously; miR-126 inhibits pancreas and liver cancer cell invasion *in vitro* with no effect on proliferation [86,87] and causes regression of overall tumor growth in an orthotopic breast cancer model [85]. Future experiments can be done to investigate apoptotic effects of miR-126 and if inhibition of miR-126 promotes invasion in non-invasive bladder cancer cells.

To examine whether miR-198 or miR-126 promotes tumor invasion *in vivo*, orthotopic transurethral inoculation of miRNA-overexpressing cell lines into nude female mice can be performed following previously published protocols [185,186] (**Figure 5.4**). Since the cells

express firefly luciferase, tumor formation and development can be monitored in real-time using non-invasive bioluminescent imaging as previously described [186]. RT4 behaves as a non-invasive papillary tumor in mice [187]. Current studies in our lab is ongoing to characterize *in vivo* the tumor forming capacity of BFTC-905, RT112, J82 and EJ138. Based on *in vitro* results, RT4_FL_198, BFTC-905_FL_198, and RT112_FL_198 are expected to form invasive and metastatic tumors. Conversely, miR-126 is expected to revert J82 and EJ138 to a non-invasive phenotype. If orthotopic experiments confirm the oncogenic and tumor suppressive roles of miR-198 and miR-126, respectively, the next step would be to examine whether pharmacological manipulations of miRNA expression in an invasive bladder cancer model can prevent invasion and metastasis.

There are two transgenic models that reproduce the development of invasive and metastatic bladder cancer in mice: the bladder-specific double knock-out of *p53* and *Pten* via surgical delivery of Cre recombinase [38], and the inactivation of *p53* and *Rb* through UPKII-driven expression of SV40T [134]. Similar to the silencing of miR-10b in a mouse mammary tumor model using antagomirs [89], an antagomir against miR-198 can be designed and administered intravenously into the metastatic murine models described. Inhibition of miR-198 should prevent tumor invasion. Likewise, systemic delivery of lipid-based synthetic miR-126 should also prevent tumor invasion. Construction of a miR-126 mimetic can follow as previously described in the transgenic lung cancer model where miR-34a was complexed with a neutral-lipid emulsion [99].

In conclusion, we have identified two miRNAs – miR-198 and miR-126 – involved in the progression of bladder UCs. Increased miR-198 is associated with certain cancers, however, we are the first to show an oncogenic effect of miR-198 *in vitro*. Furthermore, we demonstrate a putative interaction between miR-198 and the miR-200 family. While a tumor suppressive role of miR-126 has been observed in other cancers, we are the first to provide evidence of such a role

in bladder cancer. Future experiments to investigate the therapeutic potential of these miRNAs *in vivo* are warranted.

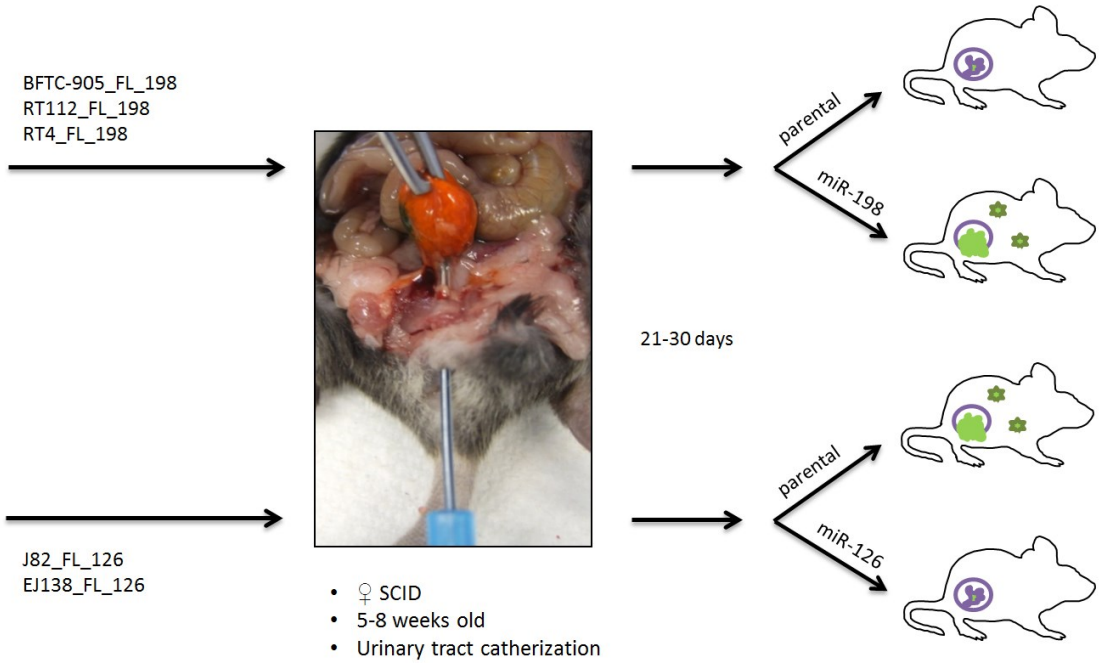

Figure 5.4 Orthotopic invasion mouse model

Five to eight weeks old female SCID mice can be used. Parental and cell lines overexpressing miR-198 or miR-126 would be injected into the bladder via the urethra with an angiocatheter. Inoculated cells are visualized in real-time through bioluminescent imaging following intraperitoneal administration of luciferin to monitor tumor formation and invasion *in vivo*. Distinct bioluminescent foci at distant sites are indicative of secondary metastatic tumor formation.

miR-126 targets ADAM9 in bladder cancer cells to inhibit invasion

Our mRNA expression array identified increased ADAM9 in muscle-invasive tumors compared to non-muscle invasive papillary tumors. This is consistent with other findings that report ADAM9 is overexpressed in invasive carcinomas [162-164,166]. In a separate panel of 103 bladder tumors, we observed high ADAM9 expression in 82.7% of muscle-invasive bladder tumors (>T2) and only 50.4% of non-muscle invasive papillary tumors (Ta and T1). Moreover,

for the first time, we observed ADAM9 expression to be a marker of poor prognosis in UC patients. Patients with elevated levels of ADAM9 displayed a shorter overall survival and disease-specific survival.

ADAM9 is a predicted target of miR-126 *in silico* and this has been verified in pancreatic cells [86]. Inhibition of ADAM9 by siRNA in invasive bladder cancer cells suppresses cell invasion by two-fold. To further assess whether miR-126 prevents acquisition of invasive traits through suppressing ADAM9, restoration of functional ADAM9 should reverse the effects of miR-126 and reestablish cell invasive properties. As such, a lentiviral ADAM9 construct can be introduced into J82_FL_126 and EJ138_FL_126 cells. Re-expression of ADAM9 in miR-126 overexpressing cells should increase invasion back to parental cell levels in the invasion luciferase assay. Similarly, if miR-126 reduces tumor invasion and metastasis in the mouse orthotopic model, overexpression of ADAM9 should revert J82_FL_126 and EJ138_FL_126 tumor cells back to an invasive phenotype.

Another method to verify the invasive effects of ADAM9 would be to administer selective ADAM9 inhibitors into J82 and EJ138 cells. To attribute the potential decrease in invasion to ADAM9, the ADAM9 siRNA knock-down cells, J82_FL_126 cells, and EJ138_FL_126 cells should not be affected by inhibitor treatment. ADAMs are zinc proteases, therefore many ADAM inhibitors contain a zinc-binding group, usually hydroxamate, to chelate the catalytic zinc ion in the active site [156]. Several specific inhibitors to ADAM17 and ADAM10 have been described. Compound INCB3619 (Incyte Corporation) has been shown to block the release of ADAM17 and ADAM10 HER ligands: TGF-α, HB-EGF, amphiregulin, and heregulin [188]. INCB3619 has also shown to synergize with paclitaxel and cisplatin in mouse xenograft models of breast cancer and head and neck cancer, respectively [188]. In a separate study, INCB3619 used in combination with gefitinib or paclitaxel was able to reduce tumor growth in mice bearing non-small cell lung cancer xenografts [189]. INCB7839 (Incyte Corporation), a similar compound to INCB3619, was evaluated in a 28-day phase 1b study to treat patients with chemorefractory

cancers [190]. Plasma levels of HER and EGFR ligands heregulin and TGF-α, both associated with poor prognosis, were reduced in patients. Six out of 20 subjects displayed disease stabilization two months after therapy. The drug was generally well tolerated with minor side effects (mild diarrhea) and no significant toxicities [190]. Another selective inhibitor of ADAM17, WAY-022 (Wyeth-Aherst) suppressed DNA replication and cell proliferation in colorectal cancer cells [191].

Four compounds have been shown to target ADAM9. The mouse prodomain of ADAM9 (proA9; amino acids 24-204) is a competitive inhibitor of human ADAM9 [192], while Rav-18 is a humanized monoclonal antibody against ADAM9 (Raven Biotechnologies, now a subsidiary of Macrogenics, San Francisco) [193]. While these two compounds are highly specific, they are not commercially available. The other two ADAM9 inhibitors, CGS27023 (GlaxoSmithKline, Stevenage, UK) and batimastat (Sigma-Aldrich), are broad-spectrum MMP inhibitors [194]. These are not as desirable because they are associated with musculoskeletal side effects and may inadvertently target protective MMPs such as MMP3 and MMP8, the inhibition of which could have pro-tumorigenic effects [195]. Unlike other members of the ADAMs family, such as ADAM17 and ADAM10, ADAM9 is not inhibited by tissue inhibitors of metalloproteinases (TIMPs) [194]. Therefore, CGS27023 and batimastat can be administered into J82 and EJ138 as a proof-of-principle experiment to test whether drug-induced inhibition of ADAM9 reduces invasion. However, use specific ADAM9 inhibitors, proA9 and Rav-18, would be preferred in clinical trials.

Another aspect to examine is tumor-stromal interdependence. It has been suggested that MMPs are secreted by stromal cells surrounding the tumor as opposed to the invading tumor [195]. For instance, ADAM9 expression was localized to stromal liver myofibroblasts, particularly at the invasive front, in human liver metastases, and secretion of soluble ADAM9 by hepatic stellate cells promoted colon cancer cell invasion *in vitro* [165]. We detected ADAM9 expression predominantly in tumor cells, but the surrounding stroma also exhibited some

ADAM9 positivity. Therefore, systemic delivery of a specific ADAM9 inhibitor in the invasive bladder orthotopic model should also be performed. Based on our studies, we provide a rationale for the therapeutic inhibition of ADAM9 in aggressive UCs.

References

1. Larsen WJ (1993) Development of the Urogenital System. Human Embryology: Churchill Lingstone Inc. pp. 235-263.
2. Wu XR, Lin JH, Walz T, Haner M, Yu J, et al. (1994) Mammalian uroplakins. A group of highly conserved urothelial differentiation-related membrane proteins. J Biol Chem 269: 13716-13724.
3. Harnden P, Eardley I, Joyce AD, Southgate J (1996) Cytokeratin 20 as an objective marker of urothelial dysplasia. Br J Urol 78: 870-875.
4. Sheinfeld J, Reuter VE, Fair WR, Cordon-Cardo C (1992) Expression of blood group antigens in bladder cancer: current concepts. Semin Surg Oncol 8: 308-315.
5. Di Como CJ, Urist MJ, Babayan I, Drobnjak M, Hedvat CV, et al. (2002) p63 expression profiles in human normal and tumor tissues. Clin Cancer Res 8: 494-501.
6. Schulz WA (2006) Understanding urothelial carcinoma through cancer pathways. Int J Cancer 119: 1513-1518.
7. Kaneko H, Watanabe H, Hosokawa Y, Urata Y, Hattori T, et al. (1984) The presence of G1 and G2 populations in normal epithelium of rat urinary bladder. Basic Appl Histochem 28: 41-57.
8. Fierabracci A, Caione P, Di Giovine M, Zavaglia D, Bottazzo GF (2007) Identification and characterization of adult stem/progenitor cells in the human bladder (bladder spheroids): perspectives of application in pediatric surgery. Pediatr Surg Int 23: 837-839.
9. Nguyen MM, Lieu DK, deGraffenried LA, Isseroff RR, Kurzrock EA (2007) Urothelial progenitor cells: regional differences in the rat bladder. Cell Prolif 40: 157-165.
10. Potten CS, Morris RJ (1988) Epithelial stem cells in vivo. J Cell Sci Suppl 10: 45-62.
11. Kurzrock EA, Lieu DK, Degraffenried LA, Chan CW, Isseroff RR (2008) Label-retaining cells of the bladder: candidate urothelial stem cells. Am J Physiol Renal Physiol 294: F1415-1421.
12. Zhang H, Lin G, Qiu X, Ning H, Banie L, et al. (2012) Label retaining and stem cell marker expression in the developing rat urinary bladder. Urology 79: 746 e741-746.
13. Karni-Schmidt O, Castillo-Martin M, Shen TH, Gladoun N, Domingo-Domenech J, et al. (2011) Distinct expression profiles of p63 variants during urothelial development and bladder cancer progression. Am J Pathol 178: 1350-1360.
14. Cohen SM (1983) Promotion in urinary bladder carcinogenesis. Environ Health Perspect 50: 51-59.
15. Johansson SL, Cohen SM (1997) Epidemiology and etiology of bladder cancer. Semin Surg Oncol 13: 291-298.
16. Cordon-Cardo C (2008) Molecular alterations associated with bladder cancer initiation and progression. Scand J Urol Nephrol Suppl: 154-165.
17. Jemal A, Siegel R, Xu J, Ward E (2010) Cancer statistics, 2010. CA Cancer J Clin 60: 277-300.
18. Ferlay J, Shin HR, Bray F, Forman D, Mathers C, et al. (2010) Estimates of worldwide burden of cancer in 2008: GLOBOCAN 2008. Int J Cancer 127: 2893-2917.
19. Knowles MA, Platt FM, Ross RL, Hurst CD (2009) Phosphatidylinositol 3-kinase (PI3K) pathway activation in bladder cancer. Cancer Metastasis Rev 28: 305-316.
20. Goebell PJ, Knowles MA (2010) Bladder cancer or bladder cancers? Genetically distinct malignant conditions of the urothelium. Urol Oncol 28: 409-428.
21. Chapman EJ, Harnden P, Chambers P, Johnston C, Knowles MA (2005) Comprehensive analysis of CDKN2A status in microdissected urothelial cell carcinoma reveals potential

haploinsufficiency, a high frequency of homozygous co-deletion and associations with clinical phenotype. Clin Cancer Res 11: 5740-5747.
22. Orlow I, LaRue H, Osman I, Lacombe L, Moore L, et al. (1999) Deletions of the INK4A gene in superficial bladder tumors. Association with recurrence. Am J Pathol 155: 105-113.
23. Simoneau M, LaRue H, Aboulkassim TO, Meyer F, Moore L, et al. (2000) Chromosome 9 deletions and recurrence of superficial bladder cancer: identification of four regions of prognostic interest. Oncogene 19: 6317-6323.
24. Cappellen D, De Oliveira C, Ricol D, de Medina S, Bourdin J, et al. (1999) Frequent activating mutations of FGFR3 in human bladder and cervix carcinomas. Nat Genet 23: 18-20.
25. Rieger-Christ KM, Mourtzinos A, Lee PJ, Zagha RM, Cain J, et al. (2003) Identification of fibroblast growth factor receptor 3 mutations in urine sediment DNA samples complements cytology in bladder tumor detection. Cancer 98: 737-744.
26. Sibley K, Stern P, Knowles MA (2001) Frequency of fibroblast growth factor receptor 3 mutations in sporadic tumours. Oncogene 20: 4416-4418.
27. Lopez-Knowles E, Hernandez S, Malats N, Kogevinas M, Lloreta J, et al. (2006) PIK3CA mutations are an early genetic alteration associated with FGFR3 mutations in superficial papillary bladder tumors. Cancer Res 66: 7401-7404.
28. Jebar AH, Hurst CD, Tomlinson DC, Johnston C, Taylor CF, et al. (2005) FGFR3 and Ras gene mutations are mutually exclusive genetic events in urothelial cell carcinoma. Oncogene 24: 5218-5225.
29. Buyru N, Tigli H, Ozcan F, Dalay N (2003) Ras oncogene mutations in urine sediments of patients with bladder cancer. J Biochem Mol Biol 36: 399-402.
30. Czerniak B, Cohen GL, Etkind P, Deitch D, Simmons H, et al. (1992) Concurrent mutations of coding and regulatory sequences of the Ha-ras gene in urinary bladder carcinomas. Hum Pathol 23: 1199-1204.
31. Zhang ZT, Pak J, Huang HY, Shapiro E, Sun TT, et al. (2001) Role of Ha-ras activation in superficial papillary pathway of urothelial tumor formation. Oncogene 20: 1973-1980.
32. Cordon-Cardo C, Dalbagni G, Saez GT, Oliva MR, Zhang ZF, et al. (1994) p53 mutations in human bladder cancer: genotypic versus phenotypic patterns. Int J Cancer 56: 347-353.
33. Cordon-Cardo C (1998) Cell cycle regulators as prognostic factors for bladder cancer. Eur Urol 33 Suppl 4: 11-12.
34. Cairns P, Proctor AJ, Knowles MA (1991) Loss of heterozygosity at the RB locus is frequent and correlates with muscle invasion in bladder carcinoma. Oncogene 6: 2305-2309.
35. Cordon-Cardo C, Wartinger D, Petrylak D, Dalbagni G, Fair WR, et al. (1992) Altered expression of the retinoblastoma gene product: prognostic indicator in bladder cancer. J Natl Cancer Inst 84: 1251-1256.
36. Aveyard JS, Skilleter A, Habuchi T, Knowles MA (1999) Somatic mutation of PTEN in bladder carcinoma. Br J Cancer 80: 904-908.
37. Cairns P, Evron E, Okami K, Halachmi N, Esteller M, et al. (1998) Point mutation and homozygous deletion of PTEN/MMAC1 in primary bladder cancers. Oncogene 16: 3215-3218.
38. Puzio-Kuter AM, Castillo-Martin M, Kinkade CW, Wang X, Shen TH, et al. (2009) Inactivation of p53 and Pten promotes invasive bladder cancer. Genes Dev 23: 675-680.
39. Li M, Zhang ZF, Reuter VE, Cordon-Cardo C (1996) Chromosome 3 allelic losses and microsatellite alterations in transitional cell carcinoma of the urinary bladder. Am J Pathol 149: 229-235.
40. Presti JC, Jr., Reuter VE, Galan T, Fair WR, Cordon-Cardo C (1991) Molecular genetic alterations in superficial and locally advanced human bladder cancer. Cancer Res 51: 5405-5409.

41. Clarke MF, Dick JE, Dirks PB, Eaves CJ, Jamieson CH, et al. (2006) Cancer stem cells--perspectives on current status and future directions: AACR Workshop on cancer stem cells. Cancer Res 66: 9339-9344.
42. Chan KS, Espinosa I, Chao M, Wong D, Ailles L, et al. (2009) Identification, molecular characterization, clinical prognosis, and therapeutic targeting of human bladder tumor-initiating cells. Proc Natl Acad Sci U S A 106: 14016-14021.
43. He X, Marchionni L, Hansel DE, Yu W, Sood A, et al. (2009) Differentiation of a highly tumorigenic basal cell compartment in urothelial carcinoma. Stem Cells 27: 1487-1495.
44. Lee RC, Feinbaum RL, Ambros V (1993) The C. elegans heterochronic gene lin-4 encodes small RNAs with antisense complementarity to lin-14. Cell 75: 843-854.
45. Griffiths-Jones S, Saini HK, van Dongen S, Enright AJ (2008) miRBase: tools for microRNA genomics. Nucleic Acids Res 36: D154-158.
46. Kozomara A, Griffiths-Jones S (2011) miRBase: integrating microRNA annotation and deep-sequencing data. Nucleic Acids Res 39: D152-157.
47. Molnar A, Schwach F, Studholme DJ, Thuenemann EC, Baulcombe DC (2007) miRNAs control gene expression in the single-cell alga Chlamydomonas reinhardtii. Nature 447: 1126-1129.
48. Zhang W, Dahlberg JE, Tam W (2007) MicroRNAs in tumorigenesis: a primer. Am J Pathol 171: 728-738.
49. He L, Hannon GJ (2004) MicroRNAs: small RNAs with a big role in gene regulation. Nat Rev Genet 5: 522-531.
50. Esquela-Kerscher A, Slack FJ (2006) Oncomirs - microRNAs with a role in cancer. Nat Rev Cancer 6: 259-269.
51. Filipowicz W, Bhattacharyya SN, Sonenberg N (2008) Mechanisms of post-transcriptional regulation by microRNAs: are the answers in sight? Nat Rev Genet 9: 102-114.
52. Jones-Rhoades MW, Bartel DP, Bartel B (2006) MicroRNAS and their regulatory roles in plants. Annu Rev Plant Biol 57: 19-53.
53. Schwarz DS, Hutvagner G, Du T, Xu Z, Aronin N, et al. (2003) Asymmetry in the assembly of the RNAi enzyme complex. Cell 115: 199-208.
54. Kiriakidou M, Tan GS, Lamprinaki S, De Planell-Saguer M, Nelson PT, et al. (2007) An mRNA m7G cap binding-like motif within human Ago2 represses translation. Cell 129: 1141-1151.
55. Petersen CP, Bordeleau ME, Pelletier J, Sharp PA (2006) Short RNAs repress translation after initiation in mammalian cells. Mol Cell 21: 533-542.
56. Vasudevan S, Tong Y, Steitz JA (2007) Switching from repression to activation: microRNAs can up-regulate translation. Science 318: 1931-1934.
57. Hobert O (2008) Gene regulation by transcription factors and microRNAs. Science 319: 1785-1786.
58. Ashraf SI, McLoon AL, Sclarsic SM, Kunes S (2006) Synaptic protein synthesis associated with memory is regulated by the RISC pathway in Drosophila. Cell 124: 191-205.
59. Schratt GM, Tuebing F, Nigh EA, Kane CG, Sabatini ME, et al. (2006) A brain-specific microRNA regulates dendritic spine development. Nature 439: 283-289.
60. Bhattacharyya SN, Habermacher R, Martine U, Closs EI, Filipowicz W (2006) Relief of microRNA-mediated translational repression in human cells subjected to stress. Cell 125: 1111-1124.
61. Calin GA, Sevignani C, Dumitru CD, Hyslop T, Noch E, et al. (2004) Human microRNA genes are frequently located at fragile sites and genomic regions involved in cancers. Proc Natl Acad Sci U S A 101: 2999-3004.
62. Tam W (2008) The emergent role of microRNAs in molecular diagnostics of cancer. J Mol Diagn 10: 411-414.

63. Tam W, Hughes SH, Hayward WS, Besmer P (2002) Avian bic, a gene isolated from a common retroviral site in avian leukosis virus-induced lymphomas that encodes a noncoding RNA, cooperates with c-myc in lymphomagenesis and erythroleukemogenesis. J Virol 76: 4275-4286.
64. Tili E, Michaille JJ, Wernicke D, Alder H, Costinean S, et al. (2011) Mutator activity induced by microRNA-155 (miR-155) links inflammation and cancer. Proc Natl Acad Sci U S A 108: 4908-4913.
65. Costinean S, Zanesi N, Pekarsky Y, Tili E, Volinia S, et al. (2006) Pre-B cell proliferation and lymphoblastic leukemia/high-grade lymphoma in E(mu)-miR155 transgenic mice. Proc Natl Acad Sci U S A 103: 7024-7029.
66. Ma X, Kumar M, Choudhury SN, Becker Buscaglia LE, Barker JR, et al. (2011) Loss of the miR-21 allele elevates the expression of its target genes and reduces tumorigenesis. Proc Natl Acad Sci U S A 108: 10144-10149.
67. Medina PP, Nolde M, Slack FJ (2010) OncomiR addiction in an in vivo model of microRNA-21-induced pre-B-cell lymphoma. Nature 467: 86-90.
68. Hatley ME, Patrick DM, Garcia MR, Richardson JA, Bassel-Duby R, et al. (2010) Modulation of K-Ras-dependent lung tumorigenesis by MicroRNA-21. Cancer Cell 18: 282-293.
69. O'Donnell KA, Wentzel EA, Zeller KI, Dang CV, Mendell JT (2005) c-Myc-regulated microRNAs modulate E2F1 expression. Nature 435: 839-843.
70. He L, Thomson JM, Hemann MT, Hernando-Monge E, Mu D, et al. (2005) A microRNA polycistron as a potential human oncogene. Nature 435: 828-833.
71. Klein U, Lia M, Crespo M, Siegel R, Shen Q, et al. (2010) The DLEU2/miR-15a/16-1 cluster controls B cell proliferation and its deletion leads to chronic lymphocytic leukemia. Cancer Cell 17: 28-40.
72. Musumeci M, Coppola V, Addario A, Patrizii M, Maugeri-Sacca M, et al. (2011) Control of tumor and microenvironment cross-talk by miR-15a and miR-16 in prostate cancer. Oncogene 30: 4231-4242.
73. Kumar MS, Pester RE, Chen CY, Lane K, Chin C, et al. (2009) Dicer1 functions as a haploinsufficient tumor suppressor. Genes Dev 23: 2700-2704.
74. Bernstein E, Kim SY, Carmell MA, Murchison EP, Alcorn H, et al. (2003) Dicer is essential for mouse development. Nat Genet 35: 215-217.
75. Gupta GP, Massague J (2006) Cancer metastasis: building a framework. Cell 127: 679-695.
76. Valastyan S, Weinberg RA (2011) Tumor metastasis: molecular insights and evolving paradigms. Cell 147: 275-292.
77. Gregory PA, Bert AG, Paterson EL, Barry SC, Tsykin A, et al. (2008) The miR-200 family and miR-205 regulate epithelial to mesenchymal transition by targeting ZEB1 and SIP1. Nat Cell Biol 10: 593-601.
78. Korpal M, Lee ES, Hu G, Kang Y (2008) The miR-200 family inhibits epithelial-mesenchymal transition and cancer cell migration by direct targeting of E-cadherin transcriptional repressors ZEB1 and ZEB2. J Biol Chem 283: 14910-14914.
79. Park SM, Gaur AB, Lengyel E, Peter ME (2008) The miR-200 family determines the epithelial phenotype of cancer cells by targeting the E-cadherin repressors ZEB1 and ZEB2. Genes Dev 22: 894-907.
80. Gibbons DL, Lin W, Creighton CJ, Rizvi ZH, Gregory PA, et al. (2009) Contextual extracellular cues promote tumor cell EMT and metastasis by regulating miR-200 family expression. Genes Dev 23: 2140-2151.
81. Kong D, Banerjee S, Ahmad A, Li Y, Wang Z, et al. (2010) Epithelial to mesenchymal transition is mechanistically linked with stem cell signatures in prostate cancer cells. PLoS One 5: e12445.

82. Wellner U, Schubert J, Burk UC, Schmalhofer O, Zhu F, et al. (2009) The EMT-activator ZEB1 promotes tumorigenicity by repressing stemness-inhibiting microRNAs. Nat Cell Biol 11: 1487-1495.
83. Valastyan S, Reinhardt F, Benaich N, Calogrias D, Szasz AM, et al. (2009) A pleiotropically acting microRNA, miR-31, inhibits breast cancer metastasis. Cell 137: 1032-1046.
84. Valastyan S, Chang A, Benaich N, Reinhardt F, Weinberg RA (2011) Activation of miR-31 function in already-established metastases elicits metastatic regression. Genes Dev 25: 646-659.
85. Tavazoie SF, Alarcon C, Oskarsson T, Padua D, Wang Q, et al. (2008) Endogenous human microRNAs that suppress breast cancer metastasis. Nature 451: 147-152.
86. Hamada S, Satoh K, Fujibuchi W, Hirota M, Kanno A, et al. (2012) MiR-126 acts as a tumor suppressor in pancreatic cancer cells via the regulation of ADAM9. Mol Cancer Res 10: 3-10.
87. Chen H, Miao R, Fan J, Han Z, Wu J, et al. (2013) Decreased expression of miR-126 correlates with metastatic recurrence of hepatocellular carcinoma. Clin Exp Metastasis.
88. Huang Q, Gumireddy K, Schrier M, le Sage C, Nagel R, et al. (2008) The microRNAs miR-373 and miR-520c promote tumour invasion and metastasis. Nat Cell Biol 10: 202-210.
89. Ma L, Reinhardt F, Pan E, Soutschek J, Bhat B, et al. (2010) Therapeutic silencing of miR-10b inhibits metastasis in a mouse mammary tumor model. Nat Biotechnol 28: 341-347.
90. Bloomston M, Frankel WL, Petrocca F, Volinia S, Alder H, et al. (2007) MicroRNA expression patterns to differentiate pancreatic adenocarcinoma from normal pancreas and chronic pancreatitis. JAMA 297: 1901-1908.
91. Ciafre SA, Galardi S, Mangiola A, Ferracin M, Liu CG, et al. (2005) Extensive modulation of a set of microRNAs in primary glioblastoma. Biochem Biophys Res Commun 334: 1351-1358.
92. Tan HX, Wang Q, Chen LZ, Huang XH, Chen JS, et al. (2010) MicroRNA-9 reduces cell invasion and E-cadherin secretion in SK-Hep-1 cell. Med Oncol 27: 654-660.
93. Kasinski AL, Slack FJ (2011) Epigenetics and genetics. MicroRNAs en route to the clinic: progress in validating and targeting microRNAs for cancer therapy. Nat Rev Cancer 11: 849-864.
94. Aigner A (2011) MicroRNAs (miRNAs) in cancer invasion and metastasis: therapeutic approaches based on metastasis-related miRNAs. J Mol Med (Berl) 89: 445-457.
95. Ebert MS, Neilson JR, Sharp PA (2007) MicroRNA sponges: competitive inhibitors of small RNAs in mammalian cells. Nat Methods 4: 721-726.
96. Krutzfeldt J, Rajewsky N, Braich R, Rajeev KG, Tuschl T, et al. (2005) Silencing of microRNAs in vivo with 'antagomirs'. Nature 438: 685-689.
97. Lanford RE, Hildebrandt-Eriksen ES, Petri A, Persson R, Lindow M, et al. (2010) Therapeutic silencing of microRNA-122 in primates with chronic hepatitis C virus infection. Science 327: 198-201.
98. Wiggins JF, Ruffino L, Kelnar K, Omotola M, Patrawala L, et al. (2010) Development of a lung cancer therapeutic based on the tumor suppressor microRNA-34. Cancer Res 70: 5923-5930.
99. Trang P, Wiggins JF, Daige CL, Cho C, Omotola M, et al. (2011) Systemic delivery of tumor suppressor microRNA mimics using a neutral lipid emulsion inhibits lung tumors in mice. Mol Ther 19: 1116-1122.
100. Liu C, Kelnar K, Liu B, Chen X, Calhoun-Davis T, et al. (2011) The microRNA miR-34a inhibits prostate cancer stem cells and metastasis by directly repressing CD44. Nat Med 17: 211-215.
101. Miller TE, Ghoshal K, Ramaswamy B, Roy S, Datta J, et al. (2008) MicroRNA-221/222 confers tamoxifen resistance in breast cancer by targeting p27Kip1. J Biol Chem 283: 29897-29903.

102. Zhong M, Ma X, Sun C, Chen L (2010) MicroRNAs reduce tumor growth and contribute to enhance cytotoxicity induced by gefitinib in non-small cell lung cancer. Chem Biol Interact 184: 431-438.
103. Holleman A, Chung I, Olsen RR, Kwak B, Mizokami A, et al. (2011) miR-135a contributes to paclitaxel resistance in tumor cells both in vitro and in vivo. Oncogene 30: 4386-4398.
104. Hwang JH, Voortman J, Giovannetti E, Steinberg SM, Leon LG, et al. (2010) Identification of microRNA-21 as a biomarker for chemoresistance and clinical outcome following adjuvant therapy in resectable pancreatic cancer. PLoS One 5: e10630.
105. Park JK, Lee EJ, Esau C, Schmittgen TD (2009) Antisense inhibition of microRNA-21 or -221 arrests cell cycle, induces apoptosis, and sensitizes the effects of gemcitabine in pancreatic adenocarcinoma. Pancreas 38: e190-199.
106. Galluzzi L, Morselli E, Vitale I, Kepp O, Senovilla L, et al. (2010) miR-181a and miR-630 regulate cisplatin-induced cancer cell death. Cancer Res 70: 1793-1803.
107. Pramanik D, Campbell NR, Karikari C, Chivukula R, Kent OA, et al. (2011) Restitution of tumor suppressor microRNAs using a systemic nanovector inhibits pancreatic cancer growth in mice. Mol Cancer Ther 10: 1470-1480.
108. Zhang X, Liu S, Hu T, Liu S, He Y, et al. (2009) Up-regulated microRNA-143 transcribed by nuclear factor kappa B enhances hepatocarcinoma metastasis by repressing fibronectin expression. Hepatology 50: 490-499.
109. Grimm D, Streetz KL, Jopling CL, Storm TA, Pandey K, et al. (2006) Fatality in mice due to oversaturation of cellular microRNA/short hairpin RNA pathways. Nature 441: 537-541.
110. Urist MJ, Di Como CJ, Lu ML, Charytonowicz E, Verbel D, et al. (2002) Loss of p63 expression is associated with tumor progression in bladder cancer. Am J Pathol 161: 1199-1206.
111. Castillo-Martin M, Domingo-Domenech J, Karni-Schmidt O, Matos T, Cordon-Cardo C (2010) Molecular pathways of urothelial development and bladder tumorigenesis. Urol Oncol 28: 401-408.
112. Yang A, Schweitzer R, Sun D, Kaghad M, Walker N, et al. (1999) p63 is essential for regenerative proliferation in limb, craniofacial and epithelial development. Nature 398: 714-718.
113. Hu P, Deng FM, Liang FX, Hu CM, Auerbach AB, et al. (2000) Ablation of uroplakin III gene results in small urothelial plaques, urothelial leakage, and vesicoureteral reflux. J Cell Biol 151: 961-972.
114. Kong XT, Deng FM, Hu P, Liang FX, Zhou G, et al. (2004) Roles of uroplakins in plaque formation, umbrella cell enlargement, and urinary tract diseases. J Cell Biol 167: 1195-1204.
115. Sesterhenn IA (2004) Urothelial carcinoma in situ. In: Eble JN, Sauter, G., Epstein, J.I., Sesterhenn, I.A., editor. Wold Health Organization Classification of Tumors: Pathology and Genetics of Tumors of the Urinary System and Male Genital Organs. Lyon: IARC Press. pp. 119-120.
116. McKenney JK, Gomez JA, Desai S, Lee MW, Amin MB (2001) Morphologic expressions of urothelial carcinoma in situ: a detailed evaluation of its histologic patterns with emphasis on carcinoma in situ with microinvasion. Am J Surg Pathol 25: 356-362.
117. Wolf H, Melsen F, Pedersen SE, Nielsen KT (1994) Natural history of carcinoma in situ of the urinary bladder. Scand J Urol Nephrol Suppl 157: 147-151.
118. Lu J, Getz G, Miska EA, Alvarez-Saavedra E, Lamb J, et al. (2005) MicroRNA expression profiles classify human cancers. Nature 435: 834-838.
119. Puerta-Gil P, Garcia-Baquero R, Jia AY, Ocana S, Alvarez-Mugica M, et al. (2012) miR-143, miR-222, and miR-452 are useful as tumor stratification and noninvasive diagnostic biomarkers for bladder cancer. Am J Pathol 180: 1808-1815.

120. Wang M, Chu H, Li P, Yuan L, Fu G, et al. (2012. [Epub ahead of print]) Genetic variants in microRNAs predict bladder cancer risk and recurrence. Cancer Res.
121. Catto JW, Miah S, Owen HC, Bryant H, Myers K, et al. (2009) Distinct microRNA alterations characterize high- and low-grade bladder cancer. Cancer Res 69: 8472-8481.
122. Dyrskjot L, Ostenfeld MS, Bramsen JB, Silahtaroglu AN, Lamy P, et al. (2009) Genomic profiling of microRNAs in bladder cancer: miR-129 is associated with poor outcome and promotes cell death in vitro. Cancer Res 69: 4851-4860.
123. Gottardo F, Liu CG, Ferracin M, Calin GA, Fassan M, et al. (2007) Micro-RNA profiling in kidney and bladder cancers. Urol Oncol 25: 387-392.
124. Hanke M, Hoefig K, Merz H, Feller AC, Kausch I, et al. (2010) A robust methodology to study urine microRNA as tumor marker: microRNA-126 and microRNA-182 are related to urinary bladder cancer. Urol Oncol 28: 655-661.
125. Ichimi T, Enokida H, Okuno Y, Kunimoto R, Chiyomaru T, et al. (2009) Identification of novel microRNA targets based on microRNA signatures in bladder cancer. Int J Cancer 125: 345-352.
126. Lin T, Dong W, Huang J, Pan Q, Fan X, et al. (2009) MicroRNA-143 as a tumor suppressor for bladder cancer. J Urol 181: 1372-1380.
127. Wang G, Zhang H, He H, Tong W, Wang B, et al. (2010) Up-regulation of microRNA in bladder tumor tissue is not common. Int Urol Nephrol 42: 95-102.
128. Gires O (2011) Lessons from common markers of tumor-initiating cells in solid cancers. Cell Mol Life Sci 68: 4009-4022.
129. Veerla S, Lindgren D, Kvist A, Frigyesi A, Staaf J, et al. (2009) MiRNA expression in urothelial carcinomas: important roles of miR-10a, miR-222, miR-125b, miR-7 and miR-452 for tumor stage and metastasis, and frequent homozygous losses of miR-31. Int J Cancer 124: 2236-2242.
130. Dalbagni G, Presti J, Reuter V, Fair WR, Cordon-Cardo C (1993) Genetic alterations in bladder cancer. Lancet 342: 469-471.
131. McConkey DJ, Lee S, Choi W, Tran M, Majewski T, et al. (2010) Molecular genetics of bladder cancer: Emerging mechanisms of tumor initiation and progression. Urol Oncol 28: 429-440.
132. Dinney CP, McConkey DJ, Millikan RE, Wu X, Bar-Eli M, et al. (2004) Focus on bladder cancer. Cancer Cell 6: 111-116.
133. Wu XR (2005) Urothelial tumorigenesis: a tale of divergent pathways. Nat Rev Cancer 5: 713-725.
134. Zhang ZT, Pak J, Shapiro E, Sun TT, Wu XR (1999) Urothelium-specific expression of an oncogene in transgenic mice induced the formation of carcinoma in situ and invasive transitional cell carcinoma. Cancer Res 59: 3512-3517.
135. Sidransky D, Frost P, Von Eschenbach A, Oyasu R, Preisinger AC, et al. (1992) Clonal origin bladder cancer. N Engl J Med 326: 737-740.
136. Fleige S, Pfaffl MW (2006) RNA integrity and the effect on the real-time qRT-PCR performance. Mol Aspects Med 27: 126-139.
137. Howlader N, Noone AM, Krapcho M, Neyman N, Aminou R, et al. (2009) SEER Cancer Statistics Review, 1975-2009 (Vintage 2009 Populations). Bethesda, MD: National Cancer Institute.
138. Garcia del Muro X, Torregrosa A, Munoz J, Castellsague X, Condom E, et al. (2000) Prognostic value of the expression of E-cadherin and beta-catenin in bladder cancer. Eur J Cancer 36: 357-362.
139. Vihinen P, Kahari VM (2002) Matrix metalloproteinases in cancer: prognostic markers and therapeutic targets. Int J Cancer 99: 157-166.
140. Campbell SC, Volpert OV, Ivanovich M, Bouck NP (1998) Molecular mediators of angiogenesis in bladder cancer. Cancer Res 58: 1298-1304.

141. Eble JN, Sauter G, Epstein JI, Sesterhenn IA (2004) Pathology and Genetics of Tumors of the Urinary System and Male Genital Organs. Lyon: IARC Press. 90-157 p.
142. Wiklund ED, Bramsen JB, Hulf T, Dyrskjot L, Ramanathan R, et al. (2011) Coordinated epigenetic repression of the miR-200 family and miR-205 in invasive bladder cancer. Int J Cancer 128: 1327-1334.
143. Adam L, Zhong M, Choi W, Qi W, Nicoloso M, et al. (2009) miR-200 expression regulates epithelial-to-mesenchymal transition in bladder cancer cells and reverses resistance to epidermal growth factor receptor therapy. Clin Cancer Res 15: 5060-5072.
144. Zhao JJ, Yang J, Lin J, Yao N, Zhu Y, et al. (2009) Identification of miRNAs associated with tumorigenesis of retinoblastoma by miRNA microarray analysis. Childs Nerv Syst 25: 13-20.
145. Wong TS, Liu XB, Wong BY, Ng RW, Yuen AP, et al. (2008) Mature miR-184 as Potential Oncogenic microRNA of Squamous Cell Carcinoma of Tongue. Clin Cancer Res 14: 2588-2592.
146. Tan S, Li R, Ding K, Lobie PE, Zhu T (2011) miR-198 inhibits migration and invasion of hepatocellular carcinoma cells by targeting the HGF/c-MET pathway. FEBS Lett 585: 2229-2234.
147. Mazumder Indra D, Mitra S, Singh RK, Dutta S, Roy A, et al. (2011) Inactivation of CHEK1 and EI24 is associated with the development of invasive cervical carcinoma: clinical and prognostic implications. Int J Cancer 129: 1859-1871.
148. Zhao X, Ayer RE, Davis SL, Ames SJ, Florence B, et al. (2005) Apoptosis factor EI24/PIG8 is a novel endoplasmic reticulum-localized Bcl-2-binding protein which is associated with suppression of breast cancer invasiveness. Cancer Res 65: 2125-2129.
149. Mork CN, Faller DV, Spanjaard RA (2007) Loss of putative tumor suppressor EI24/PIG8 confers resistance to etoposide. FEBS Lett 581: 5440-5444.
150. Mishra L, Katuri V, Evans S (2005) The role of PRAJA and ELF in TGF-beta signaling and gastric cancer. Cancer Biol Ther 4: 694-699.
151. Jiang X, Gillen S, Esposito I, Giese NA, Michalski CW, et al. (2010) Reduced expression of the membrane skeleton protein beta1-spectrin (SPTBN1) is associated with worsened prognosis in pancreatic cancer. Histol Histopathol 25: 1497-1506.
152. Wang S, Huang J, He J, Wang A, Xu S, et al. (2010) RPL41, a small ribosomal peptide deregulated in tumors, is essential for mitosis and centrosome integrity. Neoplasia 12: 284-293.
153. Wang A, Xu S, Zhang X, He J, Yan D, et al. (2011) Ribosomal protein RPL41 induces rapid degradation of ATF4, a transcription factor critical for tumour cell survival in stress. J Pathol 225: 285-292.
154. Sanfiorenzo C, Ilie MI, Belaid A, Barlesi F, Mouroux J, et al. (2013) Two Panels of Plasma MicroRNAs as Non-Invasive Biomarkers for Prediction of Recurrence in Resectable NSCLC. PLoS One 8: e54596.
155. Sasahira T, Kurihara M, Bhawal UK, Ueda N, Shimomoto T, et al. (2012) Downregulation of miR-126 induces angiogenesis and lymphangiogenesis by activation of VEGF-A in oral cancer. Br J Cancer 107: 700-706.
156. Duffy MJ, McKiernan E, O'Donovan N, McGowan PM (2009) Role of ADAMs in cancer formation and progression. Clin Cancer Res 15: 1140-1144.
157. Meyer SU, Pfaffl MW, Ulbrich SE (2010) Normalization strategies for microRNA profiling experiments: a 'normal' way to a hidden layer of complexity? Biotechnol Lett 32: 1777-1788.
158. Blobel CP (2005) ADAMs: key components in EGFR signalling and development. Nat Rev Mol Cell Biol 6: 32-43.

159. Milla ME, Leesnitzer MA, Moss ML, Clay WC, Carter HL, et al. (1999) Specific sequence elements are required for the expression of functional tumor necrosis factor-alpha-converting enzyme (TACE). J Biol Chem 274: 30563-30570.
160. Weskamp G, Kratzschmar J, Reid MS, Blobel CP (1996) MDC9, a widely expressed cellular disintegrin containing cytoplasmic SH3 ligand domains. J Cell Biol 132: 717-726.
161. Weskamp G, Cai H, Brodie TA, Higashyama S, Manova K, et al. (2002) Mice lacking the metalloprotease-disintegrin MDC9 (ADAM9) have no evident major abnormalities during development or adult life. Mol Cell Biol 22: 1537-1544.
162. O'Shea C, McKie N, Buggy Y, Duggan C, Hill AD, et al. (2003) Expression of ADAM-9 mRNA and protein in human breast cancer. Int J Cancer 105: 754-761.
163. Le Pabic H, Bonnier D, Wewer UM, Coutand A, Musso O, et al. (2003) ADAM12 in human liver cancers: TGF-beta-regulated expression in stellate cells is associated with matrix remodeling. Hepatology 37: 1056-1066.
164. Shintani Y, Higashiyama S, Ohta M, Hirabayashi H, Yamamoto S, et al. (2004) Overexpression of ADAM9 in non-small cell lung cancer correlates with brain metastasis. Cancer Res 64: 4190-4196.
165. Mazzocca A, Coppari R, De Franco R, Cho JY, Libermann TA, et al. (2005) A secreted form of ADAM9 promotes carcinoma invasion through tumor-stromal interactions. Cancer Res 65: 4728-4738.
166. Sung SY, Kubo H, Shigemura K, Arnold RS, Logani S, et al. (2006) Oxidative stress induces ADAM9 protein expression in human prostate cancer cells. Cancer Res 66: 9519-9526.
167. Peduto L, Reuter VE, Shaffer DR, Scher HI, Blobel CP (2005) Critical function for ADAM9 in mouse prostate cancer. Cancer Res 65: 9312-9319.
168. Seshacharyulu P, Ponnusamy MP, Haridas D, Jain M, Ganti AK, et al. (2012) Targeting the EGFR signaling pathway in cancer therapy. Expert Opin Ther Targets 16: 15-31.
169. Shigematsu H, Takahashi T, Nomura M, Majmudar K, Suzuki M, et al. (2005) Somatic mutations of the HER2 kinase domain in lung adenocarcinomas. Cancer Res 65: 1642-1646.
170. Raouf A, Sun Y, Chatterjee S, Basak P (2012) The biology of human breast epithelial progenitors. Semin Cell Dev Biol 23: 606-612.
171. Wang ZA, Shen MM (2011) Revisiting the concept of cancer stem cells in prostate cancer. Oncogene 30: 1261-1271.
172. Stingl J, Eaves CJ, Zandieh I, Emerman JT (2001) Characterization of bipotent mammary epithelial progenitor cells in normal adult human breast tissue. Breast Cancer Res Treat 67: 93-109.
173. Stingl J, Eirew P, Ricketson I, Shackleton M, Vaillant F, et al. (2006) Purification and unique properties of mammary epithelial stem cells. Nature 439: 993-997.
174. Garraway IP, Sun W, Tran CP, Perner S, Zhang B, et al. (2010) Human prostate sphere-forming cells represent a subset of basal epithelial cells capable of glandular regeneration in vivo. Prostate 70: 491-501.
175. Wang X, Kruithof-de Julio M, Economides KD, Walker D, Yu H, et al. (2009) A luminal epithelial stem cell that is a cell of origin for prostate cancer. Nature 461: 495-500.
176. Erman A, Veranic P, Psenicnik M, Jezernik K (2006) Superficial cell differentiation during embryonic and postnatal development of mouse urothelium. Tissue Cell 38: 293-301.
177. Corcoran DL, Pandit KV, Gordon B, Bhattacharjee A, Kaminski N, et al. (2009) Features of mammalian microRNA promoters emerge from polymerase II chromatin immunoprecipitation data. PLoS One 4: e5279.
178. Ozsolak F, Poling LL, Wang Z, Liu H, Liu XS, et al. (2008) Chromatin structure analyses identify miRNA promoters. Genes Dev 22: 3172-3183.

179. Dyrskjot L, Kruhoffer M, Thykjaer T, Marcussen N, Jensen JL, et al. (2004) Gene expression in the urinary bladder: a common carcinoma in situ gene expression signature exists disregarding histopathological classification. Cancer Res 64: 4040-4048.
180. Masui T, Mann AM, Macatee TL, Garland EM, Okamura T, et al. (1991) Direct DNA sequencing of the rat neu oncogene transmembrane domain reveals no mutation in urinary bladder carcinomas induced by N-butyl-N-(4-hydroxybutyl)nitrosamine, N-[4-(5-nitro-2-furyl)-2-thiazolyl]formamide or N-methyl-N-nitrosourea. Carcinogenesis 12: 1975-1978.
181. Druckrey H, Preussmann R, Ivankovic S, Schmidt CH, Mennel HD, et al. (1964) [Selective Induction of Bladder Cancer in Rats by Dibutyl- and N-Butyl-N-Butanol(4)-Nitrosamine]. Z Krebsforsch 66: 280-290.
182. Masui T, Mann AM, Garland EM, Cohen SM (1989) Strong promoting activity by uracil on urinary bladder carcinogenesis and a possible inhibitory effect on thyroid tumorigenesis in rats initiated with N-methyl-N-nitrosourea. Carcinogenesis 10: 1471-1474.
183. Kamijo T, Zindy F, Roussel MF, Quelle DE, Downing JR, et al. (1997) Tumor suppression at the mouse INK4a locus mediated by the alternative reading frame product p19ARF. Cell 91: 649-659.
184. Wszolek MF, Rieger-Christ KM, Kenney PA, Gould JJ, Silva Neto B, et al. (2011) A MicroRNA expression profile defining the invasive bladder tumor phenotype. Urol Oncol 29: 794-801 e791.
185. Reis LO, Sopena JM, Favaro WJ, Martin MC, Simao AF, et al. (2011) Anatomical features of the urethra and urinary bladder catheterization in female mice and rats. An essential translational tool. Acta Cir Bras 26 Suppl 2: 106-110.
186. van der Horst G, van Asten JJ, Figdor A, van den Hoogen C, Cheung H, et al. (2011) Real-time cancer cell tracking by bioluminescence in a preclinical model of human bladder cancer growth and metastasis. Eur Urol 60: 337-343.
187. Theodorescu D, Cornil I, Fernandez BJ, Kerbel RS (1990) Overexpression of normal and mutated forms of HRAS induces orthotopic bladder invasion in a human transitional cell carcinoma. Proc Natl Acad Sci U S A 87: 9047-9051.
188. Fridman JS, Caulder E, Hansbury M, Liu X, Yang G, et al. (2007) Selective inhibition of ADAM metalloproteases as a novel approach for modulating ErbB pathways in cancer. Clin Cancer Res 13: 1892-1902.
189. Zhou BB, Peyton M, He B, Liu C, Girard L, et al. (2006) Targeting ADAM-mediated ligand cleavage to inhibit HER3 and EGFR pathways in non-small cell lung cancer. Cancer Cell 10: 39-50.
190. Infante J, Burris HA, Lewis N, Donehower R, Redman J, et al. (2007) A multicenter phase 1b study of the safety, pharmacokinetics, biological activity and clinical efficacy of INCB7839, a potent and selective inhibitor of ADAM10 and ADAM17. Breast Cancer Res Treat 106.
191. Merchant NB, Voskresensky I, Rogers CM, Lafleur B, Dempsey PJ, et al. (2008) TACE/ADAM-17: a component of the epidermal growth factor receptor axis and a promising therapeutic target in colorectal cancer. Clin Cancer Res 14: 1182-1191.
192. Moss ML, Powell G, Miller MA, Edwards L, Qi B, et al. (2011) ADAM9 inhibition increases membrane activity of ADAM10 and controls alpha-secretase processing of amyloid precursor protein. J Biol Chem 286: 40443-40451.
193. Kim JM, Rha SY, Yu EJ, Kim TS, Shin YK, et al. The impact of ADAM-9 protease activity on invasiveness of gastric cancer [abstract]. In: Proceedings of the AACR-NCI-EORTC International Conference: Molecular Targets and Cancer Therapeutics; 2011 Nov 12-16; San Francisco, CA. Philadelphia (PA): AACR; Mol Cancer Ther 2011;10(11 nr C43.
194. Amour A, Knight CG, English WR, Webster A, Slocombe PM, et al. (2002) The enzymatic activity of ADAM8 and ADAM9 is not regulated by TIMPs. FEBS Lett 524: 154-158.

195. Overall CM, Kleifeld O (2006) Tumour microenvironment - opinion: validating matrix metalloproteinases as drug targets and anti-targets for cancer therapy. Nat Rev Cancer 6: 227-239.